A DISSERTATION FOR THE DEGREE OF DOCTOR OF PHILOSOPHY

Gallol based Underwater Pressure-Sensitive Adhesives with Surface Microstructure

표면 미세구조를 지닌 갈롤 기반 수중 점착소재

Advisor: Hyun-Joong Kim

by
Seong-Ju Lee

PROGRAM IN ENVIRONMENTAL MATERIALS SCIENCE
GRADUATE SCHOOL
SEOUL NATIONAL UNIVERSITY

AUGUST, 2024

SEOUL NATIONAL UNIVERSITY

GRADUATE SCHOOL

PROGRAM IN ENVIRONMENTAL MATERIALS SCIENCE

WE HEREBY RECOMMEND THE THESIS BY
Seong-Ju Lee

ENTITLED

Gallol based Underwater Pressure-Sensitive Adhesives with Surface Microstructure

BE ACCEPTED IN FULFILLMENT OF THE REQUIREMENTS FOR THE DEGREE OF DOCTOR OF PHILOSOPHY

AUGUST, 2024

COMMITTEE ON FINAL EXAMINATION

Chairman ______________________________
Prof. Cheol-Hee Ahn

Co-Chairman ______________________________
Prof. Hyun-Joong Kim

Member ______________________________
Ph.D. Ick-Kyung Sung

Member ______________________________
Ph.D. Jung-Jun Lee

Member ______________________________
Ph.D. Jung-Min Kim

Abstract

Gallol based Underwater Pressure-Sensitive Adhesives with Surface Microstructure

Seong-Ju Lee
Program in Environmental Materials Science
Graduate School
Seoul National University

Adhesives are commonly employed in both everyday life and diverse industrial applications due to their ease of application, allowing them to adhere to surfaces with slight pressure at room temperature. A variety of adhesives are commercially available, tailored for specific uses; however, these are typically effective only on dry surfaces in aerial environments. There is a growing need for adhesives capable of bonding in wet conditions or submerged environments, such as in medical wound dressings, water-based energy devices, underwater sensors, underwater maintenance, and maritime applications. Consequently, the development of advanced underwater adhesives that perform effectively across various aquatic conditions has emerged as a critical focus of adhesive research.

Achieving robust adhesion in aqueous settings poses significant challenges beyond those encountered in air. When materials are exposed to aquatic environments, they often develop a hydration layer that impedes molecular interactions essential for adhesive bonding. Additionally, water droplets trapped at the interface can diminish the effective contact area, and prolonged exposure to water may lead to adhesive degradation through processes such as plasticization, swelling, erosion, and hydrolysis. These issues make the development of effective underwater adhesives complex and demanding.

The innovation in underwater adhesives has often been inspired by natural phenomena. For instance, marine organisms such as mussels utilize catechol functionalities for durable underwater adhesion, while species like frogs and clingfish leverage unique microstructures for temporary attachment to moist surfaces. Drawing inspiration from these biological strategies, researchers have explored novel approaches to enhance underwater adhesive formulations. Nevertheless, the commercial viability of these innovations has been hindered by factors such as the high cost of DOPA and the additional costs associated with preventing oxidation.

This study employs gallic acid, a more cost-effective and commercially viable alternative derived from various plants, to synthesize adhesives containing gallol groups. These adhesives, characterized by their hydrophobic nature and low glass transition temperatures, are designed to overcome the challenges posed by hydration layers and ensure effective adhesion at room temperature. Gallol groups were integrated into the adhesive matrix through a straightforward esterification reaction with epoxy groups in the scaffold. Moreover, the scaffold polymer was transitioned from a linear to a branched structure to enhance the incorporation of gallol groups and improve overall adhesive performance, addressing the limitations typically associated with linear polymers.

To further augment the underwater performance of these adhesives, microstructural techniques were employed on the adhesive surface. The use of pattern release films facilitated the application of surface patterns through a continuous coating process, enabling rapid production. The study also evaluated the impact of varying surface microstructures on the adhesive properties in submerged conditions.

By integrating molecular-scale design strategies for gallol integration and polymer branching with macro-scale surface patterning techniques, this research successfully developed adhesives that demonstrate superior performance in underwater environments. The methodologies employed—

comprising conventional radical polymerization, the omission of protective steps for gallol, and the application of continuous coating technologies—are straightforward and compatible with existing industrial infrastructure, eliminating the need for additional facilities. This practical approach not only overcomes longstanding challenges in the commercialization of underwater adhesives but also sets forth new pathways for the development of versatile aquatic adhesives, anticipated to revolutionize the industry.

Keywords: Pressure-Sensitive Adhesives, Underwater Adhesion, Gallol,
Branched Polymer, Surface Microstructure

Student Number: 2014-20043

Table of Contents

Chapter 1

Introduction and Objectives

Chapter 2

Gallol Pressure-Sensitive Adhesives

Chapter 3

Branched Gallol Pressure-Sensitive Adhesives

Chapter 4

Surface-Patterned Gallol Pressure-Sensitive Adhesives

Chapter 5

Overall Conclusions

List of Tables

List of Figures

Chapter 1

Introduction and Objectives

1. Introduction

1.1. Pressure-Sensitive Adhesives (PSAs)

Pressure-sensitive adhesives (PSAs) are engineered to bond to surfaces upon application of minimal pressure, making them pivotal across diverse sectors including packaging, medical, electrical, and automotive industries, to name a few. Their ubiquitous applications across various domains are attributed to their ease of use and removability.

PSAs are categorized based on their physical form and the chemical composition of the adhesive formulation. From a chemical standpoint, rubber-based, silicone-based, and acrylic-based adhesives constitute the primary classes. Notably, acrylic adhesives, synthesized through the radical polymerization of acrylic monomers, are distinguished by their superior weatherability, thermal stability, and resistance to oils, attributes not as pronounced in their rubber and silicone-based counterparts. The incorporation of functional groups into these polymers facilitates the customization of adhesives for specific applications.

A critical design consideration for PSAs is the polymer's glass transition temperature (T_g), which should be substantially lower than the operational temperature to ensure adequate chain mobility and substrate wetting capabilities (Creton, 2003). The viscoelastic properties of the adhesive also play a crucial role in its performance. Optimal adhesion is achieved when the adhesive can conform to the substrate's topography, facilitated by a modulus (G) lower than the critical modulus (G_c), enabling the PSA to fill in the micro-textures of the surface. This concept was quantified by Carl Dahlquist in 1969 with the establishment of a G_c value of 0.1 MPa at 25 °C and a 1 Hz frequency, a guideline that has informed adhesive design for over four decades. The

Dahlquist criterion emphasizes the importance of maintaining a modulus below 0.1 MPa, although the specific modulus required can vary based on the application environment. Further elaboration by E.P. Chang on this principle involves segmenting G' and G" values into quadrants, suggesting applications based on their quadrant positioning (Creton*,* *et al.*, 2016). Both the glass transition temperature and modulus are paramount considerations in developing effective PSAs.

Evaluating the adhesive performance of PSAs extends beyond simple tests, given the dependency on application context and environmental conditions. The adhesive's long-term behavior does not necessarily align with short-term test results, necessitating a comprehensive evaluation approach. Initial assessments often involve examining the modulus across varying temperatures or frequencies, providing foundational insights into adhesive behavior. Although these rheological evaluations do not directly measure adhesive performance, they are instrumental in understanding the underlying mechanisms of adhesion.

Probe tack testing is instrumental in elucidating the deformation and energy absorption behaviors of pressure-sensitive adhesives (PSAs) during both adhesion and detachment phases, within relatively brief temporal frameworks. This test involves the vertical separation of a probe from the adhesive layer following a predetermined period of contact under specific pressure conditions. The tackiness, or tack, is assessed by manipulating variables such as contact duration, separation velocity, and the interactions between the probe and the adhesive, alongside the adhesive's intrinsic properties.

Peel force constitutes a critical metric for assessing adhesive efficacy. The peel test serves as a straightforward and intuitive methodology for gauging the performance of PSAs, with the peel force being adjustable based on the intended application or operational conditions through modifications in peel angle and speed. The peel strength of a PSA is typically characterized by a triad of elements: the surface characteristics, the cohesive forces within the adhesive's bulk, and the properties of the backing film (Figure 1-1).

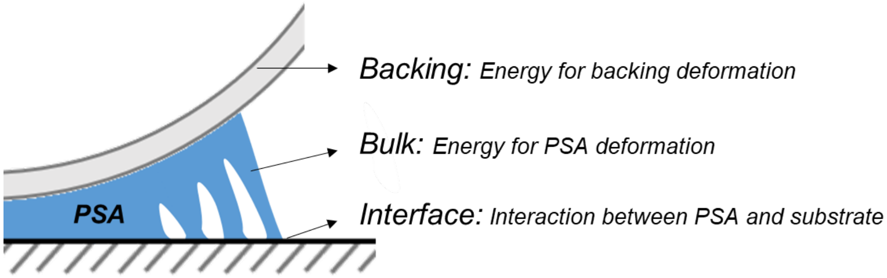

Figure 1-1. Schematic illustration of the main factors of peel adhesion force

At the interface, the strength of adhesion is significantly influenced by the physical and chemical interactions between the adhesive and the substrate. Within the adhesive's bulk, the force required to induce deformation plays a pivotal role in determining the adhesive strength. Consequently, up to a certain threshold, an increase in adhesive thickness correlates with enhanced adhesive force. Moreover, the adhesion is also impacted by the thickness and modulus of the backing material, attributed to the energy required to deform the backing, underscoring the multifaceted nature of adhesive performance evaluation.

1.2. Ways to improve adhesion force

Enhancing the adhesive force of pressure-sensitive adhesives (PSAs), aside from the influence of backing materials, hinges on the interactions at the PSA-substrate interface and the inherent properties of the adhesive material. Interface interactions necessitate a strong bond between the PSA and the substrate surface through various mechanisms. For instance, adhesion enhancement can be achieved through mechanical interlocking at a macroscopic scale, polymer chain entanglement with the substrate, or differential pressure-induced suction (Figure 1-2). Furthermore, chemical enhancements to adhesion can be achieved through the formation of covalent bonds via chemical reactions or the establishment of non-covalent interactions such as hydrogen bonds and electrostatic forces.

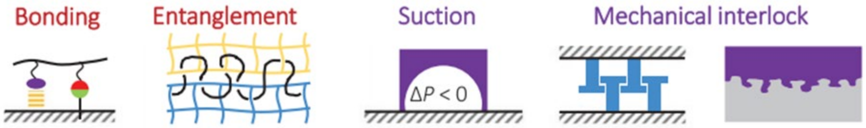

Figure 1-2. Strategies for improving interfacial adhesion force (Fan, *et al.*, 2021)

In the bulk material, adhesion improvement is achievable by optimizing energy dissipation during deformation. Energy dissipation mechanisms within the bulk help delay bond rupture at the interface, thereby enhancing adhesive force by distributing the energy that would otherwise be concentrated at the interface (Figure 1-3) (Arzt, *et al.*, 2003, del Campo, *et al.*, 2007, Rao, *et al.*, 2018, Spolenak, *et al.*, 2005).

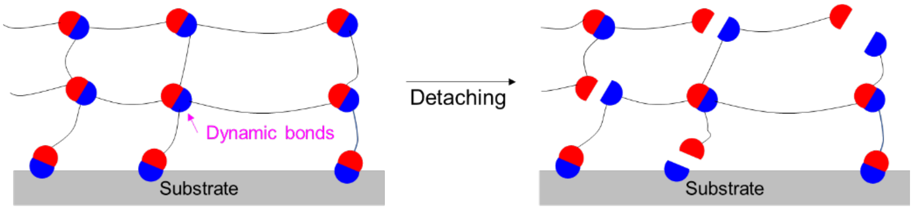

Figure 1-3. During detaching, the rupture of bulk bonds dissipates energy, which delays the debonding at the interface

One approach to augment bulk energy dissipation involves the integration of heterogeneous networks, where a rigid, brittle network is combined with a softer, more ductile one (Gong, 2014) . This configuration yields a composite network that exhibits both rigidity and toughness, delaying interfacial fractures by first breaking and dissipating energy within the rigid network upon deformation. Another strategy to enhance energy dissipation in the bulk material involves the incorporation of reversible bonds (Fan and Gong, 2021). Dynamic covalent bonds, such as disulfide, imine, and acylhydrazone bonds, as well as phenylboronate ester complexes, can undergo reversible dissociation and reformation in response to external stimuli like heat, light, or changes in pH. Additionally, non-covalent bonds, despite their individual weakness, can collectively offer significant strength. The presence of numerous weak but collectively strong non-covalent bonds in the bulk material ensures that these bonds break preferentially during deformation, thus postponing rupture at the interface and contributing to the overall durability and resilience of the PSA (Yang, *et al.*, 2020).

Table 1-1. Representative reversible bonds (Yang*, et al.*, 2020)

Bond types	**Representative bonds**
Dynamic covalent bonds	disulfide, imine, acylhydrazone, phenylborate ester complexations
Ionic bonds	iron-carboxylate coordination complex, amine-carboxylate, amine silanol, tertiary amin-carboxylate
Hydrogen bonds	carboxylic acid and hydroxyl, amine and hydroxyl, hydroxyl and hydroxyl, amine and phenol
Other noncovalent bonds	Hydrophobic interaction, dipole-dipole interaction, π-π stacks, host-guest interaction, catechol chemistry

Ionic bonds (Braccini*, et al.*, 2001, Lee*, et al.*, 2012, Roy*, et al.*, 2015, Sun*, et al.*, 2012), hydrogen bonds (Li*, et al.*, 2014, Steiner, 2002, Wang*, et al.*, 2017, Yang*, et al.*, 2018, Yang*, et al.*, 2016), hydrophobic interactions (Tuncaboylu*, et al.*, 2012, Tuncaboylu*, et al.*, 2013), π–π stacks (Jayawarna*, et al.*, 2006, Li*, et al.*, 2010, Smith*, et al.*, 2008), and dipole-dipole interactions (Bai*, et al.*, 2011, Jia*, et al.*, 2017) are typical non-covalent bonds used in adhesive materials (Table 1-1). As a reversible bond using a specific substance, there is a host-guest interaction (Ahn*, et al.*, 2013, Li*, et al.*, 2015, Ma*, et al.*, 2015, Nakahata*, et al.*, 2011, Wu*, et al.*, 2017) in which two or more molecules bind by non-covalent bonds. A typical host material is cyclodextrins. Catechol chemistry inspired by the mussels adhesion is also actively studied because it can improve bulk energy dispersibility by utilizing various covalent and non-covalent bonds (Ahn, 2017, Cheng*,* *et al.*, 2017, Lee*,* *et al.*, 2007, Liao*,* *et al.*, 2017, Waite, 2017).

The enhancement of adhesive properties through the adoption of a three-dimensional surface topology is a concept inspired by the natural adhesion mechanisms observed in geckos (Figure 1-4). The introduction of "patterned" or "fibrillar" surface structures has been demonstrated to facilitate superior adhesion on flat and rough substrates compared to conventional smooth surfaces. Contrary to the simplistic notion that adhesion directly correlates with contact area, fibrillar surfaces challenge this paradigm by exhibiting enhanced adhesive interactions through micro-scale engagement with the substrate.

The intrinsic design of fibril structures offers several mechanical advantages that contribute to their elevated adhesive performance. Primarily, the discontinuous nature of fibrils impedes the propagation of peeling forces, necessitating the initiation of new cracks for the detachment of each fibril, thus significantly increasing resistance to peeling (Figure 1-4a). Moreover, the fibrillar configuration promotes a more homogenous distribution of stress across the adhesive interface (Figure 1-4b). When subjected to external loads, this uniform stress distribution allows the adhesive bond to approach its theoretical maximum strength, ensuring optimal performance. Furthermore, fibrillar structures exhibit an inherent resilience to structural flaws (Figure 1-4c). The segmented nature of fibrils confines the extent of any defect, preventing its propagation across the adhesive interface and thereby maintaining the integrity of the adhesive bond even in the presence of imperfections. This feature underscores the robustness of fibrillar adhesive designs, making them a promising avenue for the development of advanced adhesive materials with enhanced durability and reliability (Kamperman*,* *et al.*, 2010).

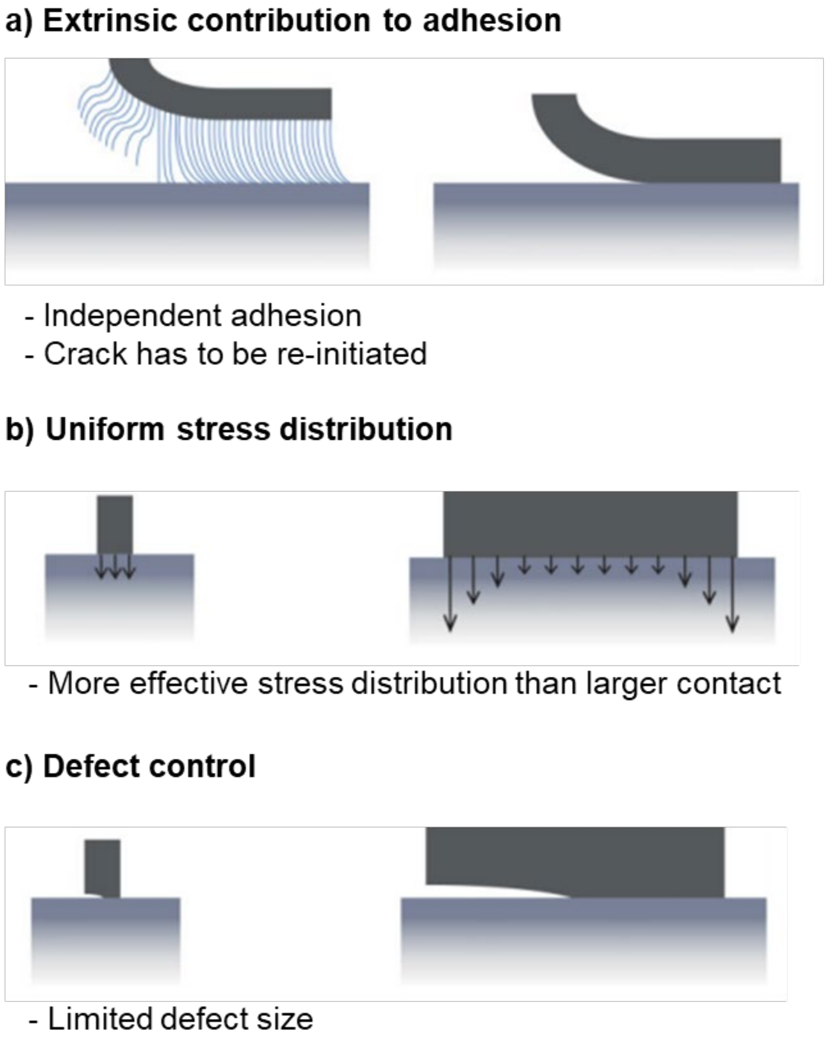

Figure 1-4. Schematic representation of adhesion mechanisms in fibrillar surfaces (Kamperman*, et al.*, 2010)

1.3. Catechol & gallol chemistry

Mussels, as sessile marine organisms, have garnered considerable attention in adhesive science due to their remarkable ability to securely attach to a variety of surfaces under aquatic conditions. The byssal threads produced by mussel feet, which exhibit strong adhesion to rocky substrates in marine environments, are rich in the catechol precursor 3,4-dihydroxy-L-phenylalanine (DOPA). Catechol's structure, characterized by a benzene ring with two adjacent hydroxyl groups, is deceptively simple. Yet, it facilitates a broad spectrum of interactions enabling adhesion to virtually any surface (Figure 1-5). Notably, catechol maintains its adhesive capabilities even in water-rich environments, although the underlying mechanisms remain partially elucidated.

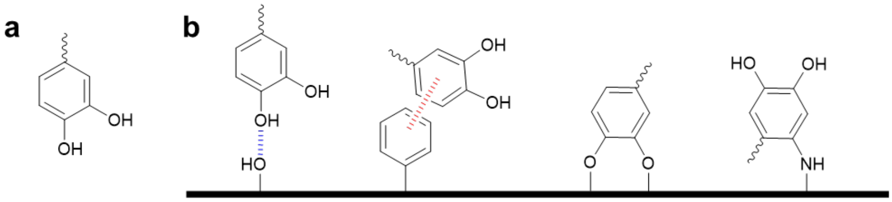

Figure 1-5. (a) Catechol structure, (b) Schematic representation of the four main catechol-surface interactions (Saiz-Poseu*, et al.*, 2019)

Conventional adhesives typically exhibit diminished bonding strength in aqueous settings, as they tend to interact with water molecules rather than establishing direct bonds with the substrate. In light of catechol's exceptional underwater adhesive properties, there has been a burgeoning interest in incorporating catechol functionalities into adhesive formulations. Research predominantly focuses on DOPA-derived materials for integrating catechol groups into organic polymers. However, challenges such as DOPA's relatively high cost and susceptibility to color change upon oxidation hinder its widespread commercial application.

Recent advancements have seen a shift towards utilizing gallic acid, a naturally abundant, cost-effective, and oxidation-resistant alternative to DOPA, offering enhanced transparency upon oxidation (Figure 1-6). Moreover, empirical evidence suggests that the tri-phenolic gallol groups, derived from gallic acid, may outperform the bi-phenolic catechol groups in adhesive strength, according to several studies. This transition towards gallic acid as a catechol alternative signifies a promising avenue for the development of efficient, durable, and economically viable underwater adhesives (Lee*, et al.*, 2021, Oh*, et al.*, 2015, Zhan*, et al.*, 2017)..

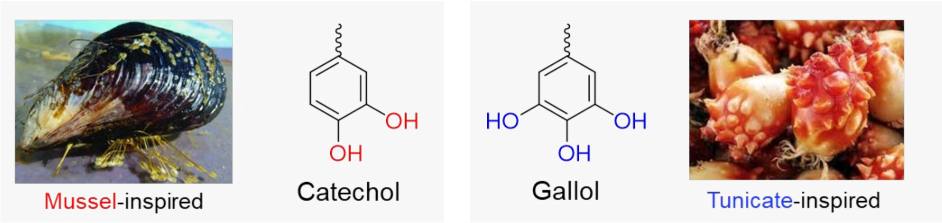

Figure 1-6. Schematic images of catechol (mussel-inspired) and gallol (tunicate-inspired) functional groups

1.4. Underwater adhesives

In numerous applications, including the medical sector, underwater equipment, and maritime industries, there is a pronounced demand for adhesives that maintain efficacy in submerged conditions. Achieving robust interfacial bonding in moist environments presents significant challenges, exceeding those encountered in dry conditions. Typically, a hydration layer forms on submerged surfaces, impeding the direct interaction between the adhesive and the substrate. Moreover, the ingress of water into the adhesive can lead to swelling or disintegration, further compromising adhesive integrity. In response to these challenges, research has pivoted towards bio-inspired catechol-based adhesive structures. However, the development of effective underwater adhesives necessitates a multifaceted approach that extends beyond merely incorporating catechol motifs.

Crucial to underwater adhesion is the ability to bypass the hydration layer enveloping the substrate and to establish direct contact (Figure 1-7). Strategies for achieving this can be categorized based on the scale of intervention. At the molecular level, rendering adhesive materials hydrophobic represents one approach, while another involves integrating water-absorbing fillers or polymers to actively displace the hydration layer from the substrate surface.

At a larger scale, engineering pathways for water egress to prevent its entrapment at the adhesive-substrate interface has proven effective (Fan and Gong, 2021, Rao*, et al.*, 2018, Zhang*, et al.*, 2021). This is achieved by crafting microstructures on the adhesive surface to facilitate water drainage, a principle observed in natural systems such as the inner surfaces of snails, tree frogs' toe pads, and clingfish suction discs (Ma*, et al.*, 2022). Moreover, the incorporation of microstructures on adhesive surfaces not only aids in dehydration but also enhances interfacial bonding strength. Emulating the suction mechanism of octopus suckers, for instance, allows for a reduction in pressure at the interface, ensuring a firm adhesion between the adhesive material and the substrate. This biomimetic approach underscores the potential of leveraging natural designs to overcome the inherent challenges of underwater adhesion, paving the way for innovative adhesive solutions across a spectrum of water-involved applications.

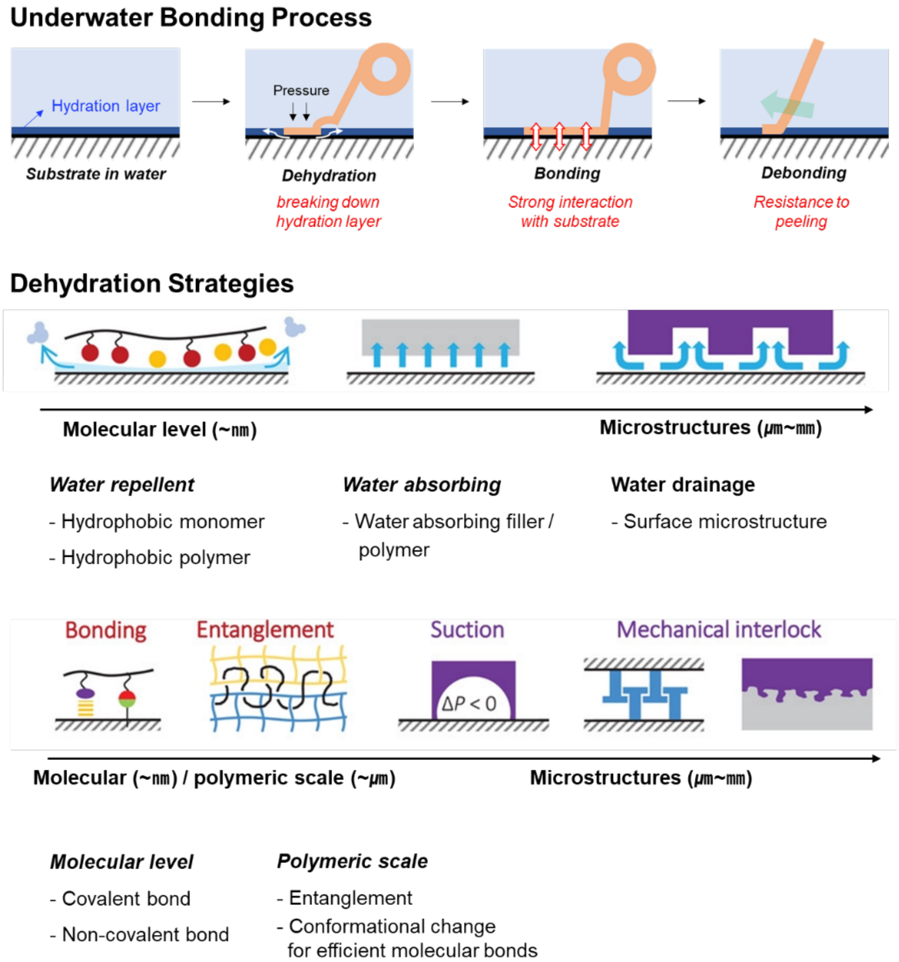

Figure 1-7. Dehydration strategies for underwater adhesives (Fan and Gong, 2021, Rao*, et al.*, 2018, Zhang*, et al.*, 2021)

2. Literature review

Research into catechol or gallol-functionalized adhesives encompasses a broad spectrum, which can be systematically categorized into three distinct areas of focus. The initial category pertains to the methodologies employed for the incorporation of catechol functional groups into adhesive matrices. This involves exploring various chemical strategies and synthesis routes to integrate catechol functionalities efficiently and stably within adhesive formulations.

The second classification relates to the specific types of materials that are endowed with catechol functional groups. This category examines the diversity of base materials, ranging from polymers to biologically derived substances, that can be functionalized with catechol to enhance their adhesive properties. The investigation into the material type is crucial, as the inherent characteristics of the base material significantly influence the overall performance and application potential of the catechol-functionalized adhesive.

Lastly, the third area of research focus delves into the engineering of microstructures on the surface of catechol-functionalized adhesives. This innovative approach draws inspiration from natural adhesion mechanisms, such as those observed in marine organisms like mussels. The implementation of microstructures aims to replicate the superior adhesive capabilities found in nature, enhancing the performance of synthetic adhesives through increased surface area, mechanical interlocking, and water displacement capabilities.

2.1. In situ polymerization / post modification

The integration of catechol functional groups into adhesives can be achieved through in situ polymerization and post-modification techniques. In situ polymerization involves the preliminary synthesis of a catechol functional group within a structure possessing a double bond, such as an acrylate group, followed by the radical polymerization of this catechol monomer with other monomers to form the adhesive. However, a notable drawback of this approach is catechol's inherent radical scavenging property, which can potentially decrease the monomer conversion rate or lower the polymerized polymer's molecular weight due to its inhibitory effect on radical propagation. To circumvent this issue, the hydroxyl groups of catechol must be protected prior to polymerization (Lee*, et al.*, 2015). Despite the additional step in the manufacturing process, incorporating catechol functional groups into adhesive materials significantly enhances adhesion. For instance, Brylee et al. synthesized a PSA by copolymerizing dopamine methacrylamide (DMA) with butyl acrylate and acrylic acid (Tiu*, et al.*, 2019). The introduction of merely 5% DMA into a conventional PSA copolymer resulted in up to a sixfold increase in the adhesive force required to detach the PSA from silica and polystyrene surfaces, markedly enhancing the 180° peel adhesion.

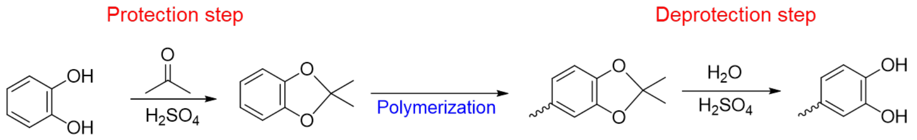

Figure 1-8. Typical catechol protection and deprotection in in situ polymerization method

Conversely, the post-modification method involves the prior polymerization of a scaffold polymer, with catechol functional groups introduced subsequently. This technique effectively negates the radical scavenging effects associated with catechol monomers and allows for a more precise comparison of different functional groups by eliminating variables such as molecular weight. Kyueui Lee and colleagues explored the impact of catechol functional groups on adhesive properties by first polymerizing an acrylic scaffold polymer containing an epoxy ring and then introducing a catechol-structured monomer (Lee, *et al.*, 2021). Their findings indicated that the catechol structure significantly improved peel strength and bulk cohesion compared to polymers containing only a benzene ring, underscoring the potential of catechol functionalization in enhancing adhesive performance.

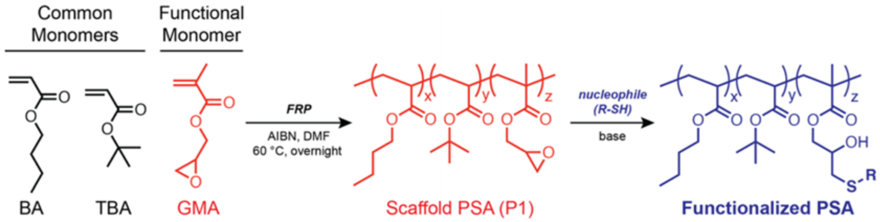

Figure 1-9. Postmodification strategy to synthesize catecholic PSAs (Lee, *et al.*, 2021)

2.2. Utilization of gallol group

The limitations associated with DOPA, notably its high cost and susceptibility to oxidation-induced discoloration, have spurred interest in gallol-based compounds as potential alternatives. Characterized by a benzene ring with three adjacent hydroxyl groups, gallol structures are prevalently found in plant-derived compounds and have shown promising results in underwater adhesive applications, often outperforming catechol-based adhesives in terms of bonding strength (Cheng*,* *et al.*, 2022, Lee*,* *et al.*, 2021, Oh*,* *et al.*, 2015, Zhan*,* *et al.*, 2017).

Bohan Cheng and colleagues explored the adhesive properties of materials featuring varying numbers of hydroxyl substitutions on benzene rings, specifically within the context of underwater adhesion (Cheng*,* *et al.*, 2022). Their findings revealed a positive correlation between the number of hydroxyl substitutions on phenolic polymers and adhesive strength. Moreover, a higher density of hydroxyl groups, resulting from increased substitutions within a confined area, was found to enhance water repellency, attributing to a more effective displacement of the hydration layer on substrates

In a related study, Kan Zhan and collaborators synthesized copolymers incorporating different phenolic groups: phenol, catechol, and gallol, employing a methoxymethyl protection/deprotection strategy (Zhan*,* *et al.*, 2017). The gallol-containing copolymers demonstrated superior adhesive performance compared to their catechol-functionalized counterparts across various conditions, including exposure to air, fresh water, seawater, and phosphate-buffered saline solutions. These studies collectively underscore the potential of gallol as a robust and efficient alternative to catechol in the development of high-performance underwater adhesives.

2.3. Surface Microstructure

The intricacies of adhesive surface microstructures can significantly enhance adhesion strength through various mechanisms. Firstly, they facilitate independent adhesion across distinct patterns, improving the overall bonding efficiency. Secondly, these structures allow for better accommodation of surface irregularities, enhancing adhesion on rough surfaces. Thirdly, they contribute to a more uniform distribution of stress across the adhesive interface, reducing the likelihood of failure under load (Kamperman*, et al.*, 2010). Furthermore, in the context of underwater adhesion, microstructured surfaces can mitigate defect formation due to water entrapment by providing channels for water to escape from between the adhesive and the substrate.

Drawing inspiration from the unique morphology of tree frog footpads, Bo Zhang and colleagues engineered a hydrogel surface adorned with hexagonal micropillars) (Zhang*, et al.*, 2021). This design significantly augmented the underwater adhesion strength of the hydrogels, making it sevenfold more effective than that of flat-surfaced hydrogels. This enhancement is attributed to the micropillars' ability to increase surface area for adhesion while facilitating water displacement, thereby improving wet adhesion.

In a study inspired by the clingfish's ability to adhere to surfaces under water, Ping Rao and collaborators investigated polyampholyte hydrogels featuring hexagonal micropatterns on their surface (Rao*, et al.*, 2018). These patterns aid in the removal of water from the adhesive interface by promoting drainage through the microstructured surface. Additionally, the hydrogels' balanced ionic charge and reversible ionic bonds contribute to superior energy dissipation within the bulk material. This energy dissipation, in conjunction with the surface patterning, synergistically enhances the adhesive force (Figure 1-10).

The presence of surface grooves and discontinuous contact patterns also plays a crucial role in hindering crack propagation during the separation of the adhesive from the substrate. The need to reinitiate cracks at each contact point, coupled with the increased compliance of these points, significantly improves the bulk deformation capabilities of the gel. This, in turn, contributes to a robust and durable adhesive bond, even in challenging underwater environments.

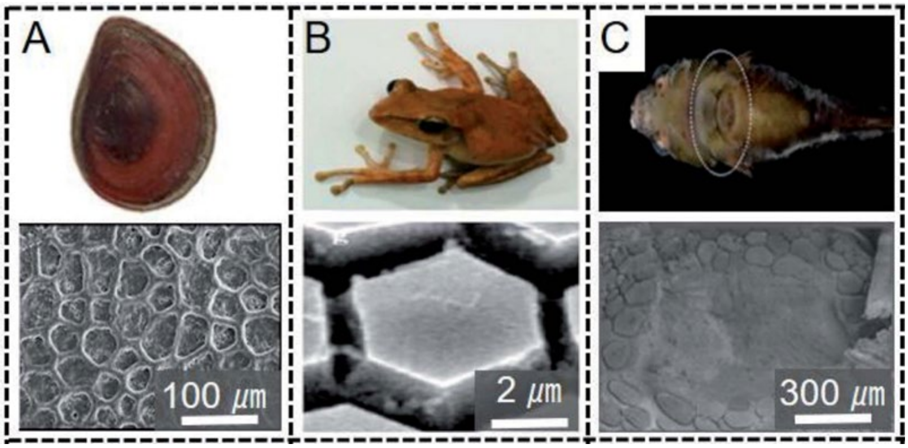

Figure 1-10. Strategy for water drainage and underwater adhesion by surface microstructure found in nature a) the microstructure of the inner surface of snails, b) tree frog's toe pad, c) clingfish adhesive disc (Ma*, et al.*, 2022)

3. Objectives

The objective of this study is to enhance the underwater adhesive properties of adhesives by substituting conventional catechol-based materials with gallol groups. These gallol groups offer economical benefits and greater transparency upon oxidation, facilitating their use in PSAs that can be activated with minimal pressure. This research integrates design strategies across both molecular and microstructural scales.

At the molecular level, a post-modification method is employed, wherein gallol groups are introduced following the initial polymerization of the polymer scaffold. This approach prevents the radical scavenging typically associated with gallol groups. The scaffold's design incorporates considerations for the glass transition temperature and modulus necessary for effective PSA performance, utilizing a process that balances simplicity with cost-efficiency for the introduction of gallol groups. The effectiveness of gallol-modified PSAs is assessed by comparing them with other polymers varying in the number of hydroxyl groups on their phenolic structures. The study further investigates how increasing gallol content influences underwater adhesion properties and addresses potential wetting challenges through strategic branching within the polymer structure. This involves monitoring changes in molecular weight, rheological behavior, and adhesion characteristics to optimize the balance between gallol content and the structural features of the polymer.

Moreover, the research explores the effects of microstructured surfaces on the gallol PSA to improve its drainage capabilities and evaluates how variations in the size of these surface patterns impact the adhesive properties. This comprehensive approach aims to develop a deeper understanding of how structural modifications at different scales influence the performance of PSAs in aquatic environments.

Chapter 2

Gallol Pressure-Sensitive Adhesives

1. Introduction

We focus on the gallol functionalization of traditional acrylic polymers using gallic acid as a cost-effective and oxidation-resistant modifier, aiming to enhance underwater adhesion properties. Gallic acid, preferred over DOPA for its economic and optical advantages, facilitates the incorporation of gallol functional groups into the polymer matrix. This functionalization introduces not only covalent crosslinks but also dynamic reversible bonds - such as hydrogen bonds, π-π interactions, and hydrophobic interactions - into the bulk material, thereby enhancing energy dissipation and delaying interfacial failure (Figure 2-1).

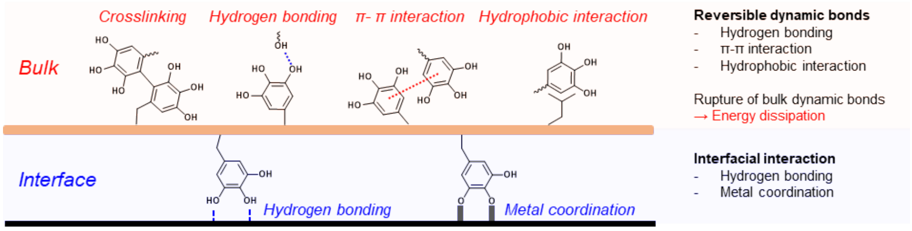

Figure 2-1. Chemical interaction of gallol functional group at bulk and interface

To use gallic acid as a modifier, a functional group capable of esterification with the carboxylic group of gallic acid must exist in the acrylic polymer. Among monomers for acrylic pressure-sensitive adhesives, hydroxyl and epoxy groups are general functional groups that can react with the carboxylic group. 4-hydroxybutyl acrylate (4-HBA) was selected for the hydroxyl group and glycidyl methacrylate (GMA) was selected for the epoxy group as a candidate functional group. And the efficiency of the two reactions was compared (Figure 2-2).

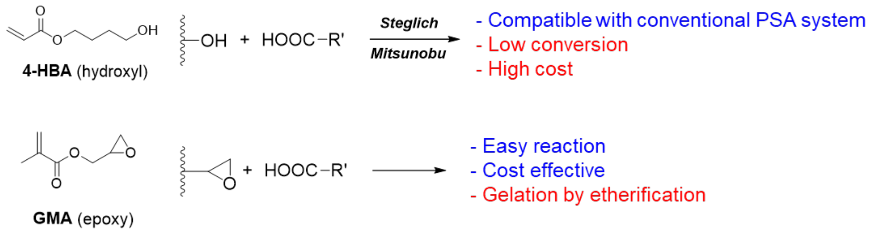

Figure 2-2. Advantages and disadvantages of reactions using hydroxyl groups and epoxy groups

Two methods were used for the reaction using the hydroxyl group: Steglich esterification and Mitsunobu reaction. First, Steglich esterification was challenging to purify because the urea by-product produced by the catalyst was insoluble in most organic solvents, and the hydroxy group conversion rate was as low as 1 %. The Mitsunobu reaction also had a low conversion rate, and both esterification reactions have the disadvantage that the amount of expensive catalyst input is too high.

In the case of the reaction using an epoxy group, the reaction was performed at 95 °C using a triphenylphosphine (TPP) catalyst and a tertiary amine catalyst. In the reaction using TPP, gelation of the reactants occurred, but in the case of using a tertiary amine catalyst, gelation did not occur. When an epoxy group and a carboxylic acid react, a secondary hydroxyl group is generated. When this secondary hydroxyl group reacts with an epoxy group again, crosslinking occurs by etherification (Figure 2-3). The tertiary amine catalyst increases the esterification selectivity of the reaction and prevents the gelation of the reactants.

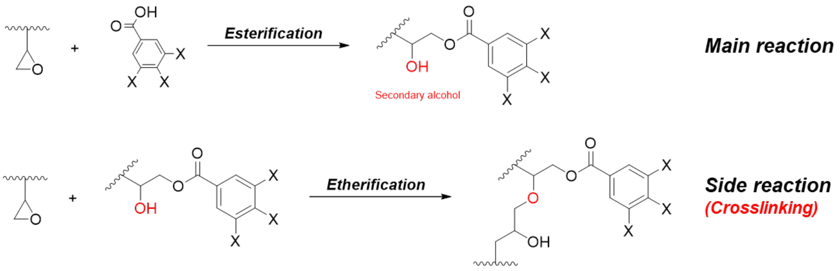

Figure 2-3. Reactional pathway of the epoxide-carboxylic acid reaction

This study involves the synthesis of a gallol PSA, with a focus on exploring its underwater adhesion attributes. And a more practical and economical approach was considered. Scaffold polymer featuring an epoxy group was fabricated and subsequently modified through post-esterification with gallic acid to circumvent radical scavenging by the gallol monomer in the polymerization step (Lee*, et al.*, 2021, Samanta*, et al.*, 2022). For comparison purposes, PSAs with a structure analogous to gallol PSA but varying in the number of hydroxyl groups on the aromatic ring were synthesized (Figure 2-4). Industrial scalability was considered during the fabrication of gallol PSA. Hence, the protection and deprotection steps to prevent the oxidation of gallol, which would increase the cost of manufacturing, were omitted from the synthesis process. Although gallol group oxidation generally compromises adhesive performance, gallol PSA exhibited markedly enhanced underwater adhesion in comparison to control group PSAs.

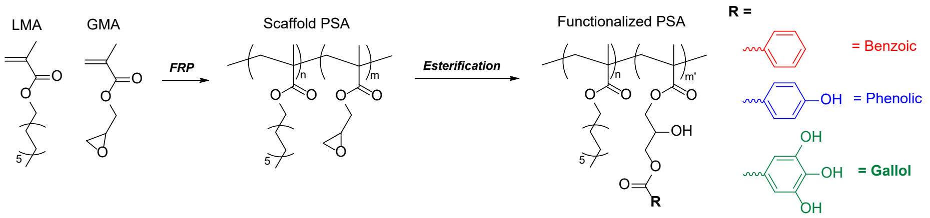

Figure 2-4. Schematic illustration of modified PSAs.

2. Experimental

2.1. Materials

Lauryl methacrylate (LMA, 96 %), glycidyl methacrylate (GMA, 97 %), azobisisobutyronitrile (AIBN, 12 % wt.% in acetone), gallic acid (97 %), benzoic acid (99.5 %), 4-hydroxybenzoic acid (99 %) were purchased from Sigma-Aldrich. 1-methylimidazole (1MI, 99 %), tetrahydrofuran (THF, 99 %), acetone (99.5 %) were purchased from Samchun Chemicals.

2.2. Synthesis of scaffold polymer

The scaffold polymer was synthesized by free radical polymerization in THF using LMA, GMA. 100 ml of THF, AIBN (1.35 g as a solution), LMA (98.30 g, 0.39 mol), GMA (1.7 g, 0.01 mol) were mixed in a 250 ml flask using Teflon stirring bar. And the flask was filled with nitrogen gas. The polymerization was initiated by immersing the flask in an oil bath at 80 °C, and the reaction was carried out for 8 h. The polymer was then precipitated in acetone to remove unreacted monomers and others. Approximately 150 ml of THF was used to re-dissolve the polymer, and the precipitation cycle was repeated three times. After the final precipitation, the polymer was dried under a high vacuum to remove solvents. Molecular weights and polydispersity of scaffold PSA were calculated by gel permeation chromatography. Polymethylmethacrylate (PMMA) calibration standards were used for calibration. The polymers were dissolved in tetrahydrofuran with a 1 mg/mL concentration. The flow rate was 1mL/min, and the refractive index detector was used for detection. Molecular weight analysis of modified PSAs was not possible due to very low intensity during

GPC analysis. This is probably due to the change in solubility following the introduction of the functional group or the interaction with GPC column. Although it was not possible to analyze the exact molecular weight, it is expected that the modified PSAs are expected to have a molecular weight similar to that of the scaffold because the post-esterification process will not significantly change the molecular weight.

2.3. Monomer conversion ratio

To determine the monomer conversion ratio, a chemical mixture before the reaction and right after the reaction was analyzed by ^{1}H NMR spectroscopy (Figure 2-5). The conversion ratio was calculated by the ratio of the vinyl peak and the epoxy group integral area before and after the polymerization).

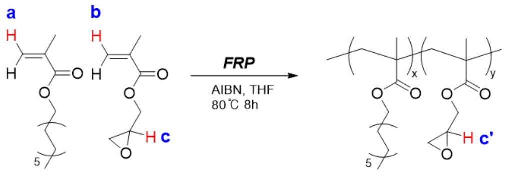

$$Conversion\ (\%) = \left\{1 - \left(\frac{H_{a+b}/H_{c'}}{H_{a+b}/H_c}\right)\right\} \times 100$$

Figure 2-5. Calculation of monomer conversion by ^{1}H NMR

2.4. Actual polymer composition

The actual molar ratio (%) between LMA, GMA in scaffold polymer was determined by ^{1}H NMR spectroscopy. Hx, Hy are standardized integral areas of LMA, GMA side chains, respectively. Alphabetic indications represent corresponding NMR peaks assigned in Figure 2-6.

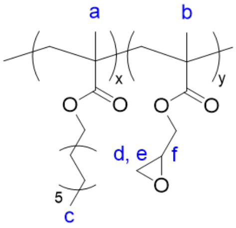

$$Hy(d),\ \ Hy(e),\ \ Hy(f) = integral\ area\ of\ the\ epoxide\ peak$$
$$3Hx(a) + 3Hx(c) + 3Hy(b) = integral\ area\ of\ the\ methyl\ peak$$

Figure 2-6. Calculation of actual monomer composition by ^{1}H NMR

2.5. Esterification of scaffold polymer

A functionalized PSA was synthesized by esterifying a scaffold polymer and three aromatic acids (Figure 2-7). (benzoic acid, 4-hydroxybenzoic acid, gallic acid) Then, epoxide conversions were calculated bu ^{1}H NMR spectroscopy (Figure 2-8).

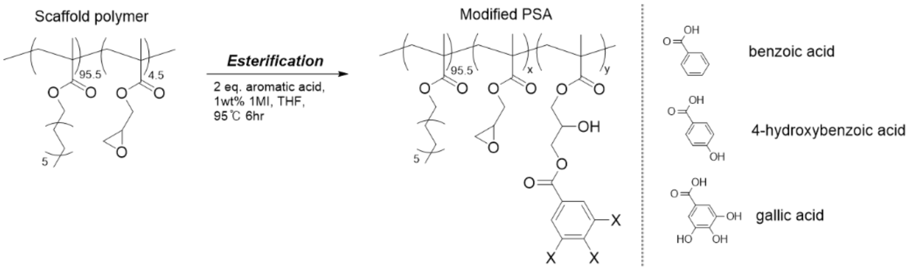

Figure 2-7. Esterification of scaffold polymer with aromatic acids

Benzoic PSA: the scaffold polymer (10 g, 4.5 mol% of the epoxide group in polymer backbone, 1 eq) and benzoic acid (0.292 g, 2.0 eq), and 1MI (0.1 wt.% of scaffold polymer) were dissolved in THF then poured into the refluxing flask. The mixture was stirred for 30min at room temperature. Then esterification was carried out in 95 °C oil bath with constant stirring. After the reaction, the mixture was cooled to room temperature. The mixture was then precipitated in acetone to remove unreacted benzoic acid. Approximately 10 ml of THF was used to redissolve the polymer, and the precipitation cycle was repeated three times. After the final precipitation, the polymer was dried under a high vacuum to remove solvents.

Phenoic PSA: The experimental procedures are indentical to the above description except for the modification reagent, 4-hydroxybenzoic acid (0.33 g, 2.0 eq).

Gallol PSA: The experimental procedures are indentical to the above description except for the modification reagent, gallic acid (0.407 g, 2.0 eq).

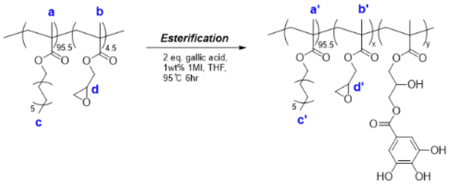

$$\text{Epoxide conversion } (\%) = \left\{1 - \left(\frac{H_{d'}/H_{a'+b'+c'}}{H_d/H_{a+b+c}}\right)\right\} \times 100$$

Figure 2-8. Calculation of epoxide conversion by ^{1}H NMR

2.6. Adhesion properties

The adhesive properties were evaluated in a dry environment, like a general PSA evaluation, and in a wet environment by being immersed in water (Figure 2-9).

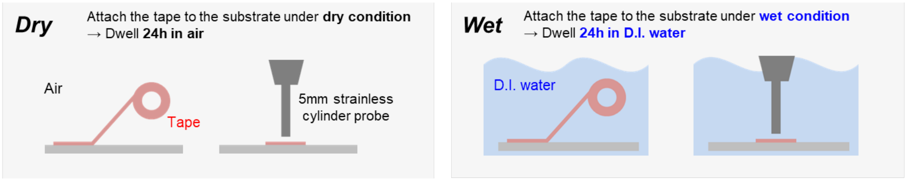

Figure 2-9. Test condition of evaluating adhesion properties

The 180° peel strength were measured using a Texture Analyzer (TA.XT plus, Stable Micro Systems) at 25 °C. Samples for underwater adhesion test were prepared by being immersed in deionized water.
180° peel strength: test speed for the peel test was 5 mm/sec, and the test angle will be 180°. All measurements were repeated more than five times. And peel strength was obtained as the average force from 20 % to 80 % of the operating range.

2.7. Rheological properties

Rheological properties were measured by using rheometer (ARES G2, TA Instruments) with 8 mm parallel plates. The evaluation conditions are as follows.

Modulus: 1.0 % strain, 1 Hz frequency, 5 °C/min heating rate with ranging −50 °C to 100 °C, Frequency sweep: 25 °C, 1.0 % strain, 0.01 to 1 Hz, Stress relaxation: 25 % shear strain, 1 min, 25 °C, Creep & Recovery: 1 kPa stress for 3 min, recovery for 9 min after stress removed, 25 °C.

3. Results & discussion

3.1. Design, synthesis, characterization

We considered the following aspects during the design of the gallol PSA: (1) The scaffold polymer has a hydrophobic structure for dehydration and water repulsion; (2) The scaffold polymer should be first polymerized and then modified with gallic acid to avoid radical scavenging by the gallol monomer (Lee*, et al.*, 2021). (3) The scaffold and modified polymers must have sufficiently low glass transition temperatures and moduli (Creton, 2003) (T_g < 25 °C and G′ < 0.1 MPa at 25 °C) to exhibit sufficient chain mobility that enables rapid wetting of the substrate with little pressure. The G′ value of 0.1 MPa is determined by the Dahlquist criterion. The Dahlquist criterion is a critical modulus mentioned by Carl Dahlquist, who worked at 3 M in 1969. Dahlquist asserted that, for a standard surface characterized by a bump radius of 5 μm and a bump height of 1 μm, PSA should exhibit a G′ value below 0.1 MPa (1 Hz, 25 °C) to facilitate flow and establish effective contact. This criterion is not absolute for all situations but is a valuable rule of thumb in designing a new PSA. The glass transition temperature (T_g) was considered to ensure minimal fluidity at room temperature, considering the intended usage temperature (Lee, 2013).

Based on these design considerations, lauryl methacrylate (LMA) was selected as the monomer for designing a hydrophobic scaffold polymer with a low T_g and G′. LMA is hydrophobic owing to the 12 carbons in the side group, and its homopolymer has a sufficiently low T_g (-65 °C) (Rogers*, et al.*, 1957). Additionally, glycidyl methacrylate (GMA) with an epoxy group was selected as a co-monomer for the esterification reaction with gallic acid. Although LMA is rarely used as a main monomer in PSA, another reason for choosing it is that general acrylic monomers of PSA, such as butyl acrylate and 2-ethylhexyl acrylate, have significant differences in reactivity from that of GMA; therefore, GMA is consumed faster than acrylic monomers in the initial stage of polymerization (Dhal*, et al.*, 1982). But, the combination of LMA and GMA results in a polymer with a random composition compared to the combination of general acrylic monomers due to little difference in the reactivity ratio.

Scaffold PSAs were synthesized through the free-radical polymerization of LMA and GMA using azobisisobutyronitrile (AIBN) as the initiator in tetrahydrofuran. The feed ratio of LMA and GMA was adjusted from 99:1 to 90:10, followed by an assessment of the adhesive properties of the resultant polymerized Scaffold PSAs. By considering their initial stickiness and peel strength, the most suitable balance was found to be the 97:3 feed ratio of LMA to GMA, which maximized GMA content without significantly compromising adhesive properties (Figure 2-10a). GPC analysis of Scaffold PSA (LMA 97: GMA 3) revealed an Mn of 213 kDa (Figure 2-10b). The actual molar ratio of LMA to GMA determined by ^{1}H NMR spectroscopy was 95.5:4.5 with a conversion exceeding 96 % (Figure 2-11, Figure 2-12).

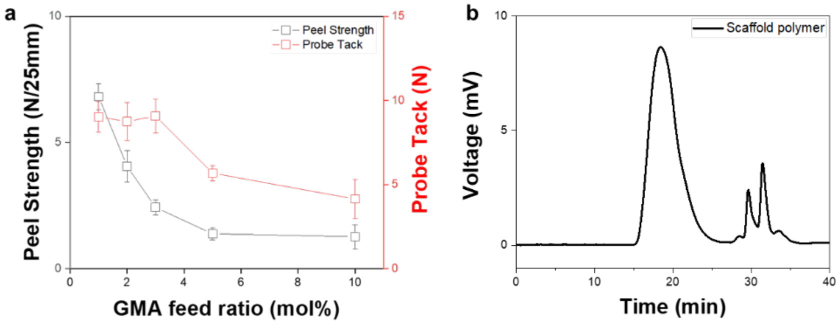

Figure 2-10. a) Adhesion properties according to the GMA feed ratio of scaffold PSA, b) GPC curve of scaffold PSA

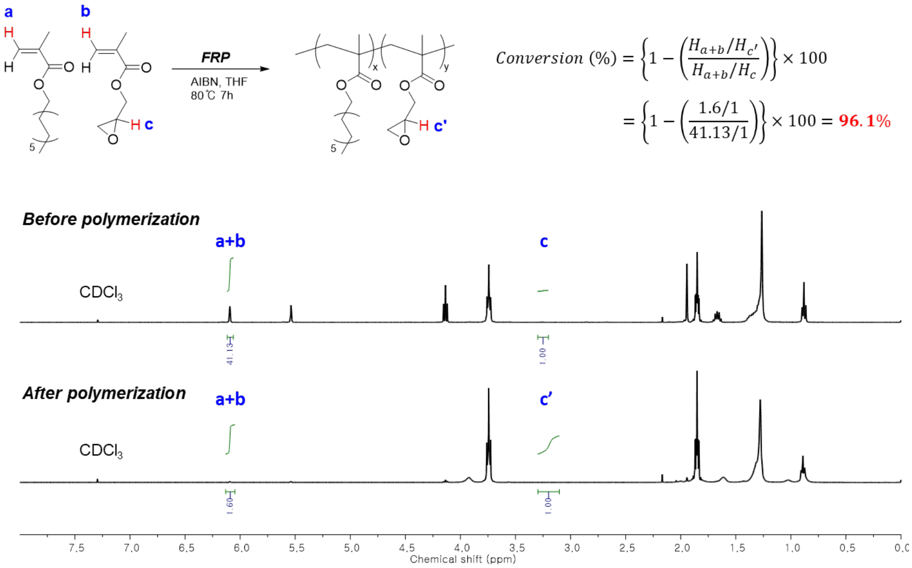

$$Conversion\ (\%) = \left\{1 - \left(\frac{H_{a+b}/H_{c'}}{H_{a+b}/H_{c}}\right)\right\} \times 100$$

$$= \left\{1 - \left(\frac{1.6/1}{41.13/1}\right)\right\} \times 100 = 96.1\%$$

Figure 2-11. Monomer conversion ratio of scaffold PSA

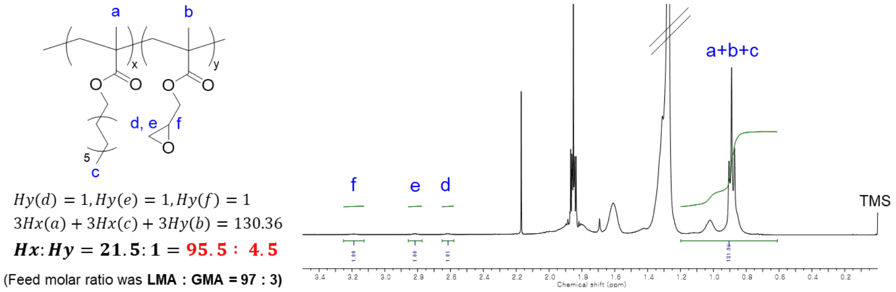

$Hy(d) = 1, Hy(e) = 1, Hy(f) = 1$

$3Hx(a) + 3Hx(c) + 3Hy(b) = 130.36$

$\boldsymbol{Hx : Hy = 21.5 : 1 = 95.5 : 4.5}$

(Feed molar ratio was **LMA : GMA = 97 : 3)**

Figure 2-12. Actual polymer composition of scaffold PSA

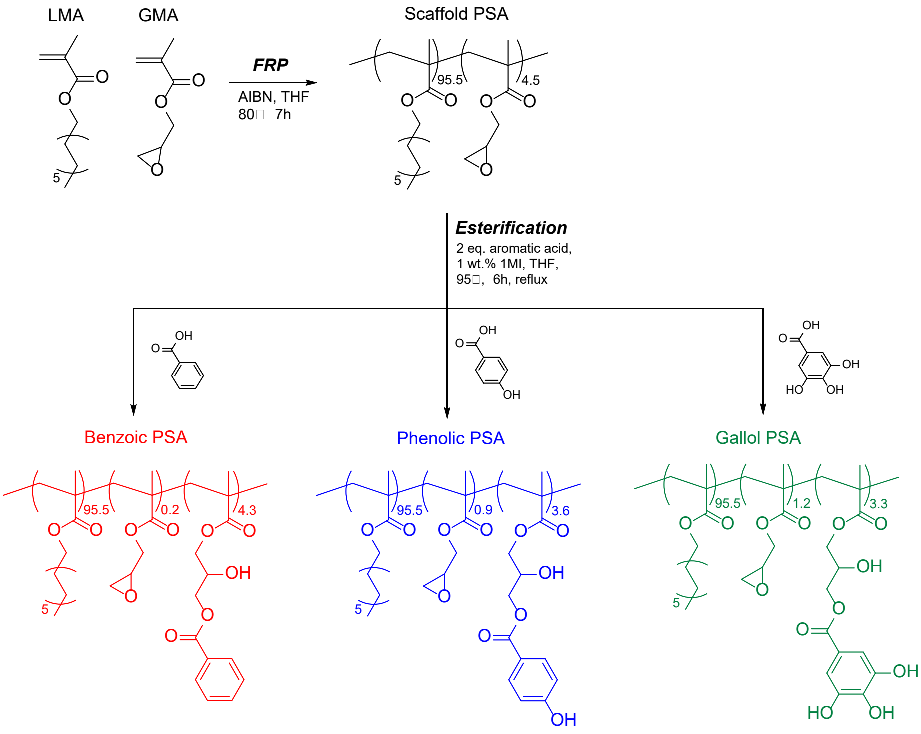

Figure 2-13. Synthesis of scaffold, benzoic, phenolic, gallol PSA

Scaffold PSA was then reacted with gallic acid to afford gallol PSA. Employing analogous procedures, benzoic PSA and phenolic PSA were synthesized by utilizing benzoic acid and 4-hydroxybenzoic acid, respectively (Figure 2-13). A minor amount of 1-methylimidazole was employed as a catalyst to mitigate unintended crosslinking between secondary hydroxyl and epoxy groups (Tran, *et al.*, 2020). After the post-esterification step, the consumption of epoxy groups in the modified polymers was measured at 4.3 %, 3.6 %, and 3.3 % for benzoic, phenolic, and gallol PSA, respectively (Figure 2-14). And gelation was not observed during the post-esterification process. Also, the epoxide conversion was similar across repetitions. The reaction conditions of all three PSAs were the same, but the epoxide conversion decreased as the number of hydroxyl groups on the aromatic ring increased owing to the difficulty in proton dissociation. The reaction conditions of all three PSAs were the same, but the epoxide conversion decreased as the number of hydroxyl groups on the aromatic ring increased owing to the difficulty in proton dissociation. Based solely on pK_a values, the pK_a value of benzoic acid is 4.20, 4-hydroxybenzoic acid is 4.55, and gallic acid is 4.21 (Zevatskii*, et al.*, 2009). This suggests that the reactivity of gallol PSA should be higher than that of phenolic PSA. However, oxidized gallic acid has a pK_a of 5.33, indicating a greater difficulty in proton dissociation (Chikere*, et al.*, 2019, Kumar*, et al.*, 2023). Consequently, it is expected that the epoxide consumption of gallol PSA would be the lowest. This post-modification method is advantageous because the molecular weights of the prepared PSAs are comparable. As the adhesive properties depend on the molecular weight, an accurate comparison of the effects of the different functional groups in the three PSAs can be achieved.

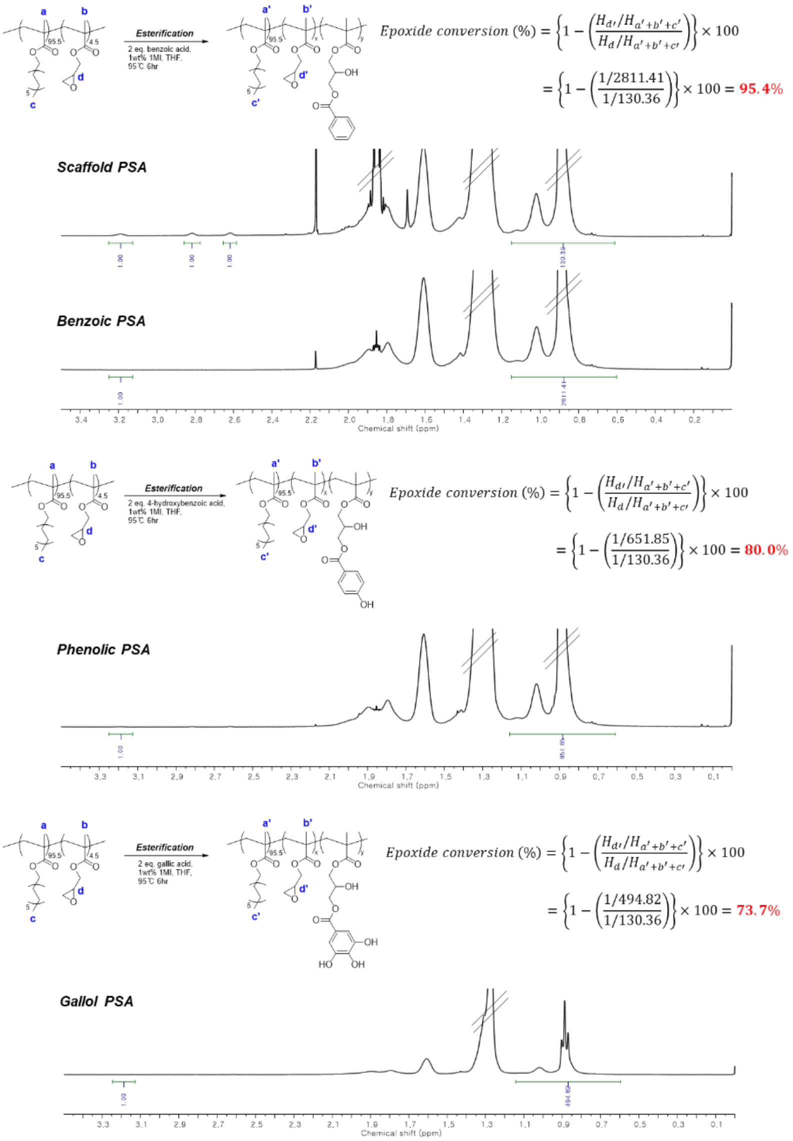

$$Epoxide\ conversion\ (\%) = \left\{1 - \left(\frac{H_{d'}/H_{a'+b'+c'}}{H_d/H_{a'+b'+c'}}\right)\right\} \times 100$$

$$= \left\{1 - \left(\frac{1/2811.41}{1/130.36}\right)\right\} \times 100 = 95.4\%$$

$$Epoxide\ conversion\ (\%) = \left\{1 - \left(\frac{H_{d'}/H_{a'+b'+c'}}{H_d/H_{a'+b'+c'}}\right)\right\} \times 100$$

$$= \left\{1 - \left(\frac{1/651.85}{1/130.36}\right)\right\} \times 100 = 80.0\%$$

$$Epoxide\ conversion\ (\%) = \left\{1 - \left(\frac{H_{d'}/H_{a'+b'+c'}}{H_d/H_{a'+b'+c'}}\right)\right\} \times 100$$

$$= \left\{1 - \left(\frac{1/494.82}{1/130.36}\right)\right\} \times 100 = 73.7\%$$

Figure 2-14. Epoxide conversion of benzoic, phenolic, gallol PSA

3.2. Rheological properties

The PSAs should have a low T_g and G′ to establish contact with the substrate surface under weak pressure. The synthesized PSAs demonstrated a G' value of 0.1 MPa or below at a frequency of 1 Hz under room temperature conditions, coupled with a T_g below 0 °C. These attributes align with the essential criteria for establishing favorable contact, facilitated by the PSA's ability to conform to the substrates through its flow characteristics (Table 2, Figure 2-15). Furthermore, the presence of additional functional groups capable of various interactions is expected to further enhance adhesion strength through increased interactions with substrates and improved cohesion in the PSA.

Table 2-1. Characterization of scaffold and functionalized PSAs

Polymer	G′ (MPa)		Tg (˚C)	Relaxation time (s)	Creep (%)	Recovery (%)
	-20 °C	25 °C				
Scaffold	0.4	0.01	-21.8	0.03	1,747	3
Benzoic	8.7	0.07	-8.6	0.05	44	60
Phenolic	4.8	0.09	-11.3	0.29	5.3	92
Gallol	2.6	0.10	-10.3	6.08	0.8	99

Incorporation of diverse functional groups led to an elevation in both the T_g and G' values; nevertheless, these values remained within the acceptable range for effective PSAs. Intriguingly, the G' values for the modified PSAs exhibited opposite trends between sub-zero temperatures and those above room temperature. In the low-temperature region, G′ increased as the number of hydroxyl groups on the benzene ring decreased. The G′ values for benzoic, phenolic, and gallol PSAs were 8.7, 4.8, and 2.6 MPa, respectively at -20 °C.

In contrast, at room temperature and higher, G′ values increased with an increasing number of hydroxyl groups. The relatively large side groups of gallol PSA increase the free volume of the polymer, thereby reducing its low-temperature G′ value (Maeda, *et al.*, 2023). This unique characteristic of exhibiting a low modulus at low temperatures and maintaining the modulus as the temperature increases indicates that gallol PSA has the potential to be applied over a broad range of temperatures without loss of adhesion strength. The tan δ data also indicate that the loss of elasticity begins at higher temperatures as the number of hydroxyl groups increases (Figure 2-16).

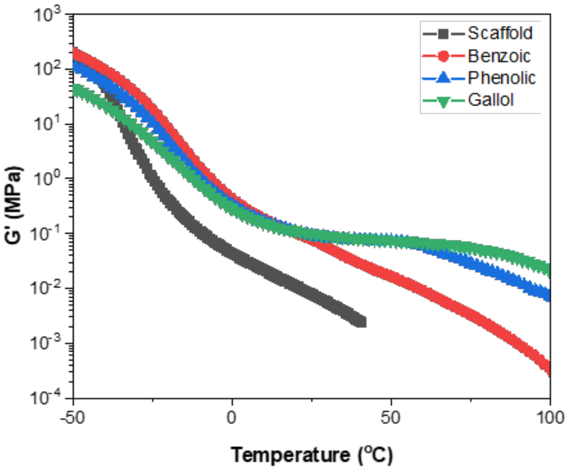

Figure 2-15. Storage modulus (G′) of scaffold and modified PSAs

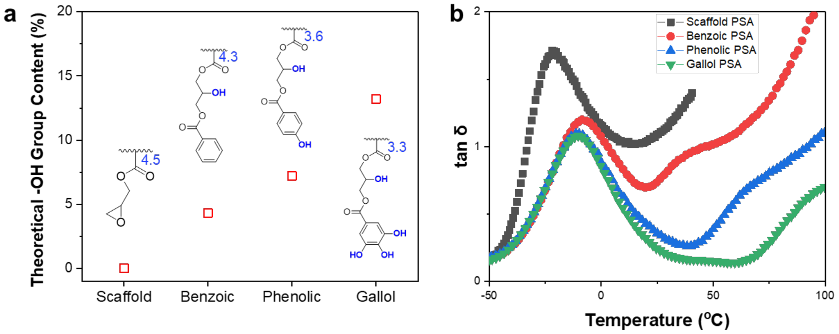

Figure 2-16. (a) theoretical -OH group content of PSAs, (b) tan δ curve of PSAs

The viscoelastic window stands out as the preeminent instrument for assessing the suitability of fabricated PSAs regarding their viscoelastic attributes. The measured G′ and G″ values within the frequency range of 0.01 Hz to 100 Hz serve as predictive indicators for the conceivable applications of the PSA (Figure 2-17a). With the sole exception of the Scaffold PSA, wherein no functional groups are introduced and consequently falls outside the low modulus region, the modified PSAs exhibit suitable G' and G" values, rendering them suitable for general adhesive applications as well as those necessitating high shear forces (Figure 2-17b).

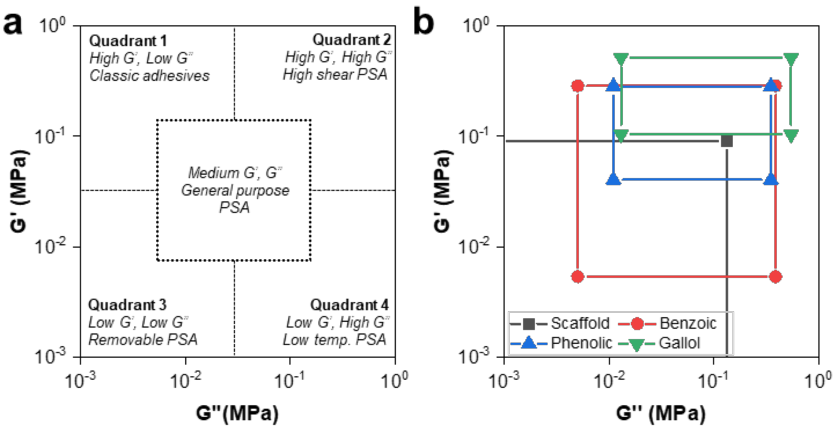

Figure 2-17. Rheological properties of scaffold and modified PSAs: (a) viscoelastic window (general PSAs)(Chang, 1997), (b) viscoelastic window

The stress relaxation of the PSAs was characterized at a strain of 25 % (Figure 2-18). The relaxation time was defined as the time required to relax to 1/e of the initial modulus. All the PSA samples reached this value within a matter of seconds. As the modified PSAs were all derived from scaffolds PSA with identical composition, molecular weight, and molecular weight distribution, the observed dissimilarity in relaxation characteristics can be attributed to the incorporated functional groups. Given the relatively limited introduction of functional groups in gallol PSA, it becomes evident that the gallol moiety exhibits more robust intermolecular or intramolecular interactions in comparison to the benzyl or phenol groups. This was corroborated by the creep recovery results (Figure 2-19). Creep and recovery tests were performed to evaluate the degree of recovery of the PSAs upon removing the constant stress (1 kPa for 180 s). While scaffold PSA and benzoic PSA exhibited constrained recuperation capacity following creep deformation, phenolic PSA and gallol PSA demonstrated marked recovery capabilities. This observation underscores the substantial impact of the presence or absence of hydroxyl groups on the recovery process. Notably, gallol PSA's nearly flawless recovery from deformation highlights its promising applications in contexts involving deformations, such as human joint skin and flexible electronic devices (Lee*, et al.*, 2019).

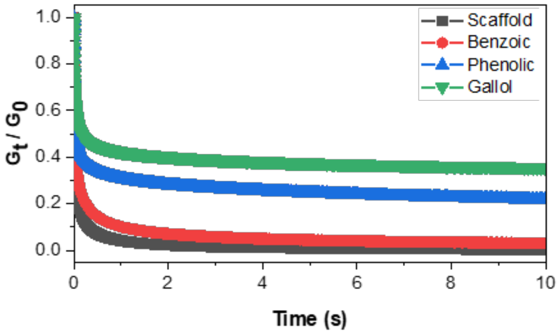

Figure 2-18. Stress relaxation of scaffold and modified PSAs

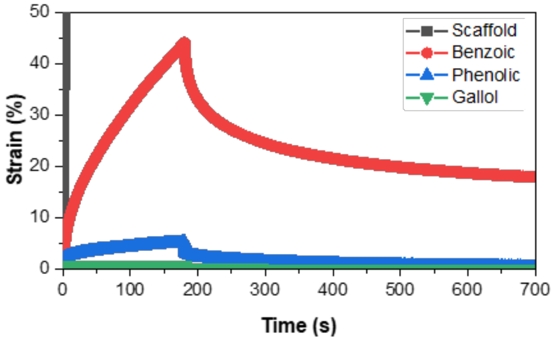

Figure 2-19. Creep and recovery of scaffold and modified PSAs

3.3. Adhesion properties

The adhesion properties of the PSAs were investigated using a 180° peel test. The PSA tapes were attached to stainless steel in air or water and then passed twice through a 2 kg rubber roller. The peel strength was measured after allowing the PSA samples to stand under ambient (dry) or underwater (wet) conditions for 24 h. The modified PSAs showed higher peel strength under dry conditions, suggesting that the modifications to the aromatic ring improved the adhesion (Figure 2-20).

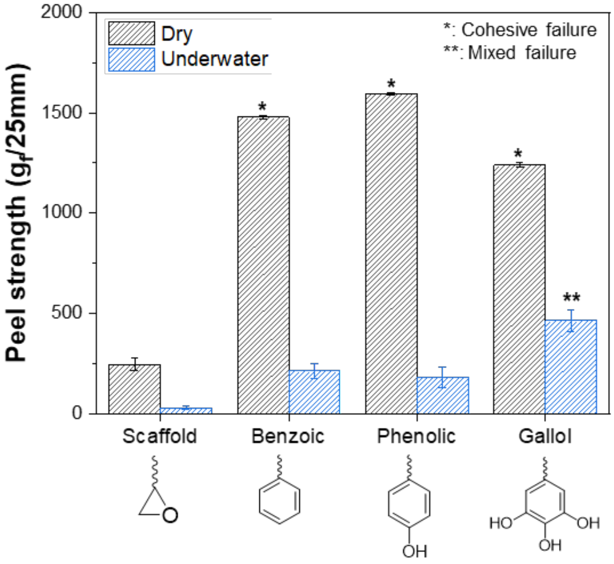

Figure 2-20. 180° peel strength results of PSAs on stainless steel substrates

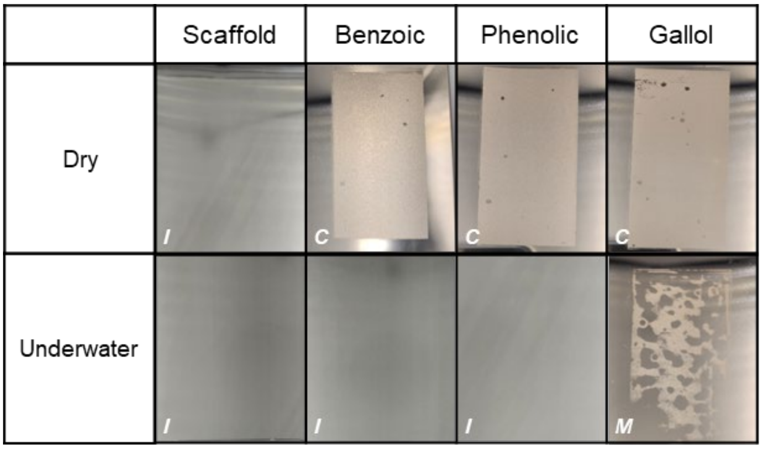

Figure 2-21. Images of the substrate surfaces after the peel test with PSAs

The modified PSAs (benzoic PSA: 1,478 g_f/25 mm, phenolic PSA: 1,595 g_f/25 mm, gallol PSA: 1,239 g_f/25 mm) showed over a five-fold increase of peel strength from that of scaffold PSA (247 g_f/25 mm). All modified PSAs failed at cohesion (Figure 2-21). Notably, gallol PSA showed the highest adhesion under underwater conditions. All PSAs except for gallol PSA exhibited a rapid drop in adhesion strength of more than 85 % [scaffold PSA: 31 g_f/25 mm (87 % ↓), benzoic PSA: 214 g_f/25 mm (86 % ↓), phenolic PSA: 184 g_f/25 mm (88 % ↓)] under underwater conditions compared to that in dry conditions. The failure mode changed from cohesive to interfacial, indicating that water weakened the interactions at the interface. Although the peel strength of gallol PSA in water decreased by 62 % (465 g_f/25 mm) compared to that under dry conditions, the failure mode exhibited a mixed characteristic, not exclusively interfacial. This was attributed to the fact that the bonding force at the interface surpassed the cohesive force, leading to the presence of PSA residues on the substrate's surface. These fracture mode changes in the PSAs indicate that, unlike the benzoic or phenolic moieties, the gallol moiety exhibited better interactions with the substrate surface under underwater conditions.

In general, adhesives that are more hydrophobic are preferred for successful dehydration (Chen, *et al.*, 2023, Cheng, *et al.*, 2022, Qin, *et al.*, 2023, Yao, *et al.*, 2023). In underwater adhesion, a critical factor is eliminating the hydration layer on the adherend's surface. The predominant approach for achieving dehydration involves the utilization of hydrophobic materials. Numerous researchers have employed strategies incorporating hydrophobic monomers, polymers, or solvents (Liu, *et al.*, 2020, Xu, *et al.*, 2017). The hydrophobic characteristics of the adhesive deter dehydration and prevent water infiltration into the bulk, thereby safeguarding the adhesive performance from deterioration (Cheng, *et al.*, 2022). From this perspective, gallol PSAs are at a disadvantage under dehydration. The contact angle values revealed by measurement show that gallol PSA is more hydrophilic than other PSAs (scaffold: 107.5°,benzoic: 103.2°, phenolic: 99.4°, gallol: 98.7°). Also, It has the highest theoretical hydroxyl group content (scaffold: OH 0%, benzoic: OH 4.3 %, phenolic: OH 7.2 %, gallol: OH 13.2 %) (Figure 2-22).

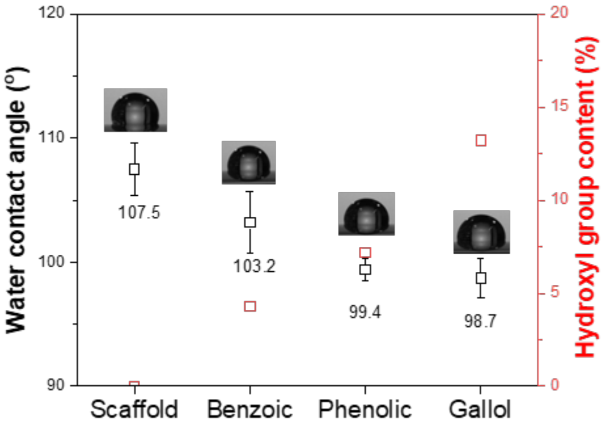

Figure 2-22. Water contact angle and theoretical hydroxyl group content of

PSAs

However, despite these dehydration-related drawbacks, gallol PSA exhibits the most robust adhesion in water. This result suggests that the gallol group possesses a distinctive structural property capable of overcoming the hindering effects of water molecules attributed to its hydrophilicity, promoting strong interactions with adherends.

4. Conclusion

This chapter aims to enhance the functionality of conventional acrylic polymers through gallol functionalization, utilizing gallic acid as a more economical and transparent alternative to DOPA for modification. Gallol functionalization enriches the polymer matrix with reversible dynamic interactions, including hydrogen bonds, π-π interactions, and hydrophobic interactions, thereby enhancing energy dissipation and interfacial durability. And PSAs with a structure analogous to gallol PSA but varying in the number of hydroxyl groups on the aromatic ring were synthesized for comparison purposes.

The adhesion and rheological properties of the modified polymers are rigorously assessed, indicating that gallol functionalization significantly improves underwater adhesion despite the polymer's hydrophilic nature, challenging the conventional preference for hydrophobic adhesives in underwater applications. The comprehensive study encompasses the synthesis, characterization, and performance evaluation of gallol-functionalized PSAs, presenting a nuanced understanding of the molecular interactions and structural dynamics at play, and highlighting the potential of gallol functionalization in advancing adhesive technologies, particularly for applications requiring robust underwater adhesion.

Furthermore, the synthesis of gallol PSA proved straightforward, eliminating the need for a gallol protection step. This manufacturing approach relies on simple processes including free-radical polymerization, esterification, and continuous liquid coating, all well-aligned with existing adhesive industry infrastructure and requiring no additional facilities. This pragmatic approach provides new insights into the catechol chemistry of PSAs for underwater adhesion, which has been challenging to commercialize over the past decade.

Chapter 3

Branched Gallol Pressure-Sensitive Adhesives

1. Introduction

Incorporating gallol moieties into acrylic-based adhesives has been identified as an efficacious strategy for augmenting their adhesive capabilities. However, this enhancement is subject to diminishing returns beyond a certain threshold of gallol integration. An escalation in the proportion of gallol groups within the adhesive matrix amplifies the interaction with the substrate and augments energy dissipation through an increased prevalence of reversible dynamic interactions. Nevertheless, this advantage is counterbalanced by the concomitant increase in the hardness of the PSAs, attributed to the elevated content of functional monomers required for gallol incorporation. Excessive hardening of the PSA impedes its ability to adequately wet the substrate, a critical prerequisite for effective adhesion, thereby paradoxically undermining adhesive performance with heightened gallol content.

Empirical evidence from the preceding analysis corroborates this phenomenon, illustrating a precipitous decline in both peel strength and probe tack when the GMA content in the scaffold polymer exceeds 3 mol%. This observation is consistent with literature on adhesives leveraging catechol and gallol functionalities, where an optimal threshold for functional group concentration is necessary to sustain or enhance adhesive performance (Lee*, et al.*, 2021, Tiu*, et al.*, 2019, Tiu*, et al.*, 2020). Given the imperative for PSAs to maintain a sufficiently low modulus to ensure effective substrate contact under minimal applied pressure, the task of balancing gallol concentration and mechanical softness emerges as a pivotal challenge, particularly in the context of underwater adhesion applications. To mitigate the increase in modulus associated with elevated gallol group content in PSAs, it becomes imperative to engineer the non-functional segments of the PSA to exhibit enhanced softness. This approach aims to counterbalance the hardening effect induced by higher concentrations of gallol groups, thereby preserving the adhesive's ability to effectively wet substrates.

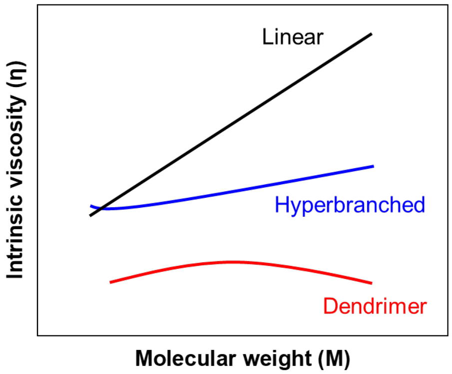

Figure 3-1. Relationship between molecular weight and intrinsic viscosity (Zheng, *et al.*, 2015)

Highly branched polymers are distinguished by their distinct properties when compared to their linear counterparts of analogous molecular weight (Zheng, *et al.*, 2015). Primarily, these polymers exhibit reduced solution viscosity, a consequence of minimized entanglement attributable to their three-dimensional conformation. Specifically, dendrimers, characterized by their regular spherical architecture, manifest a unique correlation between form and function. Similarly, hyperbranched polymers, despite an increase in intrinsic viscosity proportional to their molecular weight, experience a less pronounced viscosity escalation than linear polymers (Figure 3-1). This phenomenon is due to the reduced likelihood of chain entanglement within their densely branched structure. Consequently, the introduction of branching into linear polymers serves as an effective strategy to diminish the polymer's modulus, leveraging the inherent structural advantages of branched architectures to achieve desired mechanical softness.

The fabrication of branched vinyl polymers presents considerable challenges, primarily due to the propensity for gelation associated with multivinyl monomers. In an innovative approach to circumvent this issue, Fréchet and associates, in 1996, introduced the concept of Self-Condensing Vinyl Polymerization (SCVP) (Fréchet*, et al.*, 1995). Despite its ingenuity, the SCVP technique necessitates the utilization of specialized monomers, known as inimers, which complicates its widespread adoption. Similarly, Matyjaszewski and his team advanced the field by developing a technique for synthesizing branched polymers via Atom Transfer Radical Polymerization (ATRP) (Matyjaszewski*, et al.*, 1997). However, akin to SCVP, ATRP also demands the employment of specialized monomers, posing barriers to its industrial application. In response to these limitations, Sherrington and his collaborators devised the Strathclyde strategy, an alternative method for the polymerization of branched vinyl polymers that leverages thiol-based chain transfer (O'Brien*, et al.*, 2000) (Figure 3-2). This method distinguishes itself by being more accessible and cost-efficient compared to the previously mentioned techniques for branched polymer synthesis, offering a pragmatic solution for overcoming the challenges inherent in the production of branched vinyl polymers.

In this chapter, we endeavored to address the challenge of diminished wettability, a consequence of augmented gallol incorporation, by introducing branching within the PSA backbone, thereby rendering the adhesive matrix more pliable. This strategy is predicated on the hypothesis that a softer, more flexible backbone structure would compensate for the stiffening effect of increased gallol content, thus maintaining or enhancing the adhesive's performance characteristics.

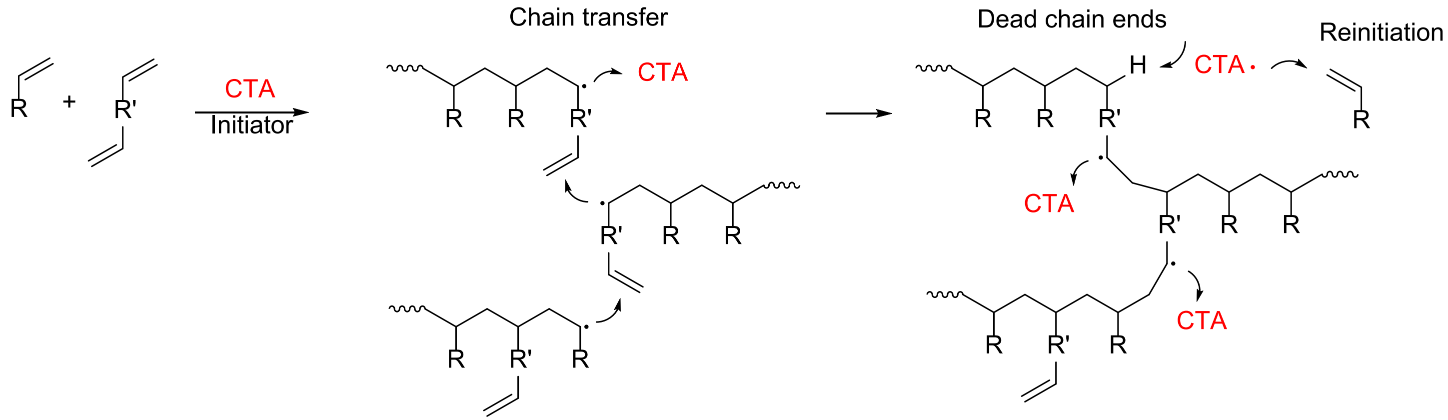

Figure 3-2. Strathclyde strategy for the synthesis of branched polymers

2. Experimental

2.1. Materials

Lauryl methacrylate (LMA, 96 %), glycidyl methacrylate (GMA, 97 %), trimethylolpropane triacrylate (TMPTA), pentaerythritol tetraacrylate (PETA), azobisisobutyronitrile (AIBN, 12 % wt.% in acetone), dodecanthiol (DDT, 98%), 1-methylimidazole (1MI, 99 %) were purchased from Sigma-Aldrich. Tripropylene glycol diacrylate (TPGDA, 90%) was purchased from Tokyo chemical industry. Methyl isobutyl ketone (MIBK, 99%), n-butanol were purchased from Samchun Chemicals. gallic acid monohydrate (98 %) was purchased from Daejung Chemicals & Metals.

2.2. Synthesis of branched scaffold polymer

The scaffold polymer was synthesized by free radical polymerization in MIBK using LMA, GMA, and multifunctional monomers (MFMs). 10 g of MIBK, AIBN (0.2 mol% of total monomers), DDT (0.5 mol% of total monomers), LMA, GMA, MFMs (variable concentration) were mixed in a 50 ml flask using Teflon stirring bar. And the flask was filled with nitrogen gas. The polymerization was initiated by immersing the flask in an oil bath at 80 °C, and the reaction was carried out for 8 h.

In consideration of mass production, adjustments have been made to the scaffold polymer manufacturing method detailed in this chapter. Previously, tetrahydrofuran (THF) was utilized as the polymerization solvent. However, the use of THF poses safety risks during mass production since the reaction temperature required for the subsequent esterification process surpasses the boiling point of THF (66 °C), thereby generating high vapor pressure. To enhance safety during the esterification process, the polymerization solvent was switched to methyl isobutyl ketone (MIBK), which has a higher boiling point (116 °C), mitigating the risks associated with high vapor pressures during large-scale manufacturing.

2.3. Monomer conversion ratio

To determine the monomer conversion ratio, a chemical mixture before the reaction and right after the reaction was analyzed by ^{1}H NMR spectroscopy (Figure 3-3). The conversion ratio was calculated by the ratio of the vinyl peak and the epoxy group integral area before and after the polymerization.

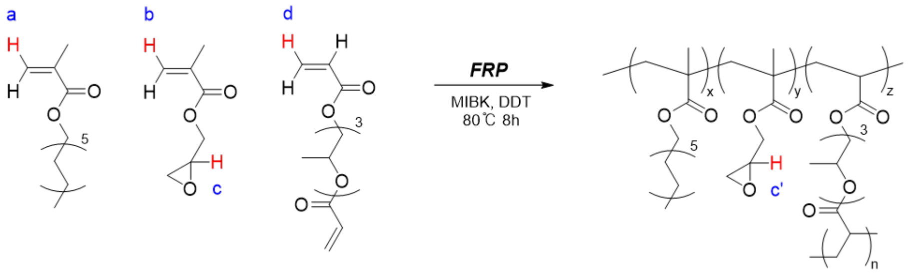

$$Methacrylate\ Conversion\ (\%) = \left\{1 - \left(\frac{H_{a'+b'}/H_{c'}}{H_{a+b}/H_c}\right)\right\} \times 100$$

$$Acrylate\ Conversion\ (\%) = \left\{1 - \left(\frac{H_{d'}/H_{c'}}{H_d/H_c}\right)\right\} \times 100$$

Figure 3-3. Calculation of monomer conversion by ^{1}H NMR

2.4. Molecular weight evaluation

Molecular weights were measured using triple detector GPC (1260 Infinity II HPLC System, Agilent). The equipment was incorporated a laser differential refractometer, differential viscometer, and right-angle laser light scattering photometer. The polymer solution obtained directly from the polymerization was diluted with tetrahydrofuran (1 mg of polymer solution per 1 ml of tetrahydrofuran) and filtered through a 0.45 μm filter. Tetrahydrofuran was used as the mobile phase.

2.4. Esterification of branched scaffold polymer

Branched gallol PSA was synthesized by esterifying a various scaffold polymers and gallic acids. Scaffold polymers (10 g, various mol% of the epoxide group in polymer backbone, 1eq) and gallic acid monohydrate (1.1 eq for epoxide group in the scaffold polymer backbone), and 1 MI (0.1 wt.% of scaffold polymer) were dissolved in n-butanol (5 g) then poured into the refluxing flask. The mixture was stirred for 30 min at room temperature. Then esterification was carried out in 100 °C oil bath with constant stirring. After the reaction, the mixture was cooled to room temperature. The mixture was then filtrated by syringe filter (pore size 0.45 ㎛). Then, epoxide conversions were calculated by ^{1}H NMR spectroscopy (Figure 2-8).

The shift to the filtration method for purifying scaffold polymers was driven by considerations for scaling up to mass production. The precipitation method previously employed proved to be highly inefficient, characterized by slow purification speeds and the excessive consumption of acetone for the purification of relatively small quantities of pressure-sensitive adhesive (PSA).

Furthermore, the approach of precipitating the reactant in acetone and subsequently removing the solvent poses significant challenges for practical implementation at industrial facilities, especially since this process often needs to be repeated several times.

In contrast, the filtration method leverages existing infrastructure within the PSA manufacturing industry. Most facilities are already equipped with pumps and filtration systems, eliminating the need for additional equipment or complex modifications. This shift not only streamlines the production process but also enhances overall efficiency compared to the previous precipitation method.

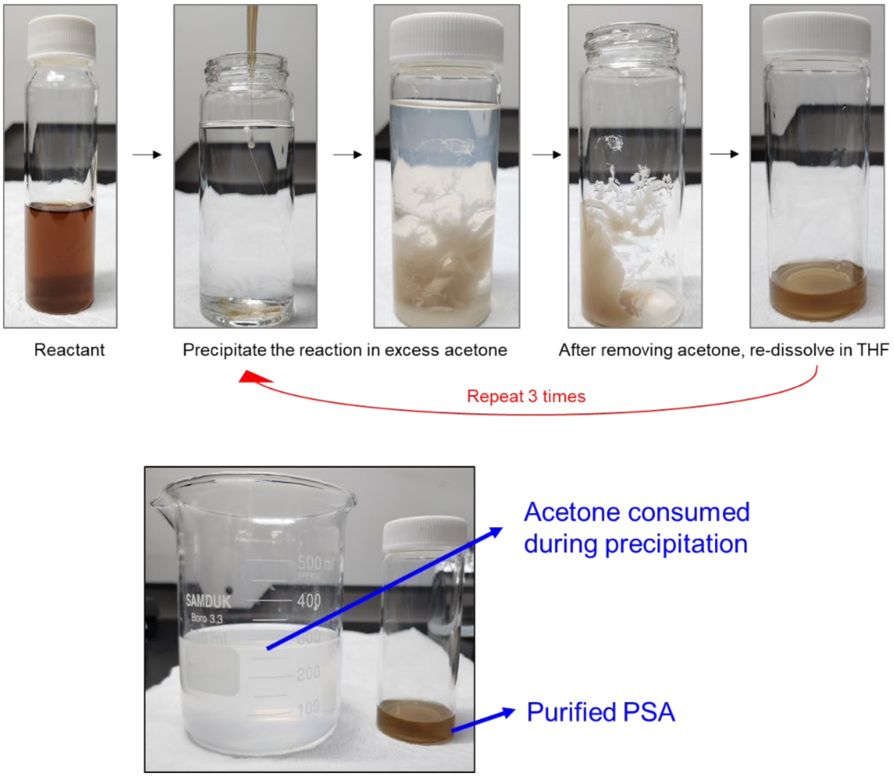

Figure 3-4. Inefficiency of precipitation processes

2.6. Adhesion properties

The 180° peel strength and probe tack were measured using a Texture Analyzer (TA.XT plus, Stable Micro Systems) at 25 °C. Samples for underwater adhesion test were prepared by being immersed in deionized water. The specific method is described in Section 2.6 of Chapter 2.

Probe tack: A cylindrical probe (stainless steel, diameter: 5 mm) was used for the probe tack test. After contact of the probe to the surface of PSA with 100 gf for 1 s, the probe was detached with 0.2 mm/sec. All measurements were repeated more than five times, and the average value was used.

2.7. Rheological properties

Rheological properties were measured by using rheometer (ARES G2, TA Instruments) with 8 mm parallel plates. The specific method is described in Section 2.7 of Chapter 2.

3. Results & discussion

3.1. Design, synthesis, characterization

The mechanism underlying the formation of branched copolymers through the copolymerization of a multifunctional monomer has been elucidated based on experimental evidence by Sherrington et al. (Slark, *et al.*, 2003). Polymerization initiation commonly occurs through primary radicals generated by the decomposition of an initiator. These radicals commence chain propagation via the copolymerization of methacrylate and a multifunctional acrylate monomer (MFAM). Within the polymerization system, the chain transfer agent, dodecanthiol, facilitates continuous generation of free radicals, leading to the formation of a "dormant" polymer characterized by numerous pendant acrylate groups.

The capability to form such dormant polymers stems from the differential reactivity ratios and chain transfer constants between methacrylate and acrylate. When designating methacrylate monomer as M_1 and acrylate monomer as M_2, the reactivity ratios typically favor the formation of more stable tertiary radicals by methacrylate, thus r_1 generally exceeds r_2. Consequently, chains formed at the early stages of polymerization predominantly contain methacrylate, whereas later stages see a higher concentration of acrylate. Furthermore, the chain transfer constants for methacrylate and acrylate differ significantly. The chain transfer constant for methacrylate radicals is approximately 0.6, while for acrylate radicals it is about 1.7. As a result, chain transfer events occur more frequently in acrylate during the initial stages, preventing gelation. In the later stages of polymerization, as the chain transfer agent becomes depleted, increased occurrences of combination and termination reactions in acrylate radicals are observed.

The degree of branching and the molecular weight of the branched polymer synthesized through the Strathclyde strategy are influenced by the number of functional groups present in the multifunctional monomer utilized. Utilizing a multifunctional acrylate with a greater number of vinyl groups results in more vinyl groups being retained in the pendant chains at the onset of polymerization. These vinyl groups can then potentially form branches or loops towards the end of the polymerization process. Interestingly, the number average molecular weight (M_n) of branched polymers, regardless of the number of functionalities, remains relatively constant. However, the molecular weights characterized by weight-average molecular weight (M_w), z-average molecular weight (M_z), and higher order averages (M_{z+1}) tend to increase with the inclusion of more functional groups in the monomer. This indicates that branched polymers derived from acrylates with higher functionalities predominantly comprise high molecular weight chains. Given that the molecular weight distribution can significantly influence the physical properties of pressure-sensitive adhesives, altering the number of acrylate functionalities in the formulation of an existing linear gallol PSA was explored to assess the resultant changes in the adhesive properties. This adjustment aims to fine-tune the performance characteristics of the PSA by manipulating the molecular architecture of the branched polymers.

The synthesis of branched scaffold polymer utilized MFAMs, each differing in the number of acryl groups to influence the degree of branching and the final properties of the adhesive. The MFAMs used include: Tripropylene glycol diacrylate with two acryl groups, trimethylolpropane triacrylate (TMPTA) with three acryl groups, pentaerythritol tetraacrylate (PETA) with four acryl groups. The scaffold PSAs were synthesized under uniform conditions regarding the initiator and chain transfer agent content to ensure consistency across different formulations. Chain transfer agent was added in equimolar proportion to the

MFAM. As the functionality of MFAM increases - ranging from two to four acryl groups - the concentration of acrylate is proportionally elevated in relation to the chain transfer agent. Furthermore, the branched scaffold PSA production was tailored based on the content of GMA to increase the introduction of gallol groups, a functional component known for enhancing adhesive properties. This strategic variation was designed to evaluate the impact of branching and increased gallol groups on the adhesive characteristics of the PSAs. This formulation provides a comparative analysis of how different multifunctional acrylates influence the structural and functional outcomes in the final PSA products (Table 3-1). During the polymerization of the scaffold polymers, there were no instances of gelation or phase separation, indicating successful maintenance of a homogeneous solution throughout the process. After the polymerization, scaffold polymers were analyszed by ^{1}H NMR spectroscopy to determine the conversion rates of methacrylate and acrylate monomers. The results demonstrated high conversion rates for methacrylate in all cases. Furthermore, the conversion rate of the acryl groups was also substantial, exceeding 70 % in every instance.

Table 3-1. Polymerization of linear and branched scaffold polymer*

Entry	Feed ratio (mol%)					MFAM functionality	Monomer conversion (%)	
	LMA	GMA	TPGDA	TMPTA	PETA		methacrylate	acrylate
S3-L	97	3	0	0	0	0 (linear)	93.2	-
S3-F2	96.5	3	0.5	0	0	2	88.4	77.4
S3-F3	96.5	3	0	0.5	0	3	88.3	70.5
S3-F4	96.5	3	0	0	0.5	4	91.7	83.8
S5-L	95	5	0	0	0	0 (linear)	91.2.	-
S5-F2	94.5	5	0.5	0	0	2	85.6	76.6
S5-F3	94.5	5	0	0.5	0	3	86.2	79.7
S5-F4	94.5	5	0	0	0.5	4	90.0	75.7
S7-L	93	7	0	0	0	0 (linear)	93.6	-
S7-F2	92.5	7	0.5	0	0	2	85.3	74.8
S7-F3	92.5	7	0	0.5	0	3	88.1	82.4
S7-F4	92.5	7	0	0	0.5	4	86.5	79.2

* Polymerization performed in MIBK at 80 ^{o}C for 8 hours under nitrogen, using 0.4 mol% of AIBN and 0.5 mol% of dodecanthiol.

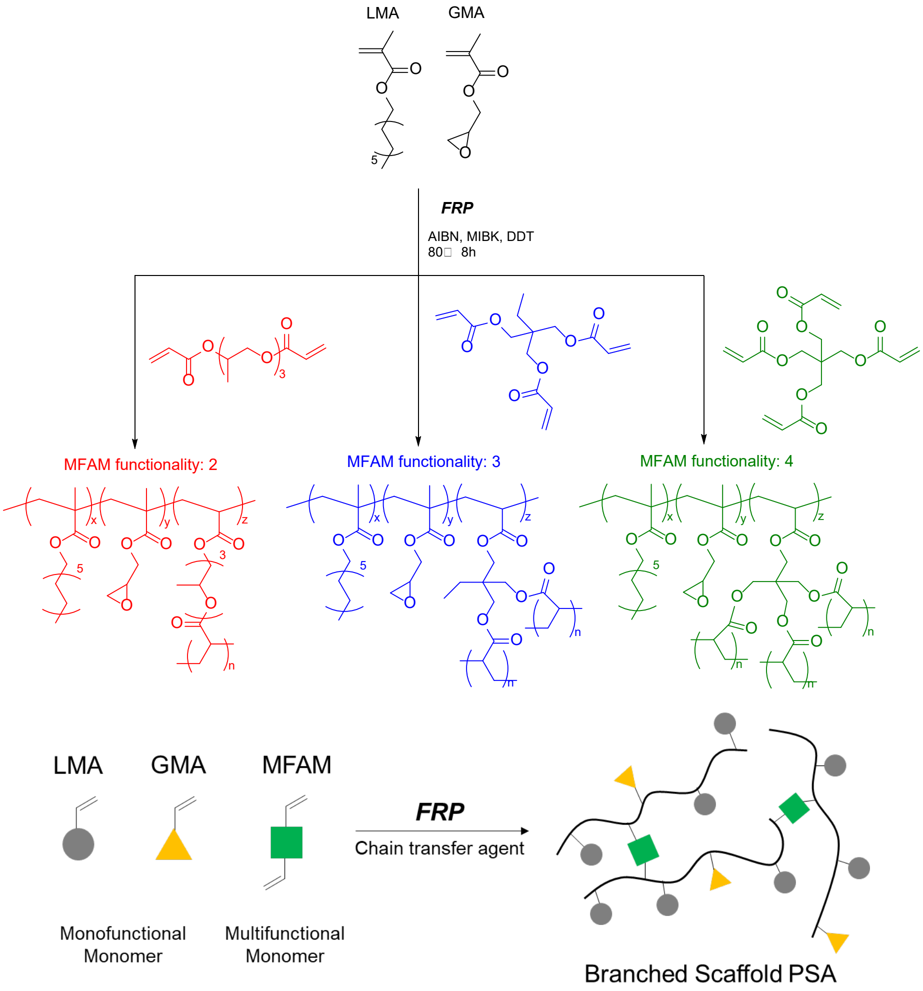

Figure 3-5. Synthesis of branched scaffold polymers by MFAM functionality

As the MFAM functionality in polymerized scaffold polymers increases, there is a corresponding increase in the concentration of acrylates in the pendant chains initiated at the onset of polymerization. Specifically, bifunctional MFAM features a single pendant acrylate double bond, trifunctional MFAM includes two, and tetrafunctional MFAM incorporates three double bonds within the pendant chain (Figure 3-5). Given that these residual acrylate groups are capable of reacting during the later stages of polymerization, an increase in MFAM functionality is likely to enhance the molecular weight of the final polymer. The results of the molecular weight analysis for these polymerized scaffold polymers are presented in Table 3-2 and Figure 3-6.

Table 3-2. TDGPC results for scaffold polymers

Entry	Molecular weight (g/mol)				M_w/M_n	α
	M_n	M_w	M_z	M_{z+1}		
S3-L	12,956	23,823	38,496	54,955	1.839	0.65
S3-F2	3,528	6,998	11,829	17,451	1.984	0.59
S3-F3	5,399	12,245	24,448	43,987	2.268	0.6
S3-F4	5,528	14,257	33,921	62,188	2.579	0.58
S5-L	12,312	22,597	36,274	51,714	1.835	0.72
S5-F2	4,122	8,525	15,077	24,950	2.068	0.6
S5-F3	5,004	10,509	19,441	31,079	2.1	0.6
S5-F4	4,589	13,524	31,063	54,111	2.947	0.52
S7-L	10,919	20,678	33,887	49,446	1.894	0.76
S7-F2	3,370	5,977	10,013	15,343	1.774	0.54
S7-F3	3,919	9,701	19,504	32,075	2.476	0.41
S7-F4	5,091	16,867	50,084	106,665	3.313	0.53

Analysis conducted using TDGPC demonstrates that all branched scaffold polymers exhibit averageable characteristics and display a broader range of properties compared to their linear counterparts. In examining branched scaffold polymers with varying MFAM functionalities, findings are consistent with previous research by the Sherrington group (Slark, *et al.*, 2003), which utilized methyl methacrylate. The results indicate that the yield remains relatively constant across different functionalities. However, there is a notable trend where yield increases as the MFAM functionality is enhanced. Additionally, the molecular weight distribution trends (M_{z+1}>M_z>M_w) also show a tendency to increase with the escalation of MFAM functionality. This suggests that higher functionality of MFAM contributes to both a greater yield and an expanded molecular weight distribution in branched scaffold polymers.

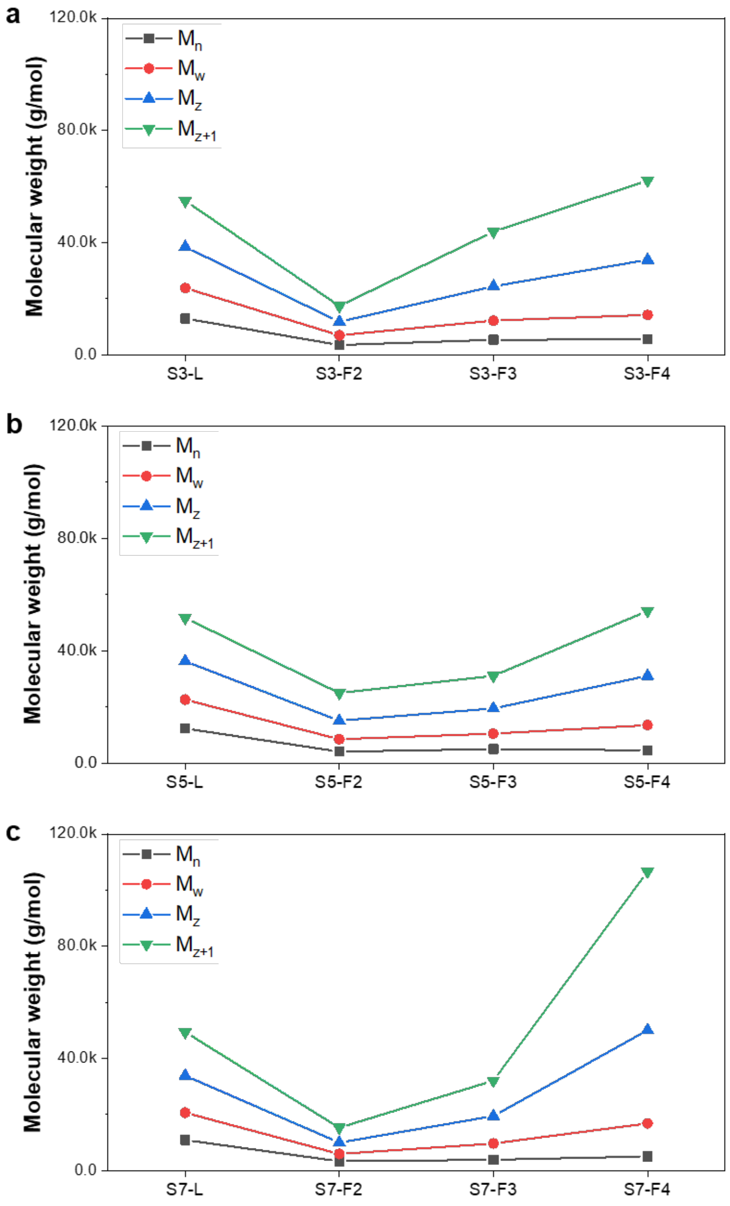

Figure 3-6. Molecular weight of linear and branched scaffold polymers with MFAM functionality. (a) scaffold 3 series, (b) scaffold 5 series, (c) scaffold 7 series

In TDGPC, the analysis involves determining the relationship between molecular size and molecular weight by employing a linear polymer as a reference. This relationship is quantitatively described by the Mark-Houwink equation (Paul*, et al.*, 2007).

$$[\eta] = KM^{\alpha}$$

Where η represents the intrinsic viscosity, and M denotes the molecular weight. The parameters K and α are specific constants known as the Mark-Houwink parameters, which characterize the viscosity-molecular weight relationship for a given polymer in a specific solvent at a particular temperature. Generally, linear PMMA polymers that exhibit a random coil conformation in solution typically have a α of approximately 0.7 (Wagner, 1987). This value reflects the proportional relationship between the intrinsic viscosity and molecular weight of the polymer under these conditions. For branched polymers, the correlation between molecular size and molecular weight is less steep compared to that observed in linear polymers. Consequently, this leads to a reduced slope in the Mark-Houwink plot, which manifests in lower values of the exponent α. All scaffold polymers incorporating MFAM and chain transfer agents demonstrate Mark-Houwink α values ranging from 0.4 to 0.65. These values are lower compared to those observed in other branched polymers, highlighting their compact and highly branched nature (Figure 3-7). Although the trend in α values with respect to MFAM functionality is not uniform, it is consistently observed that polymers with functionality 4 exhibit lower α values than those with functionality 2.

Following the polymerization process, all scaffold polymers were subjected to an esterification reaction with gallic acid monohydrate, using an equivalent ratio of 1.1 relative to their GMA feed ratio. During the ^{1}H NMR analysis, variations were observed in the extent of epoxide consumption across different samples, ranging approximately from 44.4 % to 60.4 % (Table 3-3).

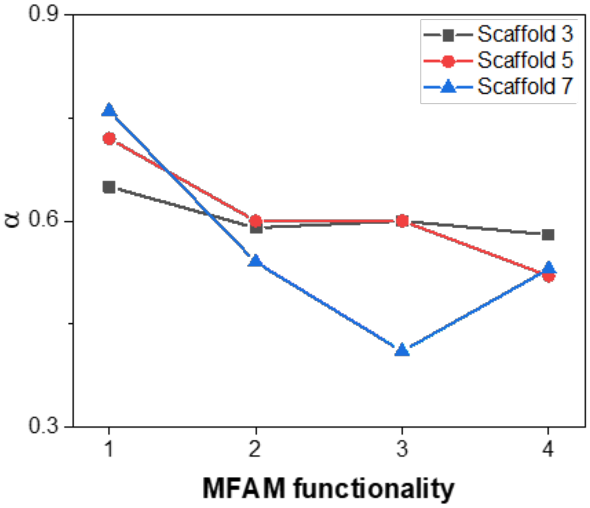

Figure 3-7. Mark-Houwink constant α with MFAM functionality of scaffold 3, scaffold 5, scaffold 7 series

3.2. Rheological properties

The objective of branching the scaffold polymer is to structurally mitigate the hardening of PSAs as the content of gallol groups increases. Gallol groups are known for their superior properties in underwater adhesive environments. To ensure that branched gallol PSAs function effectively as adhesives, they must maintain a sufficiently low G' and T_g. This allows them to wet the surface of the adherend, similar to conventional PSAs, thereby ensuring optimal adhesive performance.

The G' of gallol-functionalized PSAs exhibits a tendency to increase as the GMA content within the scaffold increases. This observation can be attributed to the relatively consistent conversion rate of epoxide groups across samples, which suggests that samples with higher GMA content contain a greater number of gallol groups. The increase in gallol groups, capable of forming diverse bonds, contributes to the observed rise in G'. However, when examining cases with comparable amounts of gallol groups, increased branching was found to substantially decrease the modulus of the PSAs, particularly at temperatures above 50 °C (Figure 3-8).

Table 3-3. Characterization of gallol functionalized PSAs

Entry	Epoxide Consumption (%)	T_g (°C)	G´ (MPa)	
			25 °C	60 °C
S3-L-G	48.7	-16.9	0.101	0.053
S3-F2-G	44.5	-13.4	0.066	0.009
S3-F3-G	47.6	-14.3	0.051	0.011
S3-F4-G	44.4	-14.2	0.072	0.016
S5-L-G	49.4	-15.5	0.150	0.086
S5-F2-G	52.9	-13.6	0.095	0.030
S5-F3-G	45.9	-13.8	0.077	0.028
S5-F4-G	46.1	-14.2	0.128	0.036
S7-L-G	53.3	-14.0	0.319	0.097
S7-F2-G	51.6	-13.9	0.179	0.046
S7-F3-G	51.6	-13.5	0.161	0.033
S7-F4-G	60.4	-13.4	0.285	0.062

Although no linear correlation was evident between the number of MFAM functionalities and modulus, MFAM functionality 4 exhibited the highest G' across all branched gallol PSA scaffold series, albeit still lower than that observed in linear gallol PSAs. Notably, scaffold series 3 and 5 demonstrated this trend even with a relatively low introduction of gallol groups. Given that an increase in MFAM functionality previously correlated with a higher proportion of high molecular weight chains, it can be inferred that the enhanced modulus observed in branched polymers may be attributed to the presence of high molecular weight chains.

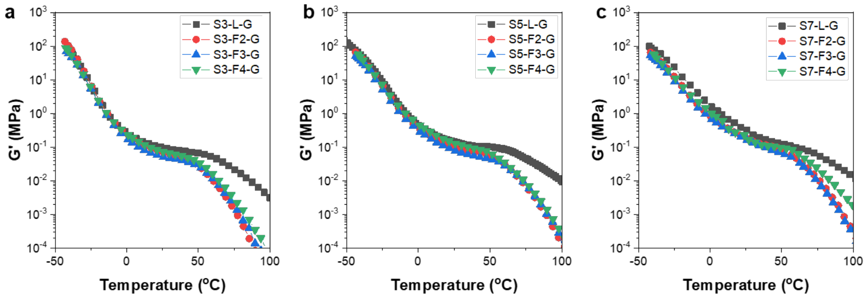

Figure 3-8. Storage modulus (G´) plot according to temperature. (a) scaffold 3 series, (b) scaffold 5 seires, (c) scaffold 7 series

While clear trends in T_g due to differences in MFAM functionality were not distinct, an increasing trend in T_g was noted with the addition of MFAM in the scaffold series. This is believed to be caused by the branching of the polymer, which typically increases the glass transition temperature.

From the perspective of linear polymers, it is well-known that T_g increases with molecular weight up to a certain threshold, after which it remains constant. The introduction of branching increases the number of chain ends and enhances the free volume, while decreasing the molecular size, the molecular weight between branches, and the average distance between chain ends. This would theoretically result in a decrease in T_g when analyzed from the perspective of linear polymers; however, an actual increase in T_g has been observed. This anomaly might be interpreted as resulting from the effects of branching points and numerous end groups on hyperbranched polymers, leading to a translational movement of the entire molecule rather than the typical segmental movement observed in linear polymers (Roovers*, et al.*, 1999). Consequently, it appears that branched polymers exhibit a slightly higher T_g compared to their linear counterparts. While this increase in T_g seems contradictory to the goal of branching, which is to soften the PSAs, it is important to note that the actual operating temperature of PSAs is significantly above T_g, typically at room temperature. Therefore, the increase in T_g is unlikely to adversely affect the wettability of branched gallol PSAs.

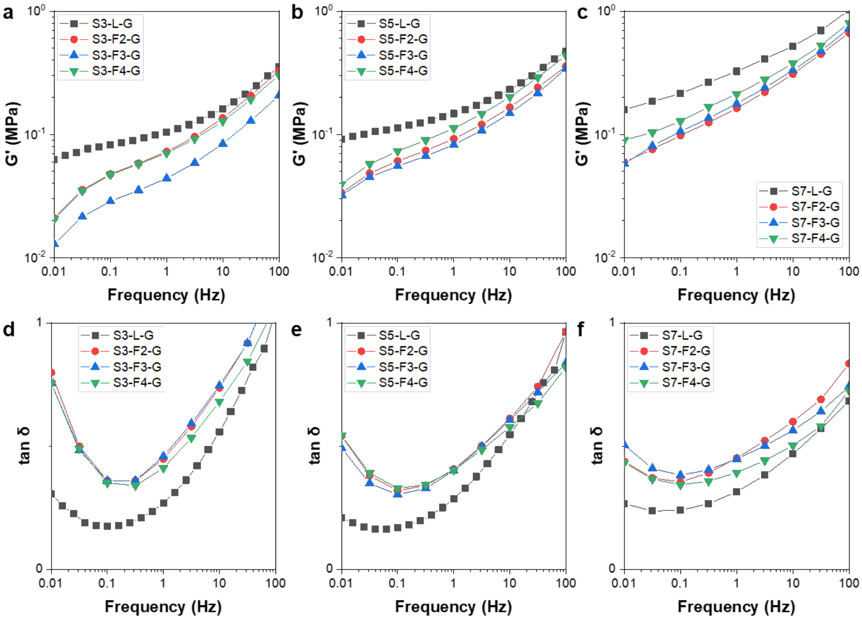

Figure 3-9. Frequency sweep results for G' (a) scaffold 3 series, (b) scaffold 5 series, (c) scaffold 7 series, and tanδ (d) scaffold 3 series, (e) scaffold 5 series, (f) scaffold 7 series

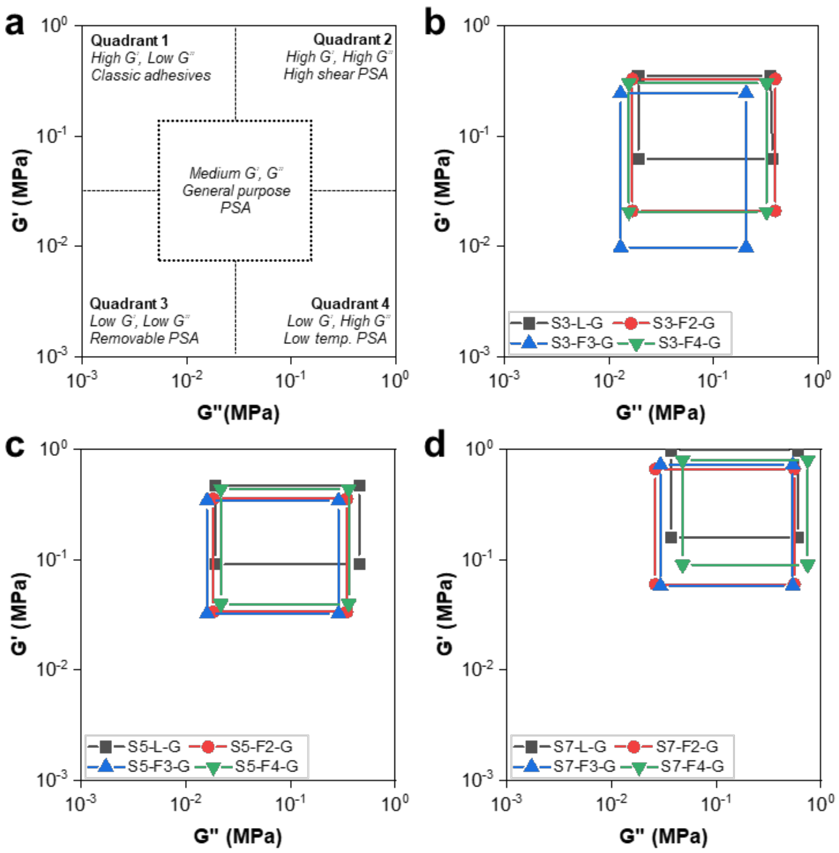

Figure 3-10. Viscoelastic window. (a) general PSAs (Chang, 1997), (b) scaffold 3 series, (c) scaffold 5 series, (d) scaffold 7 series

In the context of general PSAs, Dahlquist's criterion specifically addresses the storage modulus at a frequency of 1 Hz (Creton and Ciccotti, 2016). However, the practical application of PSAs occurs across a variety of time scales, and it is generally recognized that a frequency range from 0.01 Hz to 100 Hz more accurately reflects the conditions under which actual PSAs are utilized (Chang, 1997). At lower frequencies, approximately 0.01 Hz, the behavior is indicative of the creep characteristics of the adhesive, whereas frequencies around 100 Hz are associated with the delamination properties of PSAs. As observed during the temperature ramp evaluation, a reduction in the storage modulus across all frequencies accompanies the branching of the polymer chain (Figure 3-9). This effect is most pronounced at lower frequencies, which correspond to relatively longer time scales, and the difference in modulus at higher frequencies is less marked. This trend is also evident in the tanδ plot. The lower G' and higher tanδ at the low frequency range (0.01 Hz) attributable to branching are anticipated to enhance the wettability of the PSA into the adherend. Additionally, the smaller difference in the high frequency range compared to the existing linear polymers suggests that damage to the peel force characteristics may be minimized.

The viscoelastic plot, which utilizes a combination of G' and G'' values across different frequencies, essentially indicates that PSAs with gallol groups fall within the spectrum between high shear and general-purpose PSAs (Figure 3-10). The plot also reveals that branching serves to soften gallol PSAs. Additionally, as the concentration of gallol groups increases, there is a noticeable shift of the overall window toward quadrant 2, suggesting a transition towards properties typically associated with more elastic and less viscous materials.

3.3. Adhesion properties

The adhesion properties of the PSAs were investigated using a 180° peel test. The PSA tapes were attached to stainless steel in air or water and then passed twice through a 2 kg rubber roller. The peel strength was measured after allowing the PSA samples to stand under ambient (dry) or underwater (wet) conditions for 24 h. Figure 3-11 illustrates the peel strength under dry condition.

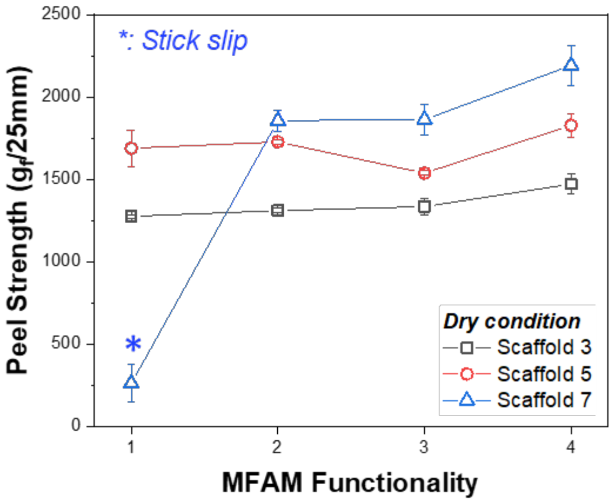

Figure 3-11. Peel strength results in dry condition

For linear pressure-sensitive adhesives PSAs, the molecular functionality was determined to be 1. In all cases except for S7-L-G, the predominant failure mode was cohesive failure (Figure 3-12). For both series 3 and series 5 scaffolds, the peel strength did not exhibit a significant variation attributable to branching. All PSAs derived from Scaffold 3 demonstrated an adhesion strength of 1,300 g_f/25mm (ranging from 1,276 to 1,471 g_f/25mm) in a dry environment, whereas Scaffold series 5 exhibited a higher adhesion level, ranging from 1,537 to 1,827 g_f/25mm. These findings suggest that the incorporation of the gallol group into the scaffold predominantly influences the adhesive strength. Given that the failure mode for all instances within the series 3 and 5 scaffolds was cohesive, and considering the uniform wetting of the adherend surface across samples, there appears to be minimal distinction in adhesion between linear and branched PSAs. This implies that the energy required for the destruction of the PSA matrix shows no significant difference. Furthermore, in relation to rheological properties, the difference in modulus between linear and branched PSAs diminishes as frequency increases (Figure 3-9). Given that around 100Hz is the deformation frequency during peel force evaluations, it can be concluded that the disparity in adhesion between the PSAs is minimal.

However, the Scaffold 7 series exhibits a distinct pattern. The branched PSA displayed a notably high peel force exceeding 1800 gf, whereas the linear gallol PSA S7-L-G demonstrated a stick-slip phenomenon during peeling, along with a significantly lower peel force of 262 gf/25mm. Observing the time-dependent peel curve for the Scaffold 7 series (Figure 3-13), the peel force of the S7-L-G sample exhibits substantial fluctuation in amplitude compared to other levels. This behavior suggests that S7-L-G does not adequately wet the surface of the adherend, leading to unstable peeling behavior. Considering that S7-L-G exhibited the highest G' and the lowest tanδ at low frequencies in the previously analyzed rheological properties, it is likely that the standard 24-hour dwell time was insufficient for S7-L-G to adequately wet the adherend, possibly due to either insufficient time or excessively high G'.

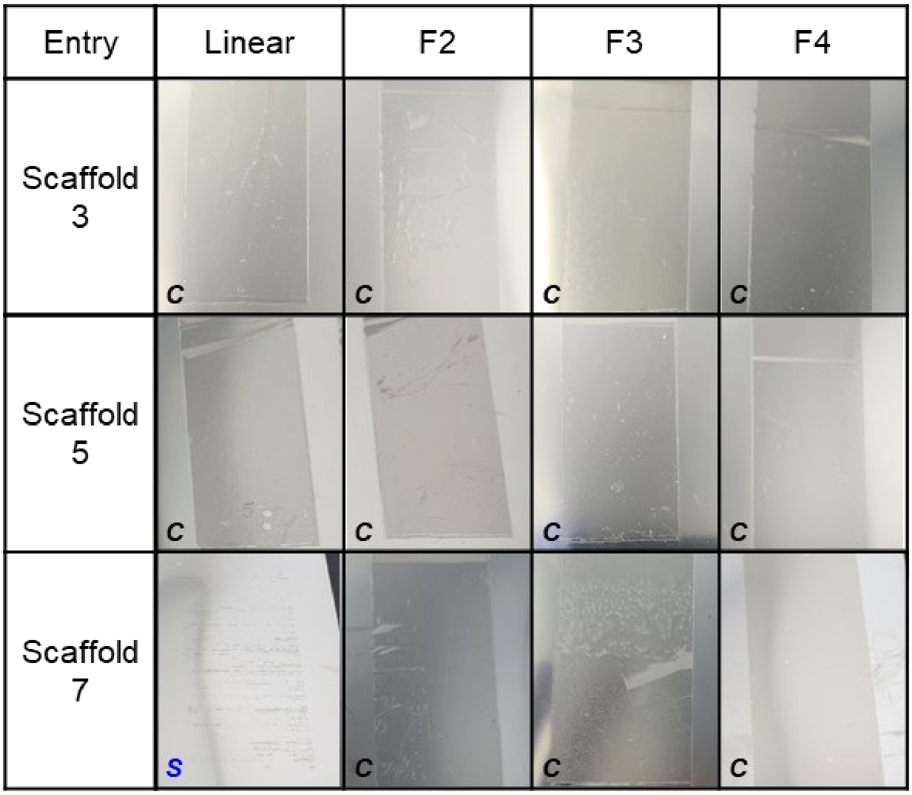

* *C: Cohesive failure, S: Stick slip*

Figure 3-12. Images of the substrate surfaces after peel test in dry condition

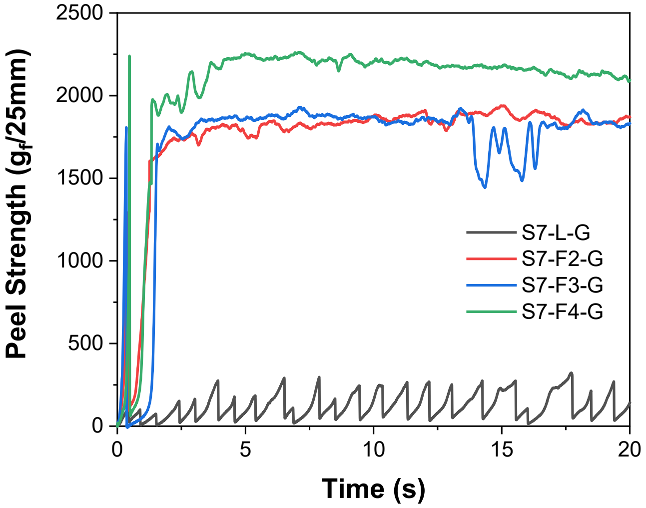

Figure 3-13. Peel curve results of scaffold 7 series in dry condition

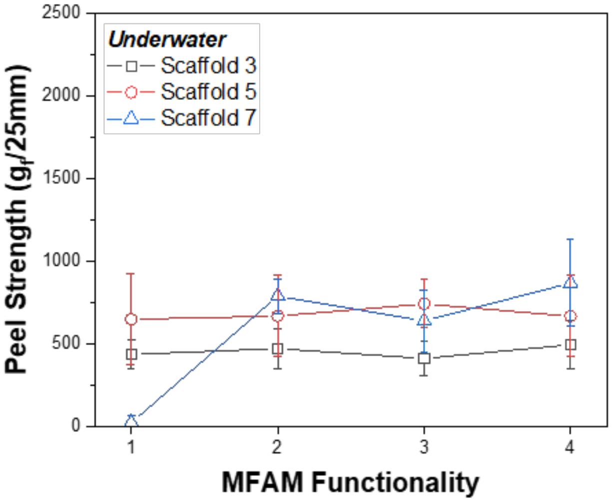

Figure 3-14. Underwater peel strength results

In terms of underwater adhesion, no significant differences were observed in peel strength between linear gallol PSA and branched gallol PSA for both the scaffold 3 and scaffold 5 series (Figure 3-14). However, a notable decline in peel strength, exceeding 60 % relative to dry conditions, was evident, with all samples demonstrating a mixed failure mode (Figure 3-15). This mode was characterized by the presence of both residue-covered and clean areas on the surface of the substrates. The scaffold 7 series also exhibited a reduction in peel strength in aquatic environments. Notably, only the linear PSA exhibited interfacial failure; a slight stain was visible on the surface of the substrate, but no residual PSA material remained. In contrast, all branched PSA samples showed mixed failure modes. The lack of residue and the detachment of S7-L-G indicate its minimal interaction with the adherend under challenging underwater conditions, likely due to inadequate wetting properties. Furthermore, the adhesion strength recorded was minimal, only a few tens of g_f, suggesting virtually no adhesive bond.

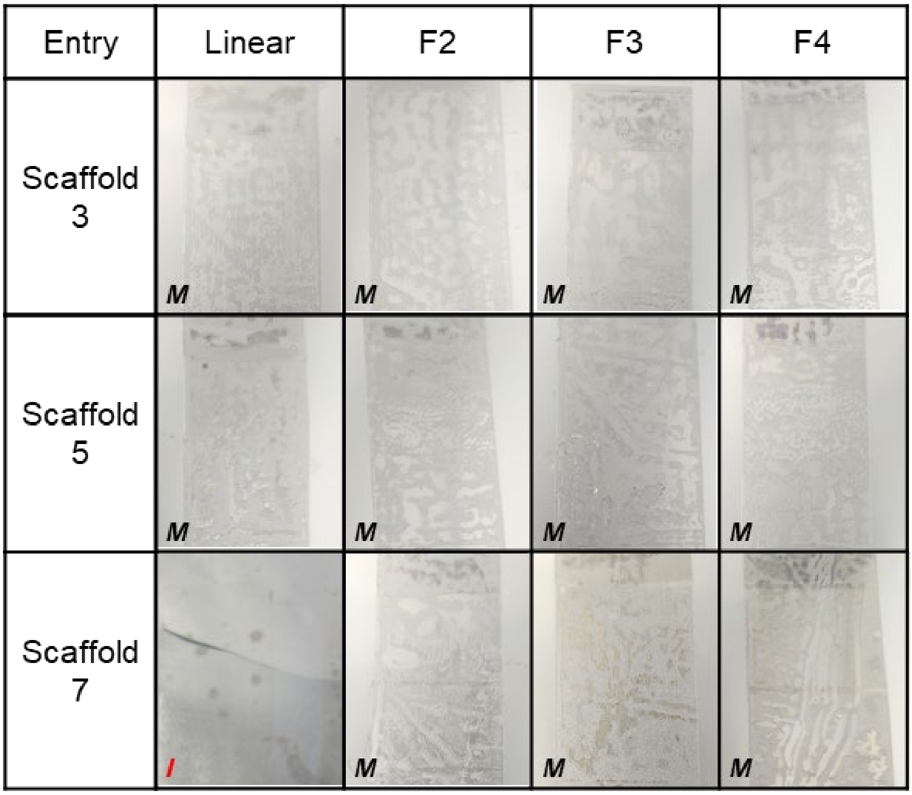

* M: Mixed failure, I: Interfacial failure

Figure 3-15. Images of the substrate surfaces after underwater peel test

It was noted that the reduction in underwater peel strength tended to lessen with an increase in the gallol group content. Specifically, compared to dry conditions, the decrease in underwater adhesion averaged 66 % for the scaffold 3 series, 60 % for the 5 series, and 61 % for the scaffold 7 series (excluding S7-L-G due to its distinct failure mode). The rate of decline in underwater adhesion compared to the dry environment was found to be similar regardless of the amount of gallol group introduced.

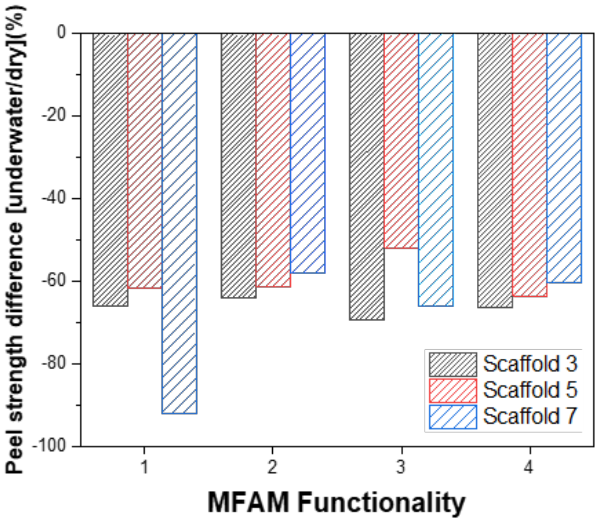

Figure 3-16. The degree of decrease in peel strength in water compared to the dry environment

However, In the probe tack evaluation, unlike in the peel strength assessment, no consistent trend emerged in relation to the amount of gallol group introduction or the branching in PSA, except for S7-L-G which exhibited the lowest tack (Figure 3-16). This contrasts with the findings from the peel strength evaluation, where a decrease in strength was noted in underwater conditions compared to the dry environment. However, in the case of probe tack, there was no significant difference between the tack levels in dry and underwater environments, with the exception of specific samples (S3-L-G, S3-F2-G, S7-L-G), where the probe tack in water appeared to be higher (Figure 3-17).

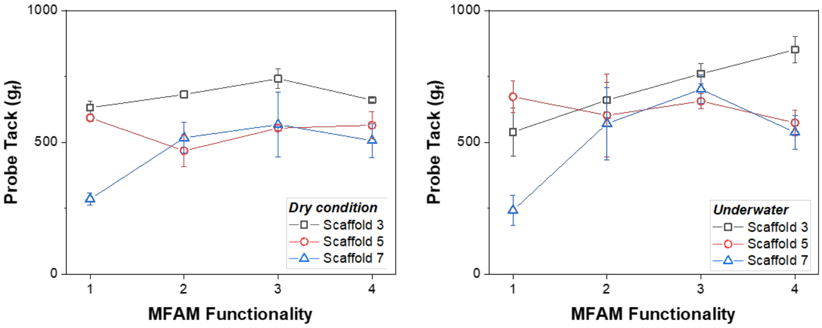

Figure 3-17. Probe tack results in dry and underwater condition

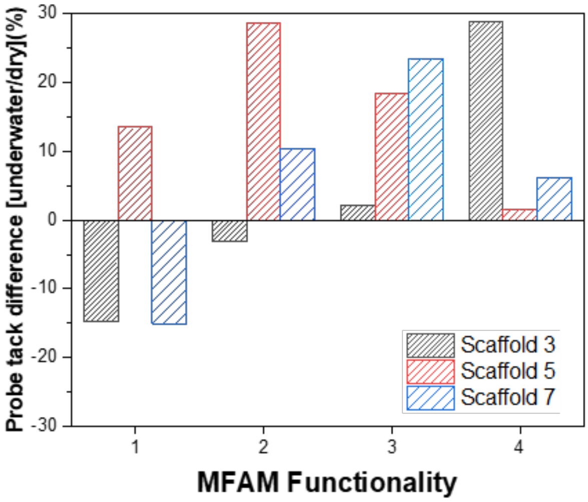

Figure 3-18. Probe tack difference between underwater/dry condition

This can be attributed to the nature of the probe tack evaluation, which applies pressure to a relatively small area (probe diameter: 5 mm). It seems that the reduction in peel strength in water, which could impede interaction with the surface of the adherend due to a hydration layer on the adherend's surface, does not significantly impact the probe tack results. This is likely because the water molecules trapped between the probe and the PSA do not interfere with contact, thus maintaining tack performance similar to that in dry conditions.

When analyzing the peel strength and probe tack curves for S7-F4-G, which demonstrated the highest adhesion in both dry and underwater conditions, distinct behaviors are observed in these two testing environments (Figure 3-18). In the dry environment, the peel strength curves among different samples exhibit small deviations in force and maintain a consistent shape, indicating stable adhesion characteristics across tests. Conversely, in the underwater environment, the peel strength curves vary significantly between samples. This variability is attributed to the random formation of adhesion defects due to water at the interface between the PSA and the adherend's surface during the preparation of samples for underwater peel testing. These defects can alter the location and shape of the interface, leading to inconsistent results. In the probe tack evaluation, although there are variations in the maximum force exerted by different samples, the overall shape of the curve remains consistent across tests. This consistency suggests that almost no defects form at the interface between the probe and the PSA during probe tack evaluation. The smaller contact area and the specific application of pressure in the probe tack test likely minimize the potential for water to interfere significantly with adhesion, unlike in the peel test where a larger surface area increases the complexity of the adhesion dynamics in the presence of water.

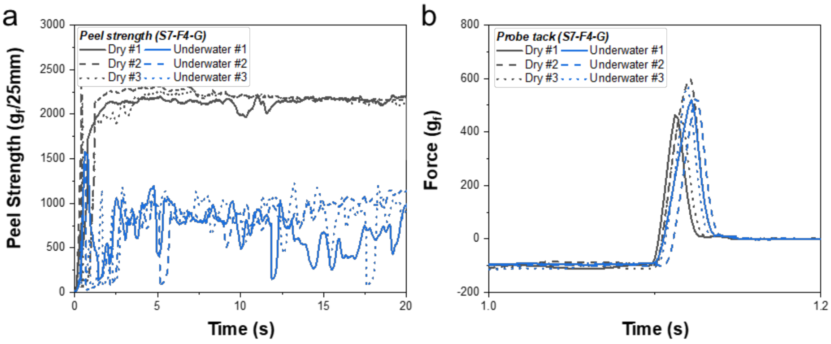

Figure 3-19. Difference in adhesion properties of S7-F4-G in dry and underwater conditions. (a) peel strength curve, (b) probe tack curve

The distinct outcomes observed in the peel test and the probe tack test can largely be attributed to differences in the contact area between the PSA and the adherend or probe (Figure 3-20). In the peel test, the interface between the PSA and the adherend is considerably larger. If water becomes trapped at this interface during adhesion, it must traverse a substantial distance to completely escape the interface. This extended path for water expulsion can complicate the adhesion process. Should water remain trapped at the interface while pressure is applied, it may disrupt the interaction between the adhesive and the adherend surface, leading to adhesion defects.

Conversely, in the probe tack test, the contact area between the probe and the PSA is much smaller, and pressure is applied to a more concentrated area. This configuration significantly reduces the distance that any trapped water would need to travel to escape. Thus, the likelihood of water causing an adhesion defect in the probe tack test is minimized. The smaller contact area and focused pressure application help to ensure that even if water is present at the interface, it can be quickly expelled, allowing for more consistent adhesion performance despite similar environmental challenges.

These findings underscore that in designing PSAs for underwater applications, it is crucial to consider both the molecular-scale properties of the PSA, such as its physical and chemical characteristics, and larger-scale properties that span from a few micrometers to millimeters or more. This dual focus is essential because the adhesion performance of PSAs under water is influenced not only by the inherent qualities of the adhesive materials but also by how these materials interact with environmental factors like water over varying scales of contact area. The interaction dynamics at these different scales can significantly affect the overall effectiveness and reliability of the adhesive under submerged conditions. This holistic approach to adhesive design ensures that PSAs are optimized for both micro-level molecular interactions and macro-level physical behaviors in aquatic environments.

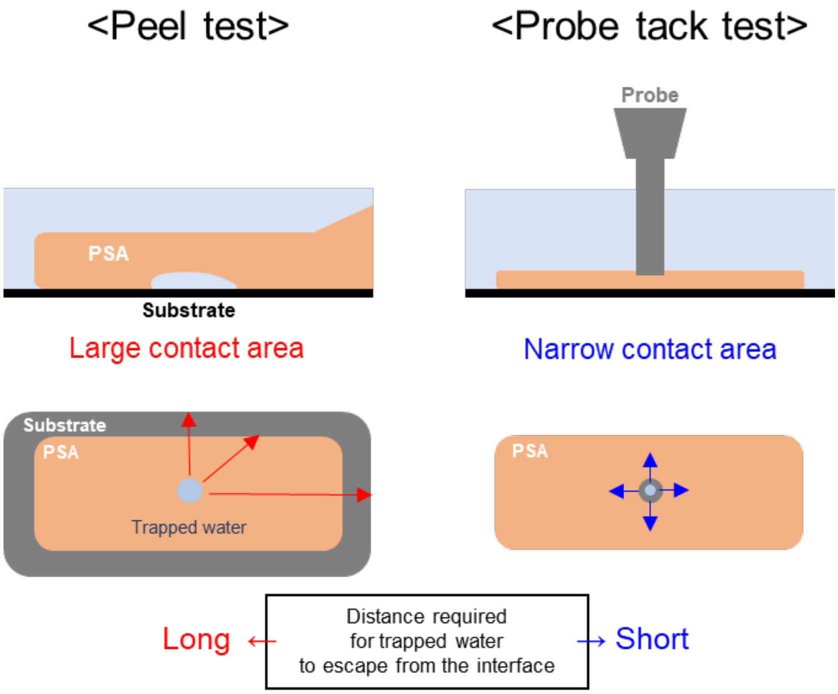

Figure 3-20. Illustration of the difference between peel test and probe tack test during underwater bonding

4. Conclusion

In this chapter, we address the issue of decreasing stickiness due to the increased hardness associated with higher gallol group content in linear gallol PSAs. To compensate for this, the polymer chains outside the gallol groups in the PSA polymer were branched to enhance softness. This branching was accomplished using the Strathclyde strategy, a common radical polymerization approach similar to that used for linear gallol PSAs. The Strathclyde method delays gel formation with a very high conversion rate by incorporating a multifunctional monomer and a chain transfer agent into the conventional system of initiator and monomer. The multifunctional monomer selected was acrylate, chosen based on the reactivity ratio with the main monomer and the chain transfer constant. The functionality of this monomer was set to 2, 3, and 4 to study the impact of these variables.

TDGPC analysis confirmed the formation of branched polymers through the reduction of the Mark-Houwink constant. Additionally, it was observed that as the functionality of the multifunctional monomer increased, the molecular weight distribution broadened, and the proportion of higher molecular weight polymers increased. In the high gallol content scaffold 7 series, the branched polymers displayed cohesive failure during peel strength testing, whereas the linear polymers exhibited stick-slip behavior, indicating that branching effectively enhances substrate wetting. Furthermore, comparisons between peel strength and probe tack revealed that as the contact area between the PSA and the substrate increases, variability among the same samples increases, leading to a decline in adhesive properties and an increase in adhesion defects.

Chapter 4

Surface-patterned Gallol Pressure-Sensitive Adhesives

1. Introduction

The findings from the evaluations of peel strength and probe tack, highlighting differences in adhesion characteristics between dry and wet environments, underscore the importance of the contact area in underwater adhesion. The presence of water lumps at the adhesive interface disrupts the interaction between the adhesive and the adherend by acting as a barrier to effective bonding. The ease with which these water lumps can be removed from the interface is inversely proportional to the contact surface area. Essentially, the larger the contact area, the more challenging it is to expel the water, as the water must travel a greater distance to be completely cleared from the interface. This phenomenon highlights the importance of considering the interface geometry and the methods of managing moisture in the design of adhesives, especially for applications involving wet or underwater conditions. Efficient water management can significantly enhance the adhesive performance by ensuring more direct contact between the adhesive and the adherend surface.

This observation aligns with strategies employed in nature to optimize adhesion under various environmental conditions. A notable example is seen in the adhesive toe pads of tree frogs and rock frogs (Drotlef*, et al.*, 2015, Xue*, et al.*, 2017). These frogs possess toe pads that are equipped with hexagonal patterns and secrete a mucous-like fluid. The mucous fluid serves as an adhesive, enabling the frogs to cling to surfaces effectively. Concurrently, the hexagonal pattern plays a crucial role by acting as a drainage system to expel excess fluid in wet conditions. This design allows the frogs to maintain strong adhesion and friction, ensuring stability even on wet surfaces. The surface patterns inspired by the tree frog's toe pads offer several advantages beyond enhancing wet adhesion. These biomimetic designs are particularly effective for adapting to structurally irregular surfaces. The patterns increase the surface area available for contact between the adhesive and the substrate, which enhances the overall adhesion strength. Additionally, the structured patterns help distribute the mechanical stress across a broader area. This distribution reduces the concentration of stress at any single point, thereby decreasing the likelihood of adhesive failure under load. Such designs not only improve the functionality of adhesives in challenging conditions but also increase their versatility across diverse applications, highlighting the potential of bio-inspired innovations in material science.

Many researchers have drawn inspiration from the tree frog's toe pad to enhance underwater adhesive technologies (Drotlef*, et al.*, 2013, Gupta*, et al.*, 2012, Iturri*, et al.*, 2015). By studying the structure of these natural adhesives, they have successfully incorporated similar patterns into synthetic materials. Techniques such as molding have been used to replicate the hexagonal pattern of the frog's toe pads on the surface of polymers like polystyrene, polydimethylsioxane (Chen*, et al.*, 2015, Iturri*, et al.*, 2015, Shahsavan*, et al.*, 2014, Wang*, et al.*, 2012, Zhang*, et al.*, 2020), polyurethane (Tsipenyuk*, et al.*, 2014, Xie*, et al.*, 2018), polycaprolactone (Shi*, et al.*, 2021) or acrylic hydrogel (Rao*, et al.*, 2018). These biomimetic patterns not only mimic the drainage function of the natural pads but also facilitate the removal of excess water from the adhesive interface. This adaptation has been shown to significantly improve the performance of adhesives in underwater environments, demonstrating the effectiveness of bio-inspired design principles in advancing material science and engineering applications.

The implementation of surface patterns inspired by natural structures, such as those found on the toe pads of tree frogs, can be achieved through various fabrication techniques. Generally, these methods can be divided into four primary categories (Zhang*, et al.*, 2022): 1) Photolithography(Gupta*, et al.*, 2012, Meng*, et al.*, 2021, Zhang*, et al.*, 2020): This process involves the use of light to transfer geometric patterns from a photomask to a light-sensitive chemical photoresist on the substrate. It is commonly used in microfabrication to create finely detailed patterns essential for electronic and microfluidic devices. Photolithography is suitable for achieving high precision and complexity in pattern design on a microscale. 2) Etching (Chen*, et al.*, 2018, Huang*, et al.*, 2022, Van Nguyen, 2019): This technique uses chemical or plasma-based processes to remove layers from the surface of a material to form patterns. Etching can be used in combination with photolithography, where the patterned photoresist acts as a mask that protects parts of the surface from being etched away, thus creating a pattern. It is effective for creating patterns on a variety of materials including metals, glass, and polymers. 3) 3D Printing (Banik*, et al.*, 2020): This additive manufacturing process creates three-dimensional objects from a digital file by laying down successive layers of material. For surface patterning, 3D printing can be used to produce complex shapes and structures that are difficult to achieve with traditional manufacturing processes. This method is particularly versatile and allows for rapid prototyping and customization. 4) Embossing (Banik and Tan, 2020, Shi*, et al.*, 2021, Xue*, et al.*, 2017): This method involves pressing a patterned tool (die) into a material to deform its surface according to the pattern. Embossing can be used on polymers and metals and is effective for large-scale production of patterned surfaces. It is commonly used for decorative and functional purposes, such as improving surface friction or enhancing visual appeal. Each of these methods has its own set of advantages and is chosen based on the requirements of the specific application, such as the type of material, the complexity of the pattern, production volume, and cost considerations.

However, traditional molding approaches for surface patterning can be highly time-consuming. Particularly with materials like hydrogels, the fabrication of even small area samples using conventional methods might take upwards of 10 hours. To address this inefficiency, an innovative approach has been adopted that leverages existing industrial techniques. The method involves the use of a patterned release film, which allows for quick and continuous surface patterning during the coating process. This technique draws from practices already established in the display industry, offering several significant advantages. Firstly, it is cost-effective as it utilizes existing equipment without the need for specialized additional machinery. Secondly, it is highly efficient, capable of achieving patterning at speeds of tens of meters per minute. This rapid processing capability not only reduces production time drastically but also enhances the scalability of manufacturing patterned surfaces on gallol PSAs and similar materials. This approach represents a practical solution to the challenges associated with traditional molding methods, particularly in high-throughput industrial applications.

2. Experimental

2.1. Materials

The patterned realease liners were supplied by O’sung Industry.

2.2. Synthesis of branched gallol pressure-sensitive adhesives

S7-F4-G was selected as the gallol PSA for surface patterning. The detailed synthesis method of S7-F4-G is described in Section 2.2 and 2.4 of Chapter 3

2.3. Preparation of surface-patterned PSA films

The S7-F4-G solution was coated on a patterned release film using a 120 μm gap applicator, ensuring a uniform coating thickness. After application, the coated film underwent a drying process at 150 °C for 5 minutes. Following the drying process, the film was laminated onto a 50 μm thickness polyethylene terephthalate (PET) sheet that had undergone corona treatment. This treatment enhances the surface energy of the PET, facilitating transcription of PSA to PET film. The lamination process effectively bonds the dried adhesive film to the PET, integrating the pattern from the release film onto the adhesive surface.

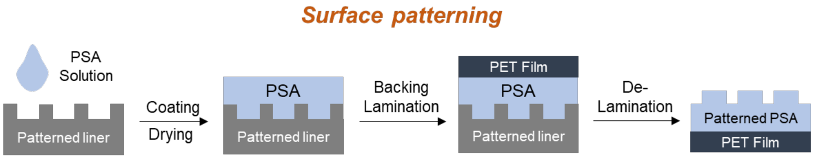

Figure 4-1. Surface patterning process

2.4. Confocal microscopy

The surface structure of PSAs was analyzed by laser confocal microscope (VK-X3000, Keyence) equipped with laser confocal optics to measure the depth of PSA surfaces. This microscope uses both 404 nm laser light sources and white light sources to obtain height information and images.

Confocal microscopy was employed to analyze both the surface pattern on the release film and the shape, length, and depth of the pattern transferred onto the PSA surface. This advanced imaging technique allows for precise, three-dimensional measurements of the microstructures on the PSA, facilitating a detailed evaluation of the pattern fidelity and quality after patterning. Additionally, confocal microscopy was utilized to assess the residue remaining on the surface of the adherend following the peel test. This analysis is crucial for understanding the efficiency and effectiveness of the adhesive interaction between the PSA and the adherend, providing insights into the adhesive's performance characteristics.

2.5. Adhesion properties

The 180° peel strength and probe tack were measured using a Texture Analyzer (TA.XT plus, Stable Micro Systems) at 25 °C. Samples for underwater adhesion test were prepared by being immersed in deionized water. The specific method is described in Section 2.6 of Chapter 2.

3. Results & discussion

3.1. Surface patterning, characterization

In studies aimed at developing underwater adhesives that mimic the surface patterns of tree frog toes, it has been found that the geometrical characteristics of these patterns - specifically the shape, size, depth, and width of the channels between the patterns - play a crucial role in influencing adhesive properties under water (Xie*, et al.*, 2018). To explore how these structural characteristics impact adhesive performance, a series of patterned liners were employed to fabricate PSAs with square-shaped patterns, each varying in size, depth, and the widths of the channels between the patterns.

The liners were numbered in ascending order, with each subsequent number representing an increase in pattern size (Figure 4-2). Liner #1 featured the smallest pattern size, with a depth of 4 μm. From Liner #2 to Liner #4, the depth of the patterns remained relatively constant; however, as the liner number increased, the pattern size became larger and the width of the drainage channels decreased. This systematic variation in pattern design across different liners allowed for a comprehensive evaluation of how different structural dimensions of the patterns influence the PSA's underwater adhesion capabilities, shedding light on optimal design parameters for enhancing performance in aquatic environments.

To fabricate the patterned PSA film, a gallol PSA solution was applied onto a patterned release liner. Given that the liner needs to be removed post-application, its surface is treated to possess low surface energy, facilitating easy removal. However, this low surface energy can pose challenges during the coating process. When the relatively high surface energy gallol PSA solution is applied directly to the release liner, it tends to bead up rather than spread evenly, leading to clumping and an uneven coating surface. To address this issue and achieve a more uniform coating, a small amount of low-molecular-weight polydimethylsiloxane was added to the gallol PSA solution - specifically 0.05 wt.% relative to the PSA solid content. PDMS is known for its ability to reduce surface tension, thus enhancing the wetting properties of the solution on the low-energy surface of the release liner. Following the application of the solution, the coated film was dried at a temperature of 150 °C for 5 minutes. This drying process is crucial for evaporating any solvents, solidifying the adhesive, and ensuring that the patterns from the liner are accurately transferred onto the PSA film. Immediately after drying, the PSA was transferred to a PET film, which had undergone corona treatment. The total thickness of PSA was 20 μm.

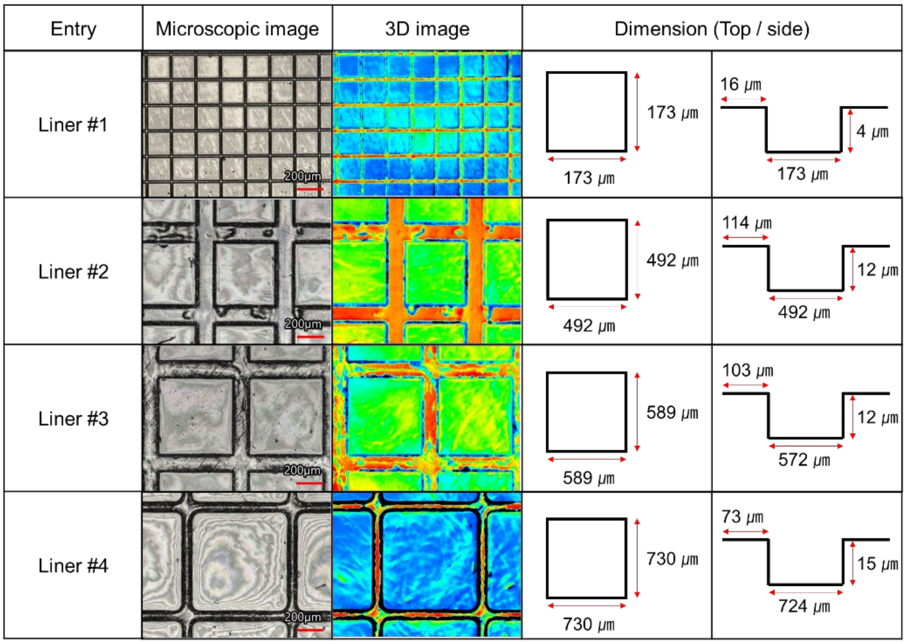

Figure 4-2. Characterization of patterned release liner

Entry	Microscopic image	3D image	Dimension (Top / side)	
PPSA #1	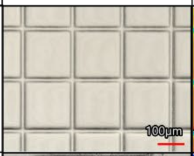	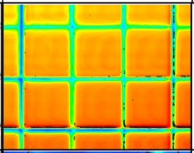	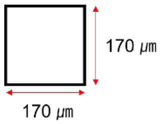	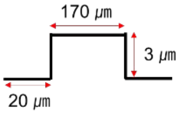
PPSA #2	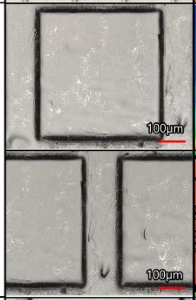	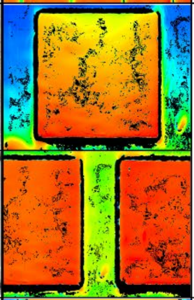	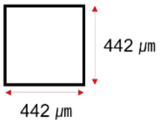	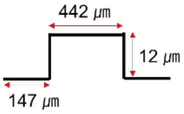
PPSA #3	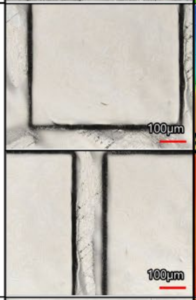	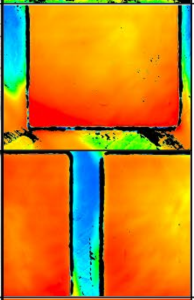	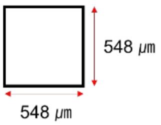	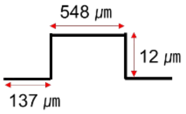
PPSA #4	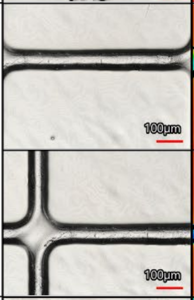	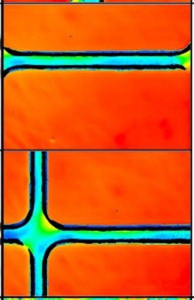	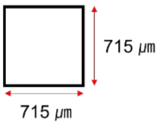	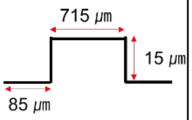
Flat PSA		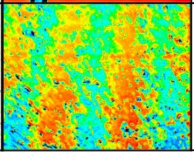	R_a: 0.164 μm	

Figure 4-3. Characterization of patterned PSA.

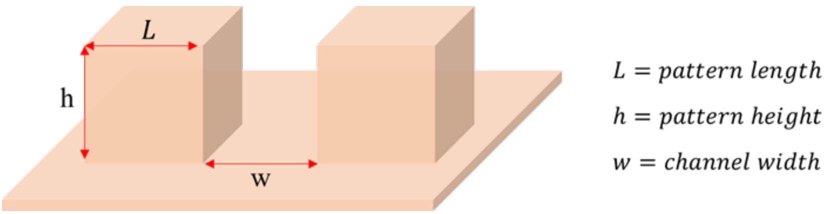

Figure 4-4. Schematic illustration of patterned PSA

Table 4-1. Pattern length, pattern height, and channel width of patterned release films and PSAs

Entry	Patterned release films				Patterned PSAs (μm)			
	L (μm)	h (μm)	w (μm)	w/L	L (μm)	h (μm)	w (μm)	w/L
PPSA#1	173	4	16	0.09	168	3	20	0.12
PPSA#2	492	12	114	0.23	442	12	147	0.33
PPSA#3	589	12	103	0.17	548	12	137	0.25
PPSA#4	730	15	73	0.10	715	15	85	0.12

After the coating process, the surface of the patterned PSA film was analyzed using confocal microscopy to assess the transfer fidelity of the patterns from the release liner to the PSA (Figure 4-3). The analysis revealed that the size of the patterns on the PSA surface were changed compared to those on the patterned liner, and the width of the drainage channels had widened. This discrepancy in pattern dimensions between the liner and the PSA film is likely attributable to the behavior of the PSA solution during the drying process. As the solvent in the gallol PSA solution evaporates under the high temperatures used for drying, the PSA material undergoes contraction. This contraction of the PSA matrix as it solidifies can cause the patterns to diminish in size and depth while simultaneously causing the channels to appear wider (Figure 4-5).

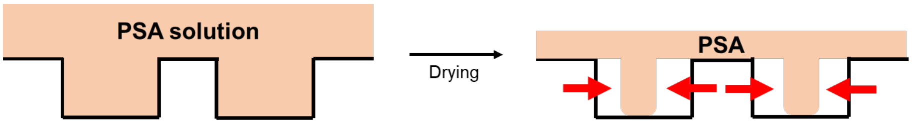

Figure 4-5. Pattern size reduction after drying process

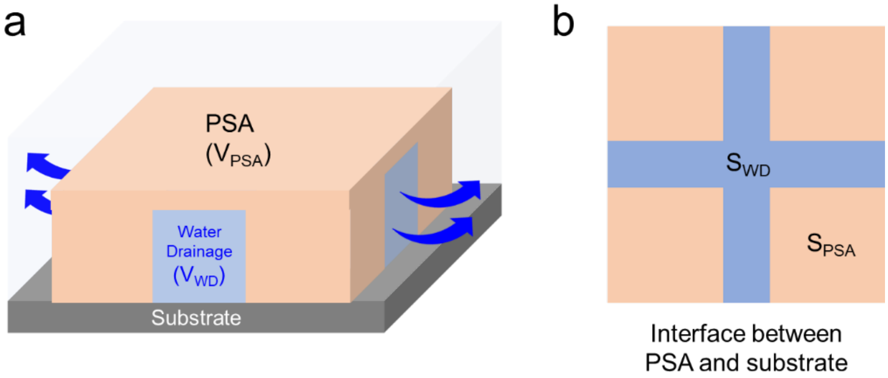

Figure 4-6. Schematic illustration of (a) patterned PSA bonded to substrate in water, (b) interface between PSA and substrate. S_{PSA}: surface area of PSA at interface, S_{WD}: surface area of water drainage

Figure 4-6a illustrates a patterned PSA bonded to an adherend submerged in water. The design of the PSA's surface facilitates the formation of a drainage channel at the interface between the adherend and the PSA, through which water can readily flow. The efficacy of water movement through this channel is directly influenced by its dimensional characteristics - specifically, the area or volume of the channel. Larger channels facilitate easier water flow, which is critical for ensuring that water can be effectively removed from the interface.

Additionally, the surface area of the PSA that is in contact with the adherend plays a pivotal role in adhesion (Figure 4-6b). This area represents the portion of the PSA that actively interacts with the adherend, affecting the strength and durability of the bond. For the analysis, although the patterns on the PSA are not perfectly rectangular, they can be approximated as rectangular parallelepipeds for calculation purposes. The calculated surface areas and volumes of the PSAs and drainage channels for an bonding area of 100 mm² are detailed in Table 4-2.

Table 4-2. Calculated surface areas and volumes of the PSAs and drainage channel for bonding area of 100 mm²

Entry	Surface area (mm^2)		Volume (mm^3)		
	PSA (S_{PSA})	Drainage (S_{WD})	PSA (V_{PSA})	Drainage (V_{WD})	V_{PSA}:V_{WD}
PPSA#1	80.1	19.9	1.940	0.060	97.3
PPSA#2	56.3	43.7	1.476	0.524	74:26
PPSA#3	64.0	36.0	1.568	0.432	78:22
PPSA#4	79.9	20.1	1.698	0.302	85:15

Calculated surface area and volume of PSAs and drainages are presented in Table 4-2. The calculated surface area available for interaction were almost similar for PPSA#1 and PPSA #4, which were the largest area, followed by PPSA #3, and PPSA #2, respectively. This hierarchy suggests that PPSA#1 and PPSA #4 potentially offer the strongest adhesion capabilities due to its larger interface with the adherend, if an ideal defect-free bond is formed between the adherend and the PSA. Conversely, the area of the drainage channels follows a reverse order, with PSA #2 providing the largest channel area, succeeded by PPSA #2, PPSA #3, PPSA #4, and PPSA #1. The size of these channels is critical, as larger channels facilitate more effective water drainage, enhancing the adhesive's performance in wet conditions. Given the observed hierarchy in surface area of the drainage channels, PPSA #2 exhibits the largest drainage area among the examined samples. This characteristic suggests that PPSA #3 is likely to possess superior drainage capacity. While PPSA #2 demonstrates a potentially superior drainage capacity due to its extensive drainage area, it is important to consider the inverse relationship between the drain area and the PSA's contact area with the adherend. As the drainage area increases, the corresponding area available for adhesive interaction decreases, which could potentially compromise the overall adhesive strength of the PSA. Therefore, a detailed examination of the ratio between the PSA area and the drainage area is essential.

When considering the volume, which accounts for the thickness of each PSA, PPSA #1 exhibits the largest volume, indicating a potentially more substantial body of adhesive material at the interface, followed by PPSA #4, PPSA #3, and PPSA #2 in descending order. Upon initial examination, the volume of the PSAs might appear to be a secondary consideration. However, the volume significantly impacts the mechanical energy required to deform the PSA during the peeling process. A greater volume of PSA indicates a larger amount of material that must be deformed, which can increase the energy required for detachment. This factor becomes particularly crucial when considering the performance of adhesives in underwater conditions, where both adhesion and ease of removal are influenced by the mechanical properties of the adhesive. Therefore, investigating the correlation between the volume of the PSA and its underwater adhesive performance is also essential. The volume of the drainage channels inversely correlates with the PSA volume, impacted by the varying thicknesses of each adhesive. The sequence from largest to smallest drainage volume is PPSA #2, PPSA #3, PPSA #4, and PPSA #1.

3.2. Adhesion properties

Adhesion property evaluations were conducted under both dry and underwater conditions to comprehensively assess the performance characteristics of the PSAs. For dry adhesion testing, measurements were taken in air, while underwater tests were performed in deionized water. The procedure involved attaching the PSA film to the adherend and allowing it to set for a period of 24 hours before measuring the peel strength.

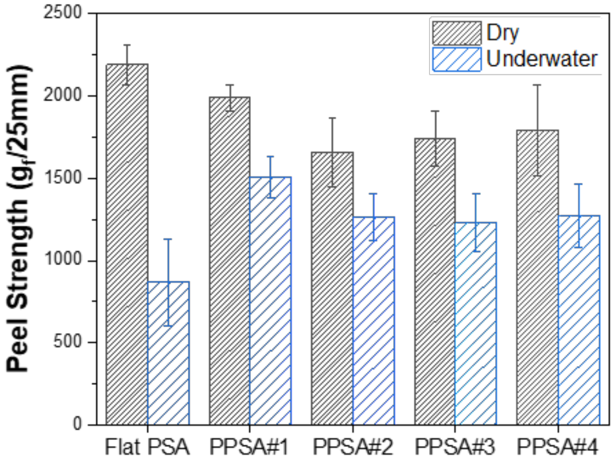

Figure 4-7. 180° peel strength results of flat PSA and patterned PSAs in dry and underwater conditions

In dry conditions, it was observed that the adhesion of patterned PSAs exhibited a slight decrease compared to that of flat PSAs; however, this difference was not statistically significant. Both types of PSAs demonstrated cohesive failure as the predominant mode of detachment, indicating that the internal strength of the adhesive material was greater than the adhesive bond between the PSA and the substrate. Furthermore, no clear relationship was identified between peel force and either the contact area or the volume of the PSA (Table 4-2). This observation suggests that the initial pattern of the PSA may undergo deformation over time due to the creeping behavior of the adhesive material. Microscopic examination of the PSA films post-attachment revealed a gradual blurring of the surface patterns, substantiating the hypothesis that structural changes occur within the PSA matrix during the dwell time (Figure 4-8). This blurring effect likely contributes to the diminished distinction in performance between patterned and flat PSA configurations under dry conditions.

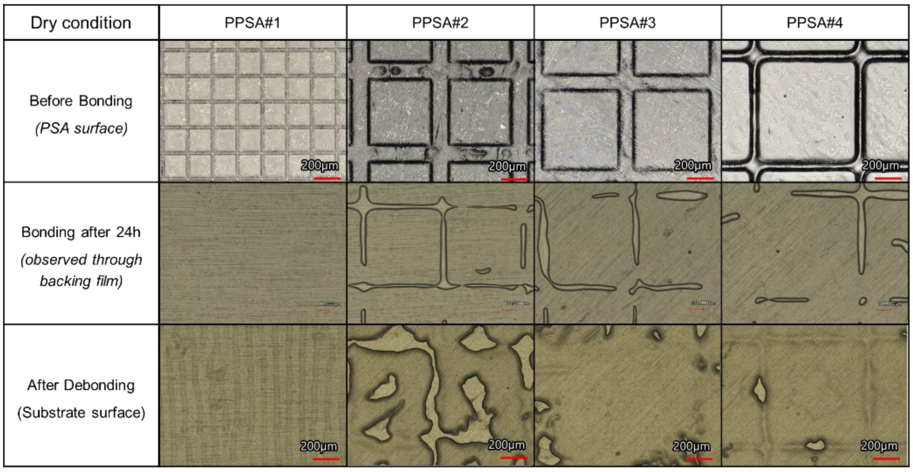

Figure 4-8. Microscopic images of before bonding, 24 hours after bonding, and after debonding (dry condition)

Microscopic analysis of the PSA films, conducted 24 hours post-attachment, revealed significant morphological changes at the microstructural level. Despite variations in the initial width (w) between the patterns, it was observed that the spaces between the patterns were progressively filled over time. This filling effect, irrespective of the original pattern width, suggests a substantial flow of the adhesive material under ambient conditions. In case of the residue from PPSA#2, which featured the widest valleys in the initial pattern of the pressure-sensitive adhesive, it was observed that the unfilled spaces remained relatively wide. However, despite these differences in the microstructure, the variations in peel strength between the patterned PSAs were not statistically significant. Further investigation predicts that with an extended attachment duration exceeding 24 hours, the valleys between the patterns will likely be completely filled, thereby homogenizing the surface texture. Consequently, when these fully filled patterned PSAs are peeled off, the peeling force required is expected to approximate that of flat PSAs. This phenomenon underscores the viscoelastic behavior of the adhesive, which facilitates the flow into the interstitial spaces of the pattern, effectively diminishing the distinctiveness of the micro-patterned structure over time. At patterned adhesive interfaces such as the gecko's foot, no increase in adhesion due to effects such as reinitiation of cracks due to the extrinsic contribution of filbril was observed, because shape collapse and adhesive failure of the patterned PSA occurred in the bulk.

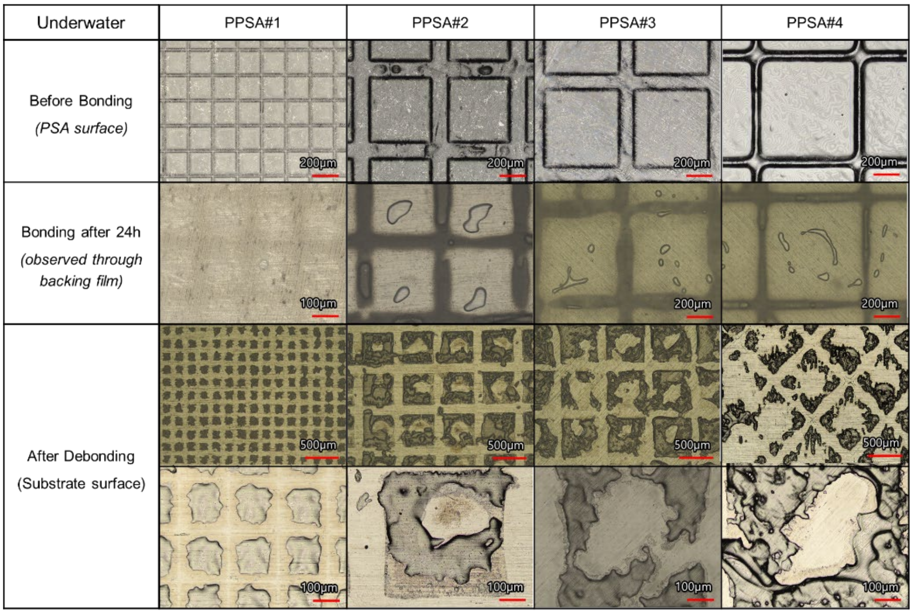

Figure 4-9. Microscopic images of before bonding, 24 hours after bonding, and after debonding (underwater)

Underwater conditions revealed distinct adhesive behaviors in contrast to those observed in dry environments. Notably, all patterned PSAs exhibited enhanced adhesion capabilities underwater compared to flat counterparts. Among these, PPSA#1, characterized by the smallest pattern size, demonstrated the most pronounced underwater adhesion, closely followed by nearly identical performances in patterns #2, #3, and #4. In dry conditions, pattern deformation over time due to creep was evident; however, underwater, the patterns retained their integrity, likely due to the channels being filled with water (Figure 4-9). Observations also revealed defects within the patterns, presumably from air or water entrapment. Residue analysis post-peeling presented consistent trends: PPSA#1 displayed filled central areas with torn edges, whereas in larger patterns (#2, #3, #4), the central regions predominantly exhibited tearing. These findings suggest that larger patterns tend to trap more defects such as water or air at the interface, thereby reducing effective interaction between the PSA and the substrate and consequently leaving fewer residues on the substrate surface after detachment.

No definitive correlation was established between the underwater peel strength and the calculated ratios of the surface area and volume of the PSAs and their drainage channels. The ranking of underwater peel strength was observed as #1 exhibiting the highest, followed by #2, #3, and #4, which were approximately equal. The sequence based on PSA surface area ratios was #1 and #4 having the highest, followed by #3 and then #2; for volume ratios, it was #1 > #4 > #3 > #2. Despite PSA #1 having the highest ratios and demonstrating superior adhesion properties, the peel strength difference between #2 and #4, which have a substantial difference in both surface area ratio (23.6 %) and volume ratio (11%), was minimal at only 2%. Conversely, #1 and #4, with almost identical surface area ratios but a 12% difference in volume ratio, showed a significant 20% difference in peel strength. These findings indicate that there is no direct quantitative correlation between the adhesion area or volume of PSA with the substrate. However, observations of the residues suggest that smaller pattern sizes potentially decrease the likelihood of interface defects between the PSA and the substrate, leading to the conclusion that smaller PSA patterns are advantageous. This highlights the importance of considering pattern size in the design of PSAs to minimize defects and enhance adhesive performance. The highest peel strength was observed in pattern #1, which featured the smallest drainage channels with dimensions of 20 μm in width and 3 μm in height. This finding indicates that even minimal channel dimensions are effective at preventing water entrapment at the adhesive interface. Furthermore, the enhanced underwater adhesion performance of all patterned PSAs compared to flat PSA substantiates the efficacy of incorporating drainage channels.

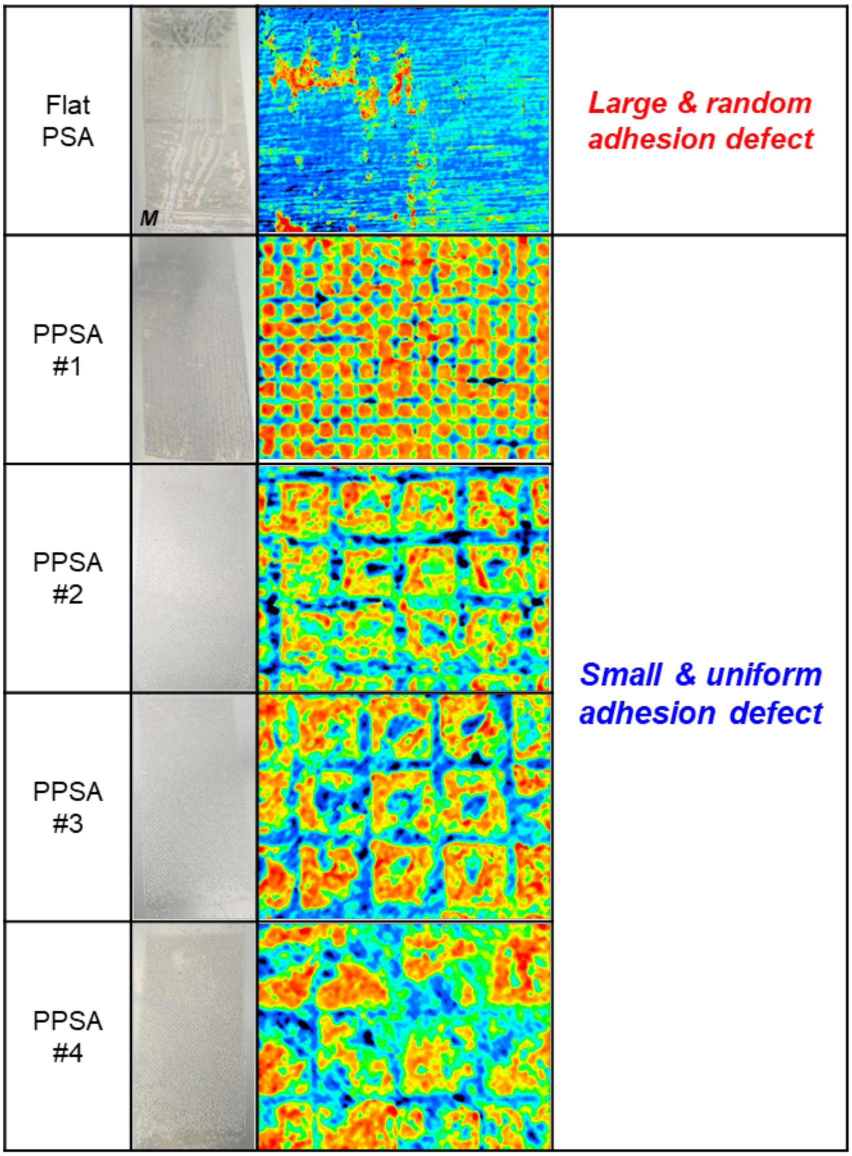

blue area: substrate, red area: PSA residue

Figure 4-10. Photographs and micrographs of PSA residues on substrate surface

Residue analysis revealed distinct differences between flat and patterned PSAs (Figure 4-10). In flat PSAs, adhesion defects were observed to exceed several millimeters in size, with irregular spatial distribution and inconsistent dimensions. Conversely, patterned PSAs demonstrated a reduction in defect size to the order of several hundred micrometers, with more systematically arranged locations and geometries relative to flat PSAs. This pattern dependency in defect formation suggests that structured pathways facilitated by the micropatterns enable more efficient water evacuation from the interface. Consequently, this structural modification not only minimizes the extent of adhesion defects but also contributes to their more uniform distribution across the adhesive surface (Figure 4-11). Such improvements are instrumental in enhancing the stability and performance of PSAs in underwater environments, underscoring the functional benefits of pattern incorporation in adhesive design.

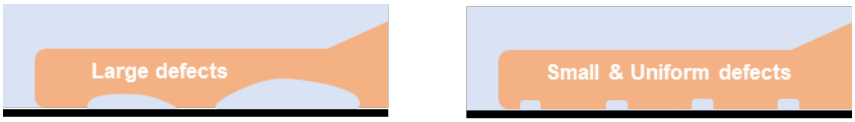

Poor dehydration

Good dehydration

Figure 4-11. Effect of surface pattern on dehydration at the interface, flat PSA (left), and patterned PSA (right)

4. Conclusion

The comprehensive investigation into patterned pressure-sensitive adhesives PSAs elucidates the significant influence of micropatterning on underwater adhesive performance. Our studies, inspired by biological entities such as tree frog toes, have demonstrated that the geometric characteristics of these patterns - namely the shape, size, depth, and width of the channels - critically affect the adhesive properties under aquatic conditions. The experiments employed a series of patterned liners to explore the effects of these structural dimensions on the adhesive's underwater capabilities.

The systematic variation in pattern size and channel dimensions across different liners allowed for an in-depth evaluation of their impacts on underwater adhesion. Smaller patterns with minimal channel dimensions proved most effective, facilitating water evacuation and preventing water entrapment at the adhesive interface. This was particularly evident in the superior performance of PPSA#1, which featured the smallest patterns and showed the highest underwater peel strength. The presence of structured drainage channels significantly enhanced adhesion by maintaining the integrity of the pattern under water, thus avoiding the common pitfalls observed in flat PSAs such as large, irregularly distributed adhesion defects. Residue analysis post-peeling revealed that patterned PSAs tend to exhibit smaller and more uniformly distributed defects compared to their flat counterparts. This finding underscores the advantage of micropatterned designs in reducing the size and variability of adhesion defects, which is pivotal for enhancing the overall stability and effectiveness of PSAs in underwater conditions.

Chapter 5

Overall Conclusions

1. Overall Conclusions

This study aimed to engineer a PSA that exhibits enhanced adhesion properties under aquatic conditions. Addressing the challenge posed by the hydration layer on substrate surfaces, this research introduces gallol groups as a cost-effective and more transparent alternative to traditional catechol-based materials. Gallol's versatility allows for strong bonding through hydrogen bonding and metal coordination at interfaces, and the formation of dynamic reversible bonds such as hydrogen bonds, π-π interactions, and hydrophobic interactions in the bulk, thereby enhancing the material's overall adhesion performance. However, excessive gallol content can lead to increased material rigidity, compromising adaptability and decreasing adhesion performance. To circumvent this issue, the study modifies the polymer backbone structure by transitioning from linear to branched polymer chains. This structural modification reduces the modulus of the polymer, facilitating the incorporation of higher levels of gallol without compromising wetting properties.

Moreover, the research incorporates microstructural design strategies to further augment underwater adhesion. By patterning the adhesive surface—similarly to biological adaptations seen in tree frogs and clingfish—enhanced drainage capabilities are achieved, effectively mitigating water entrapment issues at the interface, minimizing adhesion defects, and promoting even defect distribution. This multiscale approach not only resolves the poor underwater adhesion historically associated with conventional adhesives but also integrates seamlessly with existing industrial processes, eliminating the need for substantial additional investments. This pragmatic approach provides new insights into the catechol chemistry of PSAs for underwater adhesion, which has been challenging to commercialize over the past decade.

1.1. Gallol pressure-sensitive adhesives

The synthesis and design of gallol PSA were strategically developed based on several key principles. Firstly, the scaffold polymer underlying the gallol PSA required a hydrophobic nature to facilitate water repulsion essential for effective dehydration. Secondly, gallol groups were introduced post-polymerization to mitigate the risk of radical scavenging, which is critical for preserving the integrity of the polymer structure. Lastly, the resultant gallol PSA needed to maintain a low glass transition temperature and modulus to fulfill its role as a pressure-sensitive adhesive effectively. Gallol PSA was synthesized through the copolymerization of lauryl methacrylate and glycidyl methacrylate, followed by an esterification reaction with gallic acid to integrate the gallol groups successfully. Comparative studies were conducted with phenolic PSA and benzoic PSA, which contain fewer hydroxyl groups on their benzene rings, to evaluate the impact of functional group differences on the adhesive's properties. Rheological analysis indicated that an increase in the number of hydroxyl substitutions on the benzene ring correlates with higher G' at ambient temperatures, which in turn contributed to reduced creep behavior and enhanced recovery characteristics. Adhesive testing under dry conditions revealed that functionalization of the scaffold led to a transition in the failure mode from interfacial to cohesive, thereby enhancing the peel strength. Distinct behaviors were observed under underwater conditions, where the Gallol PSA uniquely demonstrated cohesive failure, while control group PSAs predominantly exhibited interfacial failure. This outcome underscores the unique ability of gallol groups to sustain robust interactions with the substrate interface in aquatic environments, highlighting their potential for specialized applications requiring enhanced underwater adhesion.

1.2. Branching of polymer chains

Gallol groups have proven to be highly effective in enhancing underwater adhesive properties; however, their incorporation is limited by the extent to which they increase the rigidity of the PSAs. This rigidity compromises the PSAs' fundamental ability to bond to substrates under minimal pressure conditions typical of room temperature and atmospheric pressure. To address this, the study implemented structural modifications by branching the polymer backbone of the gallol PSA, excluding the gallol functional groups. The branching process was achieved through the Strathclyde strategy, employing multifunctional acrylates and chain transfer agents, resulting in a branched scaffold synthesized with an impressive conversion rate exceeding 85%. Verification of branching was conducted using triple detection gel permeation chromatography, which indicated a reduction in the Mark-Houwink constants for the branched polymers relative to their linear analogs. The analysis further revealed that an increase in the functionality of the multifunctional acrylates broadened the molecular weight distribution. Rheological evaluations demonstrated that the branched polymers exhibited consistently lower G’ compared to their linear counterparts across a wide range of conditions. Notably, the wetting properties were significantly enhanced in the scaffold 7 series, particularly with formulations including 7 mol% GMA. Whereas the linear gallol PSA (S7-L-G) displayed stick-slip failure behaviors in dry conditions, all branched variants within the scaffold 7 series exhibited cohesive failure, achieving superior peel strength. These findings underscore the potential of polymer branching as a viable strategy to facilitate the incorporation of higher concentrations of gallol, thereby extending the utility and performance of gallol-based PSAs in demanding adhesion applications.

1.3. Surface patterning

The differences in adhesive properties between dry and underwater environments for Gallol PSA suggest that the area of the interface is an important factor in underwater adhesion. Results indicated a general decline in peel strength under submerged conditions across all samples, whereas, in some instances, probe tack measurements exhibited increased adhesion underwater. This discrepancy arises from the differential contact areas required in peel strength and probe tack tests. In peel tests, where the contact area is larger, water entrapped at the interface needs to traverse a longer path to escape, compared to probe tack scenarios. To capitalize on this understanding, patterns were introduced on the surface of S7-F4-G, which demonstrated superior underwater adhesion. Using a patterned release film, four variants of patterned PSAs, each with distinct pattern and groove dimensions, were fabricated. Confocal microscopy confirmed the successful implementation of diverse patterns on these PSAs. In dry conditions, these surface-patterned PSAs experienced a gradual degradation of the pattern structure over time, which marginally reduced their peel strength compared to flat PSAs due to incomplete sealing of the interface within 24 hours. Conversely, in submerged conditions, patterned PSAs outperformed flat PSAs in terms of peel strength. Microscopic analyses revealed that the engineered surface patterns facilitated drainage channels, effectively minimizing and uniformly distributing adhesion defects. Additionally, the impact of pattern size was assessed, indicating that smaller patterns significantly reduced the occurrence of adhesion defects during attachment. This study underscores the critical role of pattern engineering in optimizing PSA performance, particularly in challenging underwater environments.

References

Ahn, B. K., 2017, Perspectives on mussel-inspired wet adhesion, *Journal of the American Chemical Society*, **139** (30): 10166-10171

Ahn, Y., Jang, Y., Selvapalam, N., Yun, G. and Kim, K., 2013, Supramolecular velcro for reversible underwater adhesion, *Angewandte Chemie International Edition*, **52** (11): 3140-3144

Arzt, E., Gorb, S. and Spolenak, R., 2003, From micro to nano contacts in biological attachment devices, *Proceedings of the National Academy of Sciences of the United States of America*, **100** (19): 10603-10606

Bai, T., Zhang, P., Han, Y. J., Liu, Y. A., Liu, W. G., Zhao, X. L. and Lu, W., 2011, Construction of an ultrahigh strength hydrogel with excellent fatigue resistance based on strong dipole-dipole interaction, *Soft Matter*, **7** (6): 2825-2831

Banik, A. and Tan, K. T., 2020, Dynamic friction performance of hierarchical biomimetic surface pattern inspired by frog toe-pad, *Advanced Materials Interfaces*, **7** (18): 2000987

Braccini, I. and Perez, S., 2001, Molecular basis of Ca2+-induced gelation in alginates and pectins: The egg-box model revisited, *Biomacromolecules*, **2** (4): 1089-1096

Chang, E. P., 1997, Viscoelastic properties of pressure-sensitive adhesives, *Journal of Adhesion*, **60** (1-4): 233-248

Chen, D., Zhang, Y., Long, G., Liu, W., Li, X., Sun, Y. and Chang, Z., 2018, An optimal wet friction plate inspired by biological surface patterns, *Journal of*

Bionic Engineering, **15**: 872-882

Chen, G., Guo, X., Yang, C., Zhu, H., Zhang, Q. and Zhu, S., 2023, Superstrong water-resistant underwater adhesives enabled by in situ coacervation through dense hydrogen bonds, *Chemical Engineering Journal*, **460**: 141691

Chen, H., Zhang, L., Zhang, D., Zhang, P. and Han, Z., 2015, Bioinspired surface for surgical graspers based on the strong wet friction of tree frog toe pads, *Acs Applied Materials & Interfaces*, **7** (25): 13987-13995

Cheng, B., Yu, J., Arisawa, T., Hayashi, K., Richardson, J. J., Shibuta, Y. and Ejima, H., 2022, Ultrastrong underwater adhesion on diverse substrates using non-canonical phenolic groups, *Nature Communications*, **13** (1): 1892

Cheng, B. H., Yu, J. H., Arisawa, T., Hayashi, K., Richardson, J. J., Shibuta, Y. and Ejima, H., 2022, Ultrastrong underwater adhesion on diverse substrates using non-canonical phenolic groups, *Nature Communications*, **13** (1):

Cheng, H., Yue, K., Kazemzadeh-Narbat, M., Liu, Y., Khalilpour, A., Li, B., Zhang, Y. S., Annabi, N. and Khademhosseini, A., 2017, Mussel-inspired multifunctional hydrogel coating for prevention of infections and enhanced osteogenesis, *Acs Applied Materials & Interfaces*, **9** (13): 11428-11439

Chikere, C. O., Faisal, N. H., Kong Thoo Lin, P. and Fernandez, C., 2019, The synergistic effect between graphene oxide nanocolloids and silicon dioxide nanoparticles for gallic acid sensing, *Journal of Solid State Electrochemistry*, **23** (6): 1795-1809

Creton, C., 2003, Pressure-sensitive adhesives: an introductory course, *Mrs*

Bulletin, **28** (6): 434-439

Creton, C. and Ciccotti, M., 2016, Fracture and adhesion of soft materials: a review, *Reports on Progress in Physics*, **79** (4):

del Campo, A., Greiner, C. and Arzt, E., 2007, Contact shape controls adhesion of bioinspired fibrillar surfaces, *Langmuir*, **23** (20): 10235-10243

Dhal, P. K., Ramakrishna, M. and Babu, G., 1982, Copolymerization of glycidyl methacrylate with alkyl acrylate monomers, *Journal of Polymer Science: Polymer Chemistry Edition*, **20** (6): 1581-1585

Drotlef, D.-M., Stepien, L., Kappl, M., Barnes, W. J. P., Butt, H.-J. and del Campo, A., 2013, Insights into the adhesive mechanisms of tree frogs using artificial mimics, *Advanced Functional Materials*, **23** (9): 1137-1146

Drotlef, D. M., Appel, E., Peisker, H., Dening, K., del Campo, A., Gorb, S. N. and Barnes, W. J. P., 2015, Morphological studies of the toe pads of the rock frog, *Staurois parvus* (family: Ranidae) and their relevance to the development of new biomimetically inspired reversible adhesives, *Interface Focus*, **5** (1): 20140036

Fan, H. L. and Gong, J. P., 2021, Bioinspired underwater adhesives, *Advanced Materials*, **33** (44):

Fréchet, J. M. J., Henmi, M., Gitsov, I., Aoshima, S., Leduc, M. R. and Grubbs, R. B., 1995, Self-condensing vinyl polymerization: an approach to dendritic materials, *Science*, **269** (5227): 1080-1083

Gong, J. P., 2014, Materials both tough and soft, *Science*, **344** (6180): 161-162

Gupta, R. and Frechette, J., 2012, Measurement and scaling of hydrodynamic interactions in the presence of draining channels, *Langmuir*, **28** (41): 14703-14712

Gupta, R. and Fréchette, J., 2012, Measurement and scaling of hydrodynamic interactions in the presence of draining channels, *Langmuir*, **28** (41): 14703-14712

Huang, Q., Shi, X., Xue, Y., Zhang, K., Gao, Y. and Wu, C., 2022, Synergetic effects of biomimetic microtexture with multi-solid lubricants to improve tribological properties of AISI 4140 steel, *Tribology International*, **167**: 107395

Iturri, J., Xue, L., Kappl, M., García-Fernández, L., Barnes, W. J. P., Butt, H.-J. and del Campo, A., 2015, Torrent frog-inspired adhesives: attachment to flooded surfaces, *Advanced Functional Materials*, **25** (10): 1499-1505

Iturri, J., Xue, L., Kappl, M., García-Fernández, L., Barnes, W. J. P., Butt, H. J. and del Campo, A., 2015, Torrent frog-inspired adhesives: attachment to flooded surfaces, *Advanced Functional Materials*, **25** (10): 1499-1505

Jayawarna, V., Ali, M., Jowitt, T. A., Miller, A. F., Saiani, A., Gough, J. E. and Ulijn, R. V., 2006, Nanostructured hydrogels for three-dimensional cell culture through self-assembly of fluorenylmethoxycarbonyl–dipeptides, *Advanced Materials*, **18** (5): 611-614

Jia, H. Y., Huang, Z. J., Fei, Z. F., Dyson, P. J., Zheng, Z. and Wang, X. L., 2017, Bilayered polyurethane/dipole-dipole and H-bonding interaction reinforced hydrogels as thermo-responsive soft manipulators, *Journal of Materials Chemistry B*, **5** (41): 8193-8199

Kamperman, M., Kroner, E., del Campo, A., McMeeking, R. M. and Arzt, E., 2010, Functional adhesive surfaces with "gecko" effect: the concept of contact splitting, *Advanced Engineering Materials*, **12** (5): 335-348

Kumar, A., Alami-Mejjati, N., Bouvet, M. and Meunier-Prest, R., 2023, Electrochemical oxidation of gallic acid: A reexamination of the reaction mechanism in aqueous medium, *Electrochimica Acta*, **460**: 142622

Lee, H., Dellatore, S. M., Miller, W. M. and Messersmith, P. B., 2007, Mussel-inspired surface chemistry for multifunctional coatings, *Science*, **318** (5849): 426-430

Lee, K., Tiu, B. D. B., Martchenko, V., Mai, K., Lee, G., Gerst, M. and Messersmith, P. B., 2021, A modular strategy for functional pressure sensitive adhesives, *Acs Applied Materials & Interfaces*, **13** (2): 3161-3165

Lee, K. Y. and Mooney, D. J., 2012, Alginate: properties and biomedical applications, *Progress in Polymer Science*, **37** (1): 106-126

Lee, L.-H., Fundamentals of adhesion, 2013, Springer Science & Business Media

Lee, S. B., Gonzalez-Cabezas, C., Kim, K. M., Kim, K. N. and Kuroda, K., 2015, Catechol-functionalized synthetic polymer as a dental adhesive to contaminated dentin surface for a composite restoration, *Biomacromolecules*, **16** (8): 2265-2275

Lee, S. Y., Lee, J. N., Chathuranga, K., Lee, J. S. and Park, W. H., 2021, Tunicate-inspired polyallylamine-based hydrogels for wet adhesion: A comparative study of catechol- and gallol-functionalities, *Journal of Colloid and Interface Science*, **601**: 143-155

Lee, T.-H., Kim, J.-S., Lee, J.-H. and Kim, H.-J., Pressure-sensitive adhesives for flexible display applications, 2019, in *Hybrid Nanomaterials-Flexible Electronics Materials*, IntechOpen

Li, C., Rowland, M. J., Shao, Y., Cao, T., Chen, C., Jia, H., Zhou, X., Yang, Z., Scherman, O. A. and Liu, D., 2015, Responsive double network hydrogels of interpenetrating DNA and CB[8] host–guest supramolecular systems, *Advanced Materials*, **27** (21): 3298-3304

Li, F., Zhu, Y., You, B., Zhao, D., Ruan, Q., Zeng, Y. and Ding, C., 2010, Smart hydrogels co-switched by hydrogen bonds and π–π stacking for continuously regulated controlled-release system, *Advanced Functional Materials*, **20** (4): 669-676

Li, J. Y., Suo, Z. G. and Vlassak, J. J., 2014, Stiff, strong, and tough hydrogels with good chemical stability, *Journal of Materials Chemistry B*, **2** (39): 6708-6713

Liao, M., Wan, P., Wen, J., Gong, M., Wu, X., Wang, Y., Shi, R. and Zhang, L., 2017, Wearable, healable, and adhesive epidermal sensors assembled from mussel-inspired conductive hybrid hydrogel framework, *Advanced Functional Materials*, **27** (48): 1703852

Liu, J., Wang, S., Shen, Q., Kong, L., Huang, G. and Wu, J., 2020, Tough underwater super-tape composed of semi-interpenetrating polymer networks with a water-repelling liquid surface, *Acs Applied Materials & Interfaces*, **13** (1): 1535-1544

Ma, X. and Zhao, Y., 2015, Biomedical applications of supramolecular systems based on host–guest interactions, *Chemical Reviews*, **115** (15): 7794-7839

Ma, X., Zhou, X., Ding, J., Huang, B., Wang, P., Zhao, Y., Mu, Q., Zhang, S., Ren, C. and Xu, W., 2022, Hydrogels for underwater adhesion: adhesion mechanism, design strategies and applications, *Journal of Materials Chemistry A*, **10** (22): 11823-11853

Ma, X. T., Zhou, X., Ding, J. J., Huang, B., Wang, P. Y., Zhao, Y., Mu, Q. Y., Zhang, S. H., Ren, C. G. and Xu, W. L., 2022, Hydrogels for underwater adhesion: adhesion mechanism, design strategies and applications, *Journal of Materials Chemistry A*, **10** (22): 11823-11853

Maeda, M., Nobukawa, S., TAKESHITA, H. and INOMATA, K., 2023, Free volume and local dynamics in modulus-enhanced polycarbonate under addition of low-mass molecules, *材料*, **72** (1): 17-22

Matyjaszewski, K., Gaynor, S. G. and Müller, A. H. E., 1997, Preparation of hyperbranched polyacrylates by atom transfer radical polymerization. 2. kinetics and mechanism of chain growth for the self-condensing vinyl polymerization of 2-((2-bromopropionyl)oxy)ethyl acrylate, *Macromolecules*, **30** (23): 7034-7041

Meng, F., Liu, Q., Shi, Z., Tan, D., Yang, B., Wang, X., Shi, K., Kappl, M., Lei, Y. and Liu, S., 2021, Tree frog-inspired structured hydrogel adhesive with regulated liquid, *Advanced Materials Interfaces*, **8** (18): 2100528

Nakahata, M., Takashima, Y., Yamaguchi, H. and Harada, A., 2011, Redox-responsive self-healing materials formed from host–guest polymers, *Nature Communications*, **2** (1): 511

O'Brien, N., McKee, A., Sherrington, D. C., Slark, A. T. and Titterton, A., 2000, Facile, versatile and cost effective route to branched vinyl polymers, *Polymer*, **41** (15): 6027-6031

Oh, D. X., Kim, S., Lee, D. and Hwang, D. S., 2015, Tunicate-mimetic nanofibrous hydrogel adhesive with improved wet adhesion, *Acta Biomaterialia*, **20**: 104-112

Paul, C. H. and Timothy, P. L., 2007, Polymer chemistry 2nd edition, *NICE (News & Information for Chemical Engineers)*, **25** (4): 409

Qin, C., Ma, Y., Zhang, Z., Du, Y., Duan, S., Ma, S., Pei, X., Yu, B., Cai, M. and He, X., 2023, Water-assisted strong underwater adhesion via interfacial water removal and self-adaptive gelation, *Proceedings of the National Academy of Sciences*, **120** (31): e2301364120

Rao, P., Sun, T. L., Chen, L., Takahashi, R., Shinohara, G., Guo, H., King, D. R., Kurokawa, T. and Gong, J. P., 2018, Tough hydrogels with fast, strong, and reversible underwater adhesion based on a multiscale design, *Advanced Materials*, **30** (32): 1801884

Rao, P., Sun, T. L., Chen, L., Takahashi, R., Shinohara, G., Guo, H., King, D. R., Kurokawa, T. and Gong, J. P., 2018, Tough hydrogels with fast, strong, and reversible underwater adhesion based on a multiscale design, *Advanced Materials*, **30** (32):

Rogers, S. and Mandelkern, L., 1957, Glass transitions of the poly-(n-alkyl methacrylates), *The Journal of Physical Chemistry*, **61** (7): 985-991

Roovers, J., Roovers, J., Charleux, B. and Springer, Branched polymers I, 1999, 1st 1999.. ed., Berlin
Heidelberg : Springer Verlag, Berlin
New York.

Roy, C. K., Guo, H. L., Sun, T. L., Ihsan, A. B., Kurokawa, T., Takahata, M., Nonoyama, T., Nakajima, T. and Gong, J. P., 2015, Self-adjustable adhesion of polyampholyte hydrogels, *Advanced Materials*, **27** (45): 7344-7348

Saiz-Poseu, J., Mancebo-Aracil, J., Nador, F., Busque, F. and Ruiz-Molina, D., 2019, The chemistry behind catechol-based adhesion, *Angewandte Chemie-International Edition*, **58** (3): 696-714

Samanta, S., Rangasami, V. K., Sarlus, H., Samal, J. R. K., Evans, A. D., Parihar, V. S., Varghese, O. P., Harris, R. A. and Oommen, O. P., 2022, Interpenetrating gallol functionalized tissue adhesive hyaluronic acid hydrogel polarizes macrophages to an immunosuppressive phenotype, *Acta Biomaterialia*, **142**: 36-48

Shahsavan, H. and Zhao, B., 2014, Bioinspired functionally graded adhesive materials: synergetic interplay of top viscous–elastic layers with base micropillars, *Macromolecules*, **47** (1): 353-364

Shi, Z., Tan, D., Liu, Q., Meng, F., Zhu, B. and Xue, L., 2021, Tree frog-inspired nanopillar arrays for enhancement of adhesion and friction, *Biointerphases*, **16** (2):

Slark, A. T., Sherrington, D. C., Titterton, A. and Martin, I. K., 2003, Branched methacrylate copolymers from multifunctional comonomers: the effect of multifunctional monomer functionality on polymer architecture and properties, *Journal of Materials Chemistry*, **13** (11): 2711-2720

Smith, A. M., Williams, R. J., Tang, C., Coppo, P., Collins, R. F., Turner, M. L., Saiani, A. and Ulijn, R. V., 2008, Fmoc-diphenylalanine self assembles to a hydrogel via a novel architecture based on π–π interlocked β-sheets, *Advanced Materials*, **20** (1): 37-41

Spolenak, R., Gorb, S. and Arzt, E., 2005, Adhesion design maps for bio-inspired attachment systems, *Acta Biomaterialia*, **1** (1): 5-13

Steiner, T., 2002, The hydrogen bond in the solid state, *Angewandte Chemie International Edition*, **41** (1): 48-76

Sun, J.-Y., Zhao, X., Illeperuma, W. R. K., Chaudhuri, O., Oh, K. H., Mooney, D. J., Vlassak, J. J. and Suo, Z., 2012, Highly stretchable and tough hydrogels, *Nature*, **489** (7414): 133-136

Tiu, B. D. B., Delparastan, P., Ney, M. R., Gerst, M. and Messersmit, P. B., 2019, Enhanced adhesion and cohesion of bioinspired dry/wet pressure-sensitive adhesives, *Acs Applied Materials & Interfaces*, **11** (31): 28296-28306

Tiu, B. D. B., Delparastan, P., Ney, M. R., Gerst, M. and Messersmith, P. B., 2020, Cooperativity of catechols and amines in high-performance dry/wet adhesives, *Angewandte Chemie International Edition*, **59** (38): 16616-16624

Tran, T.-N., Mauro, C. D., Graillot, A. and Mija, A., 2020, Chemical reactivity and the influence of initiators on the epoxidized vegetable oil/dicarboxylic acid system, *Macromolecules*, **53** (7): 2526-2538

Tsipenyuk, A. and Varenberg, M., 2014, Use of biomimetic hexagonal surface texture in friction against lubricated skin, *Journal of The Royal Society Interface*, **11** (94): 20140113

Tuncaboylu, D. C., Argun, A., Sahin, M., Sari, M. and Okay, O., 2012, Structure optimization of self-healing hydrogels formed via hydrophobic interactions, *Polymer*, **53** (24): 5513-5522

Tuncaboylu, D. C., Argun, A., Algi, M. P. and Okay, O., 2013, Autonomic self-healing in covalently crosslinked hydrogels containing hydrophobic domains, *Polymer*, **54** (23): 6381-6388

Van Nguyen, P., 2019, Grasping interface with wet adhesion and patterned morphology: Case of thin shell, *IEEE Robotics and Automation Letters*, **4** (2): 792-799

Wagner, H. L., 1987, The Mark–Houwink–Sakurada relation for poly (methyl methacrylate), *Journal of physical and chemical reference data*, **16** (2): 165-173

Waite, J. H., 2017, Mussel adhesion – essential footwork, *Journal of Experimental Biology*, **220** (4): 517-530

Wang, K., He, B. and Shen, R.-J., 2012, Influence of surface roughness on wet adhesion of biomimetic adhesive pads with planar microstructures, *Micro & Nano Letters*, **7** (12): 1274-1277

Wang, Y., Wang, Z., Wu, K., Wu, J., Meng, G., Liu, Z. and Guo, X., 2017, Synthesis of cellulose-based double-network hydrogels demonstrating high strength, self-healing, and antibacterial properties, *Carbohydrate Polymers*, **168**: 112-120

Wu, Y. C., Shah, D. U., Liu, C. Y., Yu, Z. Y., Liu, J., Ren, X. H., Rowland, M. J., Abell, C., Ramage, M. H. and Scherman, O. A., 2017, Bioinspired supramolecular fibers drawn from a multiphase self-assembled hydrogel, *Proceedings of the National Academy of Sciences of the United States of America*, **114** (31): 8163-8168

Xie, J., Li, M., Dai, Q., Huang, W. and Wang, X., 2018, Key parameters of biomimetic patterned surface for wet adhesion, *International Journal of Adhesion and Adhesives*, **82**: 72-78

Xu, Y., Liu, Q., Narayanan, A., Jain, D., Dhinojwala, A. and Joy, A., 2017, Mussel-inspired polyesters with aliphatic pendant groups demonstrate the importance of hydrophobicity in underwater adhesion, *Advanced Materials Interfaces*, **4** (22): 1700506

Xue, L., Sanz, B., Luo, A., Turner, K. T., Wang, X., Tan, D., Zhang, R., Du, H., Steinhart, M., Mijangos, C., Guttmann, M., Kappl, M. and del Campo, A., 2017, Hybrid surface patterns mimicking the design of the adhesive toe pad of tree frog, *ACS Nano*, **11** (10): 9711-9719

Xue, L., Sanz, B. n., Luo, A., Turner, K. T., Wang, X., Tan, D., Zhang, R., Du, H., Steinhart, M. and Mijangos, C., 2017, Hybrid surface patterns mimicking the design of the adhesive toe pad of tree frog, *ACS Nano*, **11** (10): 9711-9719

Yang, J., Bai, R. and Suo, Z., 2018, Topological adhesion of wet materials, *Advanced Materials*, **30** (25): 1800671

Yang, J. W., Bai, R. B., Chen, B. H. and Suo, Z. G., 2020, Hydrogel adhesion: a supramolecular synergy of chemistry, topology, and mechanics, *Advanced Functional Materials*, **30** (2):

Yang, Y., Wang, X., Yang, F., Shen, H. and Wu, D., 2016, A universal soaking strategy to convert composite hydrogels into extremely tough and rapidly recoverable double-network hydrogels, *Advanced Materials*, **28** (33): 7178-7184

Yao, L., Lin, C., Duan, X., Ming, X., Chen, Z., Zhu, H., Zhu, S. and Zhang, Q., 2023, Autonomous underwater adhesion driven by water-induced interfacial rearrangement, *Nature Communications*, **14** (1): 6563

Zevatskii, Y. E. and Lysova, S. S., 2009, Empirical procedure for the calculation of ionization constants of organic compounds in water from their molecular volume, *Russian Journal of Organic Chemistry*, **45** (6): 825-834

Zhan, K., Kim, C., Sung, K., Ejima, H. and Yoshie, N., 2017, Tunicate-inspired gallol polymers for underwater adhesive: a comparative study of catechol and gallol, *Biomacromolecules*, **18** (9): 2959-2966

Zhang, B., Jia, L. H., Jiang, J. R., Wu, S. S., Xiang, T. and Zhou, S. B., 2021, Biomimetic microstructured hydrogels with thermal-triggered switchable underwater adhesion and stable antiswelling property, *Acs Applied Materials & Interfaces*, **13** (30): 36574-36586

Zhang, L., Chen, H., Guo, Y., Wang, Y., Jiang, Y., Zhang, D., Ma, L., Luo, J. and Jiang, L., 2020, Micro–nano hierarchical structure enhanced strong wet friction surface inspired by tree frogs, *Advanced Science*, **7** (20): 2001125

Zhang, Y., Wan, X., Xu, X., Teng, P. and Wang, S., 2022, Recent progress of tree frog toe pads inspired wet adhesive materials, *Biosurface and Biotribology*, **8** (4): 279-289

Zheng, Y., Li, S., Weng, Z. and Gao, C., 2015, Hyperbranched polymers: advances from synthesis to applications, *Chemical Society Reviews*, **44** (12): 4091-4130

List of Publications

This Ph.D. dissertation is based on the following publications.

I. Lee, S.J., Back, J.H., Kim, J.S., Han, G.Y., Kim, Y.D., Kim, H.-J., 2023, Surface-patterned gallol pressure-sensitive adhesives for strong underwater adhesion, *Materials & Design,* **236**:112505

II. Lee, S.J., Back, J.H., Han, G.Y., Kim, Y.D., Kim, H.-J., Highly branched, gallol functionalized underwater pressure-sensitive adhesives with surface microstructure, in preparation

국문 초록

점착제는 상온에서 약한 압력만으로도 표면에 달라붙을 수 있는 사용의 단순성으로 인해 우리의 일상 생활과 산업에서 널리 사용되고 있다. 현재 다양한 용도의 점착제가 상업적으로 출시되어 있는데, 이들은 대부분의 경우 건조한 고체 표면에서만 작동한다. 그러나 의료 분야의 상처 드레싱, 수계 에너지 장치, 수중 센서, 수중 수리 및 해양 산업과 같은 많은 응용분야에서는 습한 표면이나 수중에 잠긴 표면에 접착할 수 있는 점착 소재를 필요로 한다. 따라서 수중 환경에서 다양한 용도로 뛰어난 성능을 발휘할 수 있는 새로운 수중 점착제의 개발은 점착소재 연구의 중요한 목표 중 하나이다.

하지만 물 속에서 강력한 점착력을 구현하는 것은 공기 중에서 같은 수준의 성과를 얻는 것보다 더 어렵다. 일반적으로 대부분의 재료가 수중 환경에 노출될 때 표면에는 물에 의한 수화층이 형성되어 점착소재와 피착재 간의 분자 수준의 상호작용을 방해하기 때문이다. 또한 계면에서 빠져나가지 못하고 갇힌 물방울은 점착소재와 피착재의 접촉 면적을 감소시키는 문제가 있고, 점착 소재가 장기간 물에 노출되면 물의 침투로 인해 점착 소재의 가소화, 팽창, 침식, 가수 분해 등의 문제를 발생시킬 확률이 높기 때문에 수중 점착 소재의 개발은 여전히 큰 도전과제이다.

수중 점착소재의 개발은 종종 자연에서 영감을 받아 이루어진다. 홍합과 같은 해양 생물은 영구적인 수중 접착을 달성하기 위해 카테콜 작용기를 활용하고, 개구리나 학치류는 독특한 미세 구조를 통해 물이 존재하는 표면에 일시적으로 달라붙을 수 있다. 이에 많은 연구자들은 자연 생물들의 독특한 전략에 영감을 받아 수중 점착

소재를 개발해왔다. 하지만 가격 경쟁력이 요구되는 점착테이프의 특성 상 카테콜기 도입을 위한 원료인 도파민의 상대적으로 비싼 가격과 산화 방지를 위한 추가 공정에 따른 비용 등은 카테콜계 수중 점착 테이프의 상용화에 장애물이 되고 있다.

본 연구에서는 벤젠링에 3개의 수산기가 달려 카테콜과 유사한 기능을 할 수 있으면서도, 다양한 식물에서 추출되어 도파민에 비해 가격경쟁력이 우수한 갈산을 원료로 사용하여 갈롤기를 가진 점착제를 제조하였다. 높은 소수성을 띠면서도 낮은 유리전이온도를 가지는 주 단량체로 스캐폴드 고분자를 구성해 수화층 극복과 상온에서의 젖음성을 확보하고자 하였고, 스캐폴드 내 에폭시기와 갈산의 간단한 에스터화 반응을 통하여 갈롤기를 도입하였다. 그리고 갈롤 점착제와 유사한 구조를 가지는 점착소재와의 비교를 통해 수중 환경에서 갈롤기만이 가지는 특수성을 확인하였다.

갈롤기는 수중 점착력 향상에 효과적이나 도입량에는 상한이 존재한다. 갈롤기가 많아짐에 따라 점착소재의 흐름성이 낮아져 피착재 표면에 젖어들어갈 수 있는 능력이 떨어지기 때문이다. 본 연구에서는 점착소재 내 갈롤기 외의 부분인 스캐폴드 고분자의 구조를 선형에서 분지형으로 변화시켜 갈롤기 도입량의 상한을 늘려 점착 성능을 향상시키면서도 선형 고분자가 가지고 있던 젖음성 문제를 극복하였다.

또한 수중 점착 성능을 추가적으로 향상시키기 위하여 점착소재 표면에 미세구조를 부여하였다. 표면 미세구조는 패턴 이형필름을 사용하여 빠른 속도로 점착 필름 생산이 가능한 연속코팅공정 방식을 채택하였고, 표면 미세구조의 종류를 달리하여 표면 미세구조의 크기가 수중 점착 특성에 미치는 영향을 확인하였다.

결론적으로 본 연구는 갈롤기 도입과 고분자의 분지화라는 분자 스케일의 설계와 표면 패터닝을 통한 거시 스케일의 전략을 복합 적용하여 수중 환경에서도 우수한 점착 특성을 나타내는 점착소재를 성공적으로 개발하였다. 일반적인 라디칼 중합을 통한 합성, 그리고 패턴 이형필름을 활용한 연속코팅 기술과 같은 간단한 공정을 적용하여 추가 설비가 필요 없이 기존 점착소재 산업 인프라를 그대로 활용할 수 있다. 이러한 실용적인 접근법은 지난 십 년 이상의 기간 동안 상용화하에 어려움을 겪어온 범용 수중 점착소재 개발에 새로운 전략을 제공할 수 있을 것으로 기대된다.

키워드: 점착제, 수중 접착, 갈롤, 분지형 고분자, 표면 미세구조

학 번: 2014-20043